Performance Assessment Methods for the Behaviour of Natural and Artificial Harbour Inlets.

by

S.O.Vithana

B.Sc.(Hons) (Sri Lanka), C.Eng.(Lond.)

Thesis presented for the degree of
Master of Engineering Science
at the University of Adelaide,
Australia.
- February 1991 -

CONTENTS

SYNOPSIS

Maintenance of sufficient depths for safe navigation of vessels at an inlet to a natural or artificially constructed harbour exposed to littoral drift is one of the main problems the harbour authorities are facing when maintaining a commercial port. The increasing popularity for bulk handling of cargo has brought into use bigger bulk carriers and container vessels over recent decades. In order to cater for these new larger vessels, the harbour authorities today face the dredging problem with added difficulty of maintaining much deeper harbour basins and approach channels. Therefore, accurate prediction of sedimentation behaviour is extremely important in the design of a harbour to establish maintenance dredging costs.

In this research project an extensive library search was undertaken to look for the methods available for assessment of the behaviour of harbour inlets. Major contributions to the literature have been reviewed and presented in this thesis. Using a sophisticated computer software package, an attempt was made to simulate turbulent flow across a simplified navigational channel section dredged at an inlet and to predict resulting sand movement in the channel.

For comparison, the flow across the channel was represented by two turbulent models, the K-Epsilon model and the Mixing Length model, and the sand movement was simulated using two methods which are based on different concepts for defining the sediment transport. The Shield's formula (46) is based on the assumption that shear stress is the main parameter defining sediment transporting power. In the method proposed by Ackers and White (1) the average flow velocity is used in preference to shear stress in defining the sediment movement. A Profile Model was used for morphological evolution of the channel bed.

A Physical Model was built and tested to validate the numerical models.

DECLARATION

This thesis contains no material which has been accepted for the award of any other degree or diploma in any university, and, to the best of my knowledge and belief, contains no material previously published or written by another person, except where due reference is made in the text. I consent to the thesis being made available for photocopying and loan if accepted for the award of the degree.

S.O.Vithana

ACKNOWLEDGEMENTS

The author wishes to thank all those who helped to make this thesis possible. The assistance of the staff of the Civil Engineering Department, Instrumentation Laboratory, and Computing Office and also fellow post-graduate students is acknowledged. Messrs Roger Chan, Eric Browne and G.Gibson are acknowledged for the assistance given in the numerical modelling work. Mr.C.W.Haese and his staff, and Mr.W.Eidam and his staff specially Mr.R.Marcussen are also thanked for their part in the construction of the physical model. Special thanks are due to the Australian International Development Assistance Bureau for the award of the research scholarship and the friendly staff for all the assistance extended to make my stay in Australia memorable. The author acknowledges the financial support for the hire of the commercial computer software package by the Civil Engineering Department.

Thanks also are due to Mr.R.Culver without whose supervision, inspiration and persistence none of this would have been possible and last, but not least, to my wife, Ramani for her continual support and encouragement.

Chapter 1

Introduction

Tidal inlets on sea coasts are exposed to a great variety of continuously changing parameters such as tides, currents, waves and sediment movements. The fact that these parameters are interrelated and the inlets are in a dynamic situation which adjusts continuously according to these changes, makes analysis of the behaviour of tidal inlets one of the most difficult tasks in hydraulic engineering.

The main flow in a tidal inlet on a year-round basis is caused by astronomic tides. However, the combined effect of density gradients and eddy generated velocity gradients may increase the flow in an inlet to several times that of the tidal flow.

A tidal inlet on a littoral drift shore can be divided into four sections:

1. *the Gorge Channel* - the section with minimum cross- sectional area between barriers.

2. *the Ocean Section* - the ocean part of the channel which may contain shoals or bars and one or more channels.
3. *the Bay Section* - which may include shoals and channels.
4. *the Intermediate Section* - between the ocean section and the gorge.

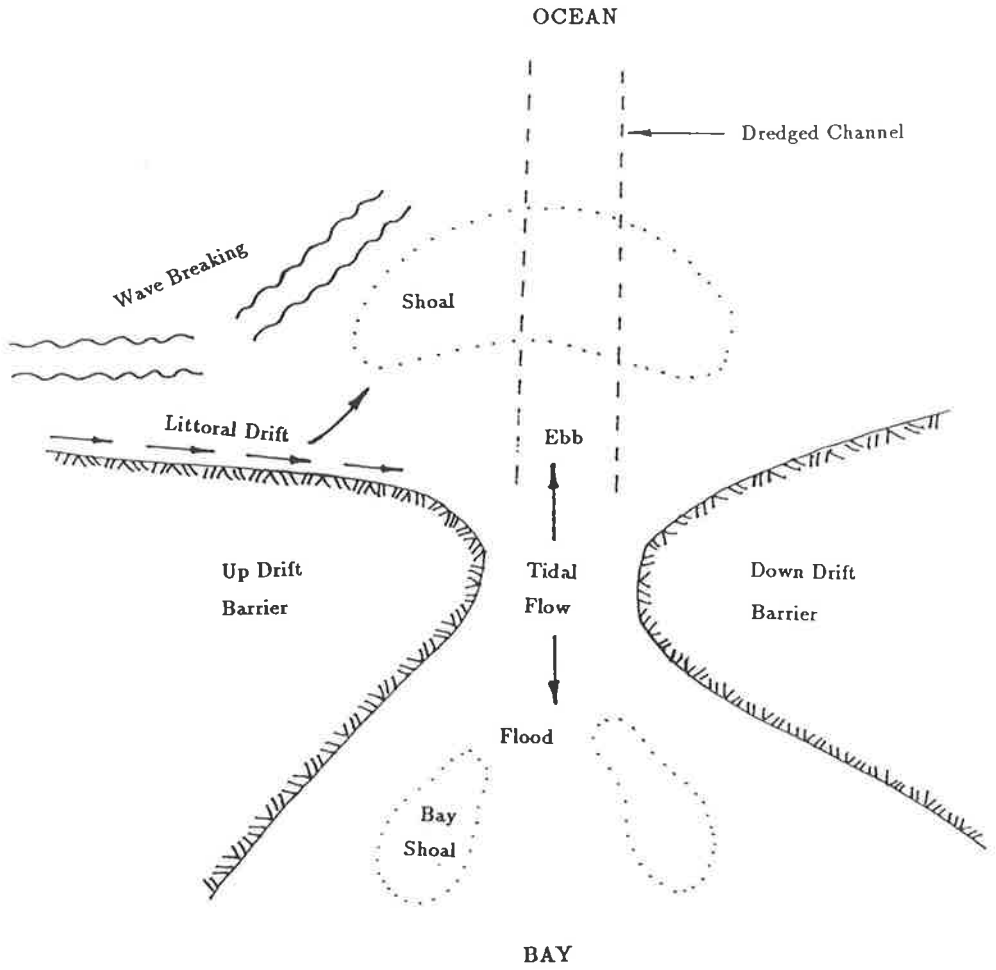

Figure 1.1: Typical Layout of A Tidal Inlet

The ocean section with its dynamic bars and shoals is the most active part of the inlet system. The entrance behaviour is an integrated result of inputs and outputs of material which are ever-changing in accordance with tides, currents and extreme events.

With respect to sediment transport there is a marked difference between the transport pattern and modes in the ocean section and the bay section. The difference lies in the wave action in the ocean entrance, which may include wave breaking over the shoals and bars causing a strong increase of mass transport influencing inlet flow, thereby inlet geometry. Wave breaking increases bed and particularly suspension load. This favours sediment transport by flood currents towards the bay and its shoals.

Moving towards the gorge channel wave action gradually reduces and becomes of lower order. Consequently bed load increases and predominates.

Near the shore turbulence caused by breaking waves initiates suspension of sediment and any longshore currents superimposed on fluid motion cause a net alongshore transport of the sediment, which is known as littoral drift. The quantity of littoral material pouring into the inlet from adjacent shores depends upon many partly interrelated factors including the longshore flux of wave energy in the vicinity of the entrance, the flux of wave energy and the tidal flow into the entrance, its geometric shape, the shoreline geometry on either side of the entrance, material characteristics and ready availability of alluvial shore and bottom material.

Generally speaking, any tidal inlet is in a state of very short term dynamic equilibrium because the conditions of flow, waves and sediment transport are always changing.

On littoral coastline the sediment transport caused by currents and waves often present major problems in regard to planning, operation and maintenance of ports. Moreover, sediment transport, erosion and accretion are very complex phenomena, which are still far from being fully understood in quantitative terms. Many projects have failed or have incurred unexpectedly high maintenance costs because of inadequate treatment of these problems.

When dredging is required the costs are usually critical to the economic feasibility of a project and in the design of a harbour the determination of capital and maintenance dredging volumes is of vital concern. Thus the accurate prediction of sedimentation behaviour is extremely important to fix dredging costs during the design assessment of the various alternatives.

Accurate sedimentation prediction usually requires detailed field surveys to determine the existing local conditions and factors such as : current velocities; velocity patterns; sediment type and concentrations and effective sea floor roughness. Accuracy of the sedimentation prediction can be further improved by carrying out a trial dredging investigation. Conducting such an investigation is also expensive but it can be considered necessary when the costs of the capital and maintenance dredging are relatively large in a given harbour location.

The design relationship between the dimensions of a harbour or bay and its channel connection to the ocean in early years was largely based on empirical formulae, experience and judgement because of the limited technical information available to solve these complex sedimentation problems. Even though such methods are good practical tools to solve physical problems, their wider applications are limited because of the substantial approximations made in deriving such formulae. With the increased demand for better navigation facilities, the need to understand flow characteristics in inlets and accurate prediction of shoaling rates became vital for proper designing of harbour inlet facilities to reduce maintenance problems. As a result of the advancements made in the fields of inlet tidal hydraulics and sedimentary aspects, as described in Chapters 2 and 3, the early empirical and statistical methods are now being gradually replaced by rational hydraulic modelling of the inlet hydraulics, with the inclusion of wave effects and their combined sedimentary response.

Simple methods for sedimentation prediction have been derived based on empirical formulae or with strong schematization of the relevant transport processes. Such methods should be used only when trial dredging results are available to calibrate the empirical coefficients or when a high accuracy of predicted sedimentation rates is not expected.

One of the most important new developments in hydraulic engineering of recent times is undoubtedly the development of numerical mathematical modelling, made possible by the ready availability of powerful digital computers. In such a model physical processes formulated by mathematical expressions are handled in the form of a discrete numerical elements and after validation they are often sufficiently reliable for practical applications.

Some of the advantages of these mathematical models over physical models are : the numerical model can take into account any physical phenomena that can be described in mathematical form, which would be impossible or very costly to simulate in physical models; scale effects as such do not exist in numerical models, however, similar errors due to discretization are introduced by the numerical representation of the mathematical equations; such a model can be stored and remobilized at insignificant cost compared to a physical model.

The limitations of application of mathematical models are set by inadequate knowledge in terms of quantitative description of the physical process to be modelled, inaccuracies in the numerical solution techniques, insufficient input data and by computer capacity and costs.

As described in Chapter-5, an attempt was made in this research project, using two separate numerical models, one to simulate turbulent flow across a navigational channel dredged through a sloping coastline and the other to predict dynamic siltation in the channel. A physical model was used to attempt validation of the numerical models. An important factor of the study was to assess the 'computational feasibility' of attempting problems of this scale on

other than 'super computer' scale machines.

For comparison, the flow was simulated using two turbulent models, the sophisticated K-Epsilon model and the Mixing Length model. A powerful computer software package, FIDAP, which uses the finite element method to solve the differential equations in the turbulent models was used to simulate flow.

As described in Section 5.4, sand transport was simulated using a simple depth averaged model.

Chapter 2

Literature Review

2.1 Introduction

In this chapter, reference has been made to contributions made by various investigators from 1930 up to the most recent developments. Only those papers which have made significant contributions towards proper interpretation of the inlet system have been reviewed and presented in chronological order. A list of all references has been presented in the bibliography at the end of the thesis.

Since methods of analysis to be presented are too numerous, the literature review chapter has been divided into separate sections so that assessment methods for stability of inlets, sedimentation at inlets and flow in inlets can be discussed separately. Current methods of analysis of inlets has been reviewed in a separate chapter in further detail.

2.2 Stability Relationships

At tidal inlets on littoral shore-line there are two opposing processes; on the one hand the littoral drift which is carried to the entrance by waves and flood currents form deposits in inner and outer bars, shoals and flats and attempt to close the inlet; on the other hand ebb tidal and other currents tend to flush these deposits away and maintain the cross sectional area of the inlet channel. Although the recognition of the importance of the tidal flow as the primary agent in maintaining the channels and inlets in lagoons and estuaries was generally accepted, it was not until 1928 that the hydraulic conditions in an inlet were expressed in a rational manner by Earl I. Brown (7).

Recognizing an intimate relationship between the size of the interior bay and the inlet, Brown deduced the equation:

$$Q = 12054\ c\ a \sqrt{\frac{a}{PL}} \sqrt[4]{H^2 - h^2} \tag{2.1}$$

in which,

Q = total tidal flow (tidal prism), in cu.ft.
c = hydraulic constant,
a = cross-sectional area of the inlet, in sq.ft.
P = wetted perimeter of the inlet, in ft.
L = length of the inlet, in ft.
H = mean tidal variation in the sea, in ft.
h = mean tidal variation in the basin, in ft.

In 1931, O'Brien (36) made an exhaustive study of the inlets and beaches of the Pacific Coast of the United States. After studying a plot of the tidal prism against area he suggested the famous empirical relationship:

$$A = 4.69 \times 10^{-4} \times P^{0.85} \tag{2.2}$$

in which,

P = tidal prism measured in cu.ft. between MLLW and MHHW,

A = cross-sectional area of the inlet below mean sea level, in sq.ft.

Even though the phenomena involved seemed too complex to yield so simple relationship, comparison by a number of investigators on other inlets has shown a surprisingly small deviation from O'Brien's equation for large and small inlets, with and without training jetties.

For a given tide, studying the maximum velocity of flow in an inlet which varies with the inlet cross-sectional area, Escoffier (16) presented a concept in 1940 to define the stability of an inlet. As shown in Figure 2.1, critical cross- sectional area, A_c^*, represents a division between stable and unstable conditions.

It is noted that in the stable area of the curve, the inlet tends to be stable by countering any area change by a velocity change that will tend to reduce the area change. In the unstable area of the curve, any area change will result in a velocity change that will tend to increase the area change.

One disadvantage of this concept is that, if maximum velocity associated with the critical cross-sectional area is less than the "threshold velocity" required to move sand, it is clear that the inlet would tend to close under the depositional action of waves and currents. Thus the critical cross- sectional area would only be meaningful in terms of some average tidal range conditions.

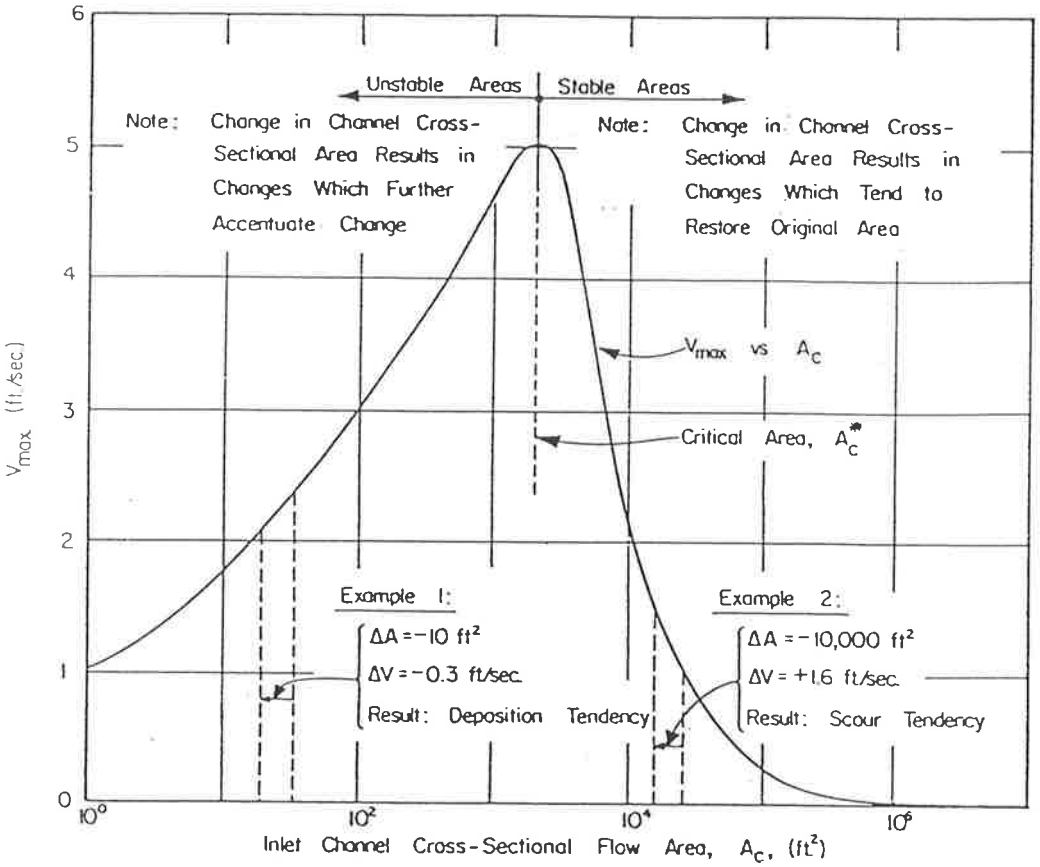

Figure 2.1: Illustration of Escoffier's Stability Concept

In 1951 Keulegan (30) undertook the analytical study of the hydrodynamics of the inlet-bay system and derived a theoretical equation relating the water level fluctuations in a basin relative to sea. The phase lag between bay and ocean tides, dimensionless values of maximum inlet velocity, and bay amplitude were presented as functions of the so-called "repletion coefficient", K, defined as :

$$K = \frac{T}{2\pi a_0} \frac{A_C}{A_B} \sqrt{\frac{2ga_0}{K_{en} + K_{ex} + fl/4R}} \tag{2.3}$$

in which,

T = tidal period, in secs.
a_0 = half tide range in ocean, in ft.
A_C = cross-sectional area of inlet, in sq.ft.
A_B = plan area of bay, in sq.ft.
l = length of inlet, in ft.
f = Darcy-Weisbach friction factor,
R = hydraulic radius of the inlet, in ft.
K_{en} = entrance loss coefficient,
K_{ex} = exit loss coefficient.

Some restricting hypotheses he assumed were that the flow section is constant during a tidal cycle, the banks of the bay are assumed to be vertical, and level variation is same at all points of the lagoon. These assumptions diminish the practical interest of the results obtained. However, this method has been considered to represent the inlet hydraulic characteristics adequately by many investigators in their studies.

In 1967, O'Brien (38) reanalysed all available data on areas of tidal inlets, and their corresponding tidal prisms and observed that for unimproved inlets, the data agreed well with :

$$A = 2.0 \times 10^{-5} \times P \tag{2.4}$$

in which,

A = minimum flow area of the inlet below MSL, in sq.ft.
P = tidal prism corresponding to the diurnal or spring range of tide, in cu.ft.

He further observed that;

1. the equilibrium minimum flow area of an improved or unimproved inlet is controlled by the tidal prism.
2. the equilibrium flow area of an inlet depends to a minor extent, if at all, on bed material size and tractive forces.

Inlet studies have been carried out by various investigators to study the relationship between the tidal prism and the inlet cross-sectional area ending up by deriving empirical formulae similar to O'Brien's equation.

1. In 1972, Johnson (26)

$$A = 3.2 \times 10^{-4} \times P^{0.88} \tag{2.5}$$

2. In 1976, Jarrett (25)

$$A = 0.56 \times 10^{-4} \times P^{0.95} \tag{2.6}$$

In 1973, Curtis Mason (10) made a comparison of O'Brien's formula for tidal flow through inlets by using the following regime equations for steady flow in alluvial channels and rivers.

1. Lacey's expression (31).

$$A = 1.40\, Q^{0.83}, \quad for\ sand\ of\ 0.2mm. \tag{2.7}$$

in which,

A = cross-sectional area of the channel in sq.ft.

Q = steady discharge in cusecs.

2. Blench's equation (4).

$$A = 1.51\ Q^{0.83},\quad for\ sand\ of\ 0.2mm. \tag{2.8}$$

3. Simons and Albertson equation (47).

$$A = 2.0\ Q^{0.86},\quad for\ R \leq 7ft. \tag{2.9}$$

$$A = 6.3\ \sqrt{Q} + 1.52\ Q^{0.86},\quad for\ R > 7ft. \tag{2.10}$$

in which,

R = hydraulic radius, in ft.

Assuming average discharge over one-half a tidal cycle and taking tidal period for the semidiurnal cycle to be 44,700 seconds, O'Brien's formula reduces to the form:

$$A = 2.3\ Q^{0.85} \tag{2.11}$$

A quantitative comparison of the equation 2.11 with the regime equations showed that O'Brien's formula was in good agreement with Simons and Albertson equation for the assumed conditions. Mason concluded that inlet channels are in a state of equilibrium similar to the regime flow in channels and rivers.

A method was presented by O'Brien and Dean (39), in 1972, for investigating the stability of coastal inlets against closure due to transport and deposition of sand in the inlet cross-section, utilizing earlier contributions made by Keulegan (30), O'Brien (36) and Escoffier (16). A measure of stability, β-stability index, has been defined to represent the capacity of an inlet to remain stable under condition of deposition.

$$\beta = \int_{A_C^*}^{A_{CE}} (V_{max} - V_T)^3\, dA_C \tag{2.12}$$

where,

A_C^* = critical cross-sectional area as defined by Escoffier,

V_{max} = maximum flow velocity corresponding to A_C^*,

V_T = "threshold velocity" of sand transport,

A_C = cross-sectional area of inlet,

A_{CE} = existing cross-sectional area of the inlet under review.

V_{max} has been defined as a function of A_C using repletion coefficient (30) and O'Brien's stability equation, (equation 2.2).

The stability equations proposed by several investigators correlating the tidal prism with the inlet area do not relate the variation of tidal prism with the change in values of range of tide, size of sand forming the channel, and roughness coefficient of the flow. A formula has been presented by Muthusamy Krishnamurthy (35), in 1977, to show the effect of the aforementioned variables on the tidal prism.

$$P = 1.25 \times By_0 \times V_{f_c} \times T \times \left(1 + \frac{2a_0}{\pi y_0}\right)\left(\ln \frac{10.93y_0}{k}\right) \qquad (2.13)$$

in which,

B = width of inlet, in ft.

y_0 = depth of flow at MSL, in ft.

V_{f_c} = friction velocity corresponding to critical shear stress, in $ft./sec.$

T = tidal period, in sec.

a_0 = amplitude of ocean tide, in ft.

k = roughness coefficient of flow.

The above formula has been derived based on the following assumptions.

1. the tide level at the ocean end of the inlet is assumed to vary sinusoidally.
2. the shape of the cross section of the inlet is approximated by a rectangular channel.
3. the velocity distribution over the depth is assumed to follow the logarithmic law.
4. for the inlet to be in equilibrium, the net sediment transport through the inlet should be zero.

Analysis of this theoretical formula revealed that;

1. the effect of the size of the bed material and roughness coefficient on tidal prism are not very significant.
2. the range of the tide on the tidal prism appears to be small, when the depth of the channel is large.
3. if the grain size of 0.5 mm is assumed, for corresponding computed values of V_{f_c} and k and using a typical tidal period of 44,700 seconds, and a range of tide of 4.0 ft., equation 2.13 reduces to :

$$A = 2.36 \times 10^{-5} \times P \tag{2.14}$$

which is comparable to O'Brien's formula, equation 2.4.

The important conclusion that can be made by reviewing all stability relationships is that the main parameter affecting the stability of an inlet channel is the flow through the inlet. The other factors, such as, the size of the bed material and roughness coefficient, and range of the tide has little effect when compared to the effect of the flow through the inlet. Thus, a thorough knowledge of the flow conditions in tidal inlets is essential for better understanding of the behaviour of inlets.

2.3 Flow in Tidal Inlets

All stability analysis methods described in Section 2.2 conclude the fact that behaviour of an inlet system is governed by the characteristics of flow through the inlet. Whether a particular inlet would remain stable or not will depend upon the ability of flow in the inlet to flush out the sediment brought to the inlet by various processes. As mentioned in Chapter-1 in tidal inlets, the tidal flow has been considered to be the main flow effect. Thus a thorough knowledge of the tidal flow through inlets is required to evaluate their behaviour.

In this section, contributions made by various investigators to describe the tidal flow in inlets in a rational manner using hydraulic principles, have been presented.

According to the available literature, Earl I. Brown (7) appears to be the first person to investigate the dynamics of tidal motion in a bay connected to the ocean by an inlet. In 1928 he presented mathematical relationships representing the tidal flow in an inlet based on the following assumptions; that flow in the inlet is equivalent to an open channel of uniform cross-section and linear bottom friction under the influence of surface slope, the surface slope will vary with relative levels of sea and basin, and the surface variations both in sea and basin are sinusoidal.

Later, in 1951, Keulegan (30) treated the same problem but included the square friction law in the inlet and predicted a non-sinusoidal oscillation in the bay elevation.

As a means of studying the behaviour of Burrand Inlet in British Columbia, W. Douglas Baines (2) presented a mathematical model in 1957 which provided a good approximation to the flow.

Considering a simple Bay-Inlet layout as shown in Figure 2.2 and applying

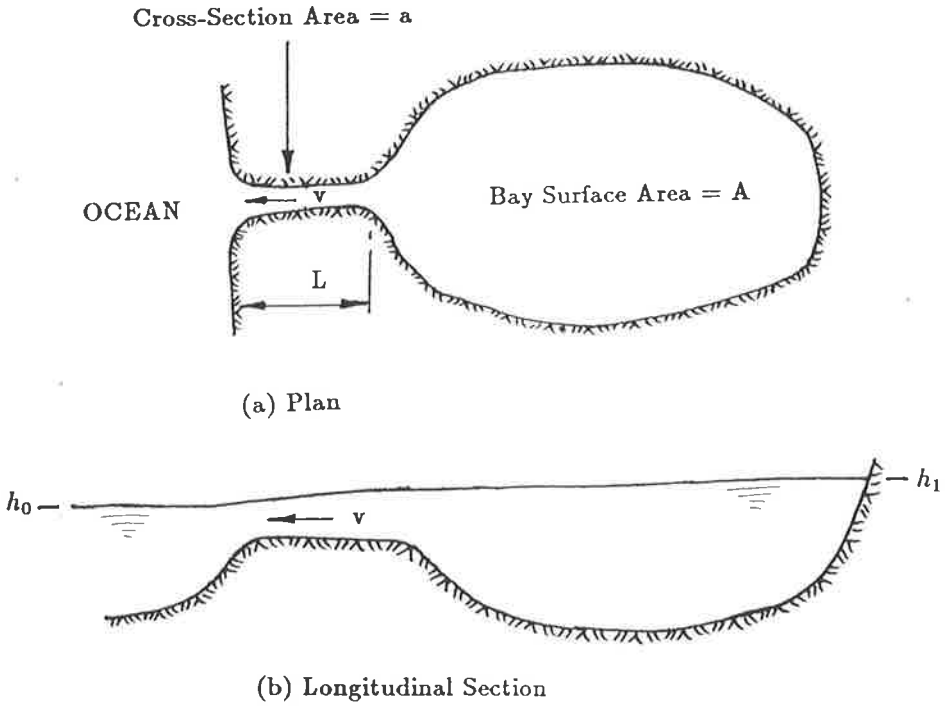

Figure 2.2: Sketch of a bay with a constricted entrance channel

the continuity equation and dynamic equation presented by Einstein (15) a simplified solution has been obtained:

$$\frac{dv}{dt} = \frac{gH}{L}\cos\frac{2\pi t}{T} - f\frac{v|v|}{8R} - \frac{ga}{La}\int_0^t v\,dt \qquad (2.15)$$

where,

v = mean velocity in the channel,

H = half range of tide,

L = length of channel,

T = period of tide,

f = friction factor,

R = hydraulic radius of the channel at mean tide,

a = cross-sectional area of the channel,

A = surface area of the bay.

Water level variation in the ocean has been assumed to be a cosine curve.

Equation 2.15 has been solved by the Laplace transformation. Discharge at the inlet has been evaluated using this equation and results have shown good agreement showing the validity of the model.

In 1967, Jacobus van de Kreeke (24) presented a mathematical model to describe the water-level fluctuations and flow in inlets as a function of ocean tide and fresh water inflow. Assuming one-dimensional flow and applying the equations of continuity and motion to the Inlet-Bay system he derived:

$$\frac{dh_b}{dt} = \frac{A_c}{A_b}\sqrt{\frac{2g}{R+1}(h_s - h_b)} + \frac{Q_R(t)}{A_b} \tag{2.16}$$

where,

h_b = bay water level,

h_s = sea water level,

A_c = cross-sectional area of the inlet channel,

A_b = horizontal bay area,

$Q_R(t)$ = fresh-water inflow,

R = $\int_0^L \frac{2g}{c^2 h} dx$ = a dimensionless resistance coefficient,

c = Chezy's coefficient,

h = water depth in inlet channel.

by whom?

The numerical method has been applied to Macquarie Harbour Inlet, Tasmania. For the case of no fresh-water inflow, the results have been compared with those obtained with Keulegan's method (30) and found to be in close agreement.

Shemdin and Forney (45) proposed a method to investigate tidal motion in single or multiple basin connected to the ocean by an inlet. Non-sinusoidal tidal motion in the ocean and square friction law in the inlet are considered. Applying the equations of motion and continuity he presented the following relationship.

$$h_s = h_b + \left(\frac{A_b}{A}\right)\frac{L}{g}\frac{d^2h_b}{dt^2} + \left(1 + \frac{r}{h}L\right)\frac{1}{g}\left(\frac{A_b}{A}\right)^2\frac{dh_b}{dt}\left|\frac{dh_b}{dt}\right| \tag{2.17}$$

in which,

h_s = sea water level,
h_b = bay water level,
A_b = horizontal bay area,
A = cross-sectional area of the inlet channel,
L = length of channel,
r = friction coefficient,
h = water depth in inlet channel,
t = time.

The method has been applied to Boca Raton inlet, Florida. The calculated tidal elevation and velocity in the inlet are found to be in reasonable agreement with measured values.

A study has been undertaken by Dennis, Lanan and Dalrymple (12) to document the past and present characteristics and trends of Delaware's two major tidal inlets. In order to gain a better understanding of the overall hydraulics, a one-dimensional numerical model has been presented.

The vertically integrated differential equation of motion is written in a semi-linearized form for flow in the x-direction as:

$$\frac{\partial q}{\partial t} = -gD\frac{\partial \eta}{\partial x} - \frac{\tau}{\rho} \tag{2.18}$$

in which,

q = discharge per unit width in the x-direction,

t = time,

D = total depth $= h + \eta$,

h = depth at MSL,

η = tide displacement above MSL,

x = horizontal distance coordinate in flow direction,

ρ = mass density of sea water,

τ = frictional stress on the bottom of water column,

$= \rho f \frac{q|q|}{8D^2}$

f = Darcy-Weisbach friction factor.

The one dimensional continuity equation is:

$$\frac{\partial \eta}{\partial t} + \frac{\partial q}{\partial x} = 0 \tag{2.19}$$

Using a Keulegan (30) type inlet equation to relate the flow through the inlet to inlet characteristics the differential equations have been solved numerically.

Comparison of results obtained from the model with tide and current measurements recorded at the inlets has shown a good correlation but has underpredicted the peak discharge and overpredicted the peak tidal amplitude.

The sediment stability of these two inlets have been further investigated by adopting the concepts developed by Escoffier (16), O'Brien (38) and Jarrett (25). Overall, the results of the stability and prism-area concepts have revealed that neither of the inlets is presently in equilibrium, which agreed well with the observed depositional characteristics of the inlet.

2.4 Sedimentation at Inlets

Sediment transport in the form of grains rolling along the bed is referred to frequently as bed load, and material carried in suspension by the turbulence generated in the current is regarded as suspended load. The simplest form of sediment transport is that caused by a current alone, such as in river flow or by tidal currents, where the influence of waves is insignificant. The sediment transport that takes place in an inlet channel is partly bed load and partly suspended load.

In the ocean section and the intermediate section of an inlet the bulk of the transport may take place in suspension. For fine-grained materials the suspended load in strong currents is many times larger than the bed load, and thus the major cause of problems.

Waves play a decisive role in coastal sediment transport processes. While river sediment transport is largest at the greatest depth of the river cross-section, and theoretically zero at the shoreline, the opposite is the case for wave-generated littoral drift. Here the sediment transport capability increases as the water gets shallow, and in the breaker zone where there is massive wave stirring taking place, exceedingly high concentrations of suspended sediment occur.

The breaking of waves generates great turbulence at the plunge point which brings large quantities of sediment into suspension. The orbital water velocity caused by movement of the waves would move this suspended sediment in back-and-forth motion . Substantial drift of sediment may occur when a current, such as a tidal current, is superimposed on each wave motion. In these cases, the transport capacity is much higher than that of the current alone, since the orbital wave motion at the bed generates a high concentration of suspended sediment near the bed, which in turn is transported by the current.

Where the bottom consists of fine sand or coarse silt the concentration of suspended sediment is determined by the waves and the currents. Concentrations within a few centimeters from the bottom are governed by wave heights and periods, while the concentration distribution from this thin bottom layer to the surface is governed by the current generated turbulence. The bottom-layer concentration, and therefore the transport capacity, decreases as the depth increases.

As mentioned in Chapter-1, an accurate sedimentation prediction requires a detailed field investigation to determine local relevant parameters. The accuracy of the computed sedimentation rate depends upon the accuracy with which the actual transport processes are represented in the method of prediction.

Due to the extreme difficulty of making observations and measurements in this region, and due to the high degree of complexity of the phenomena involved, no proper theoretical method for predicting sedimentation at entrance to an inlet was available until recently. Various empirical formulae and simple methods with strong schematization of the relevant processes involved have been presented. Nevertheless, they have proven to be useful as practical tools. Some such methods have been presented in this section and the current methods of analysis of sedimentation rates at inlets have been described in Chapter-3.

It has been experienced in the field of maintenance dredging that sedimentation occurs whenever dredging is carried out to deepen an area previously in natural equilibrium. The sedimentation rate increases as a function of the thickness of the dredged layer and bottom tends to shoal back to its equilibrium elevation. Based on this experience several methods of an empirical nature have been presented for predicting shoaling rates.

1. The Balanin formula presented by Djunkovski and Smirnov (13), in 1957, assuming the shoaling rate is proportional to the thickness

of dredging, describes the time variation of shoaling in a dredged channel.

$$h_t = \frac{1-(1-p)^t}{(1-p)^t}(H - H_0) \tag{2.20}$$

where,

h_t = thickness of the sediment transport after t-years, in ft.
H = channel depth, in ft.
H_0 = initial natural depth, in ft.
p = a coefficient characteristic of sedimentation at the place in question.

2. In an empirical method presented in 1982 for predicting shoaling rate in channels dredged at tidal inlets, Galvin (19) assumed the initial rate of shoaling is a function of the initial dredged depth. Assuming the sediment bypassing (across) the inlet is proportional to the rate of energy expended by the flow, he derived the formula:

$$Shoaling\ Rate = K\left[1 - \left(\frac{d_1}{d}\right)^m\right] \tag{2.21}$$

where,

d_1 = natural depth before dredging,
d = depth at any time after dredging,
$K = \frac{RQ}{CW}$
= characteristic shoaling rate,
Q = longshore transport rate,
R = fraction of Q carried into the channel,
C = length of dredged channel,
W = width of dredged channel,
m = 5/2 ; for constant discharge before and after dredging,

m = 3/2 ; for constant velocity before and after dredging.

3. Assuming that the shoaling rate is proportional to the relative bottom elevation, Vincente and Uva (50) presented a method in 1984 for predicting shoaling in dredged channels and basins:

$$\frac{dC}{dt} = K\,(C_e - C) \tag{2.22}$$

where,

C = different bottom elevations at instant t,

C_e = a constant that represents the bottom natural equilibrium elevation in the zone studied,

K = sedimentation coefficient.

Integration of equation 2.22 yields;

$$C = C_0 + (C_e - C_0)\left(1 - e^{-Kt}\right) \tag{2.23}$$

where,

C_0 = initial generic elevation.

4. One of the empirical procedures used in USA and presented by Trawle (49) considers the shoaling rate to be proportional to the area of the dredged channel section, measured below the natural equilibrium elevation.

5. In 1984, Forman and Vallianos (17) presented an empirical method to predict shoaling rate in an inlet based on the assumptions that the longshore transport of sediment is a function of wave height squared and the sediment transport capacity is proportional to the depth:

Daily shoal volume in the ocean bar channel

$$= C\, Q_g \frac{H_i^2}{\sum_{i=1}^{360} H_i^2} \left[1 - \left(\frac{d_1}{d_2}\right)^{5/2}\right]$$

in which,

Q_g = total volume of longshore sediment transport to the inlet each year,

H_i = average wave height for the i^{th} day of the year,

d_1 = predredging depth,

d_2 = depth of the dredged bar channel,

C = potential shoaling rate (portion of the gross longshore transport deposited in the channel).

William and Robert (52), in 1978, carried out an investigation to study selected basic flow and sediment transport characteristics of tidal inlets. A simple numerical hydraulic-sediment transport model applied to an idealized inlet-bay system, designed to have typical inlet characteristics, was used in their study. The numerical model used was formulated as follows.

1. Continuity equation.

$$V A_c = A_b \frac{dh_b}{dt} \tag{2.24}$$

in which,

V = inlet velocity,

A_c = inlet cross-sectional area,

A_b = bay surface area,

h_b = bay water level.

2. One-dimensional equation for motion along the inlet channel axis.

$$-g\frac{d\eta}{dx} = f\frac{V|V|}{8R} + V\frac{dV}{dx} + \frac{dV}{dt} \qquad (2.25)$$

in which,

η = water surface elevation,
R = channel hydraulic radius,
x = the distance along the channel axis,
f = channel friction factor.

3. The rate of sediment transport, Q_s, across the minimum cross-sectional area (B) portion of the inlet was taken as:

$$Q_s = k\sum_{i=1}^{N} B\left(|V| - V_c\right)^3 \qquad (2.26)$$

in which,

V_c = "threshold velocity" of sediment transport,
N = number of grid channels,
k = unknown constant.

Numerical integration of the equations has revealed the influence of tide type, storm surges, bay surface area, channel resistance, and the addition of a second inlet on sediment transport rate.

With the interpretation of flow in inlets in terms of their hydraulic behaviour the literature shows development of numerous methods for quantitative prediction of sedimentation in inlets based on various hypothesis, such as, longshore transport is proportional to the longshore energy flux, by-passing of sedimentation across inlets is proportional to the rate of energy dissipated in the flow etc. However, because of the limitations of computation capabilities most of these methods were limited to numerical solution of simplified differential equations.

These methods have been applied to investigate sediment movement at various tidal inlets and have found to perform reasonably well within the limits of the assumed conditions. Presentation of the fine details of all such methods would be beyond the scope of this thesis.

Chapter 3

Current Methods of Analysis of Harbour Inlets

3.1 Introduction

It has been established that in the littoral zone, the major part of the sediment movement takes place in suspension caused by the turbulent flow. In turbulent flow movement of the particles in suspension is described by the diffusion-convection equation which was apparently first presented by Schmidt (44), in 1925, in studies of dust in the atmosphere. Since in the current methods of analysis, sedimentation rates are usually predicted using the theory of sediment suspension in turbulence, the general form of the diffusion-convection equation has been described in detail in Section 3.3. Much research work has been carried out by using this equation to analyse suspended sediment movement in different environments; some key contributions have been reviewed in Section 3.4.

3.2 Early Theoretical Approaches.

As presented in Section 2.2, early methods of analysis of inlets passing through the littoral zone were based on empirical formulae where flow in the inlet (tidal prism) is related to the cross-sectional area as a measure of assessing the flushing ability of an inlet system. Even though the stability of an inlet could be assessed within the limits of assumptions made, quantitative prediction of shoaling rates cannot be performed by using such methods.

As a result of the advancements made in the fields of inlet hydraulics, sedimentary aspects and mathematical modelling, the early empirical methods have been gradually replaced by rational hydraulic modelling of the inlet hydraulics, wave effects and the combined sedimentary response. Thus, various methods have been developed for quantitative prediction of shoaling rates at inlets. However, as described in Section 2.4, because of the limitations of computation resources, most of these methods were limited to numerical solution of only the simplified differential equations.

Even though movement of sediment in suspension had been described by the diffusion equation in early 1930s (see Section 3.4) its practical applications, except for the simplified versions, were limited because of the complexity of the diffusion equation and the limitations of computation capabilities to solve realistic elaborations of these equations.

3.3 Diffusion-Convection Equation for Suspended Sediment Concentrations

Turbulence is the most important process involved in the suspension of sediment. The turbulent motion results from eddies that are swirling in an

irregular manner as they are carried along by the flow. The eddies are being formed continuously by the shearing action of the fluid while eddies already in existence are shrinking in scale and are being ultimately dissipated into heat.

The diffusion mechanism involves two essential features. One is the simple transport (advection) which results from the turbulent velocity fluctuations, and the other is a mixing (diffusion) of the transported fluid as it is advected.

To derive the equation for unsteady, non-uniform distribution of sediment in a two-dimensional steady, uniform turbulent flow consider the diffusion of suspended sediment particles of uniform size, shape and density.

With reference to Figure 3.1, in a small time, Δt, the flow of sediment into an element of volume minus the flow out is equal to the change in concentration in the volume. The width of the element normal to the xy-plane is taken to be unity.

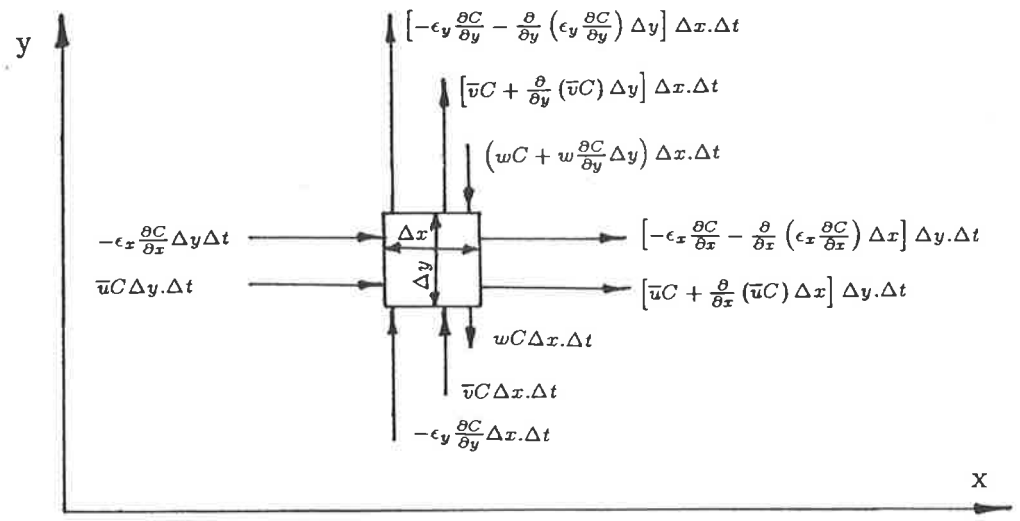

Figure 3.1: Transport of sediment into and out of an element

There is no contribution of sediment through the faces parallel to the xy- plane because the mean velocity and concentration gradient normal to the faces are

both zero. The differential equation for the concentration can be written as follows:

$$\left[-\frac{\partial}{\partial x}(uc)+\frac{\partial}{\partial x}\left(\epsilon_x\frac{\partial c}{\partial x}\right)-\frac{\partial}{\partial y}(vc)+\frac{\partial}{\partial y}\left(\epsilon_y\frac{\partial c}{\partial y}\right)+w\frac{\partial c}{\partial y}\right]\Delta y\Delta x\Delta t = \frac{\partial c}{\partial t}\Delta x\Delta y\Delta t \qquad (3.1)$$

in which,

u, v	=	mean components of velocity in x & y directions,
c	=	mean concentration of sediment,
ϵ_x, ϵ_y	=	diffusion coefficients of sediment in x & y directions,
w	=	sediment fall velocity.

The continuity equation for the system can be written as:

$$\frac{\partial u}{\partial x}+\frac{\partial v}{\partial y}=0 \qquad (3.2)$$

Equations 3.1 and 3.2 can be combined to yield:

$$-u\frac{\partial c}{\partial x}-v\frac{\partial c}{\partial y}+\epsilon_x\frac{\partial^2 c}{\partial x^2}+\frac{\partial \epsilon_x}{\partial x}\frac{\partial c}{\partial x}+\epsilon_y\frac{\partial^2 c}{\partial y^2}+\frac{\partial \epsilon_y}{\partial y}\frac{\partial c}{\partial y}+w\frac{\partial c}{\partial y}=\frac{\partial c}{\partial t} \qquad (3.3)$$

Equation 3.3 is the differential equation for unsteady, non-uniform distribution of sediment in a two-dimensional steady, uniform turbulent flow. It can be solved numerically when the flow velocities, the sediment mixing coefficients and the sediment fall velocities are known.

If the sediment distribution is steady and uniform, and the mean flow is horizontal; then $\partial c/\partial t = 0$, $v = 0$, and all derivatives with respect to x are zero. Also, $\epsilon_y = \epsilon_s =$ diffusion coefficient of sediment.

Substituting these in equation 3.3 and integrating with respect to y yields:

$$c\,w \;+\; \epsilon_s \frac{\partial c}{\partial y} \;=\; 0 \tag{3.4}$$

The diffusion coefficient ϵ_s is generally a function of y that must be known before equation 3.4 can be solved for c.

Equation 3.4 was developed by Schmidt(44), in 1925, in connection with studies of dust in the atmosphere and by O'Brien(37), in 1933, in studies of suspended sediment in streams.

3.4 Equations for Distribution of Suspended Sediment in Turbulent Flow.

Because of the complicated form of the differential equation for unsteady non-uniform distribution of sediment, equation 3.3, with several independent variables involved and also for the reason of limited computation capabilities available at the time, it seems that no attempts have been made to solve it until recently. However, Kalinske (27) in 1940 presented a method to obtain a mathematical solution to equation 3.3 by making the following simplifying assumptions: the concentration at any point does not change with time; flow is horizontal,i.e. $v = 0$; ϵ_y does not vary with y and $\frac{\partial^2 c}{\partial x^2}$ is negligible in comparison to $\frac{\partial^2 c}{\partial y^2}$. With these assumptions equation 3.3 reduces to:

$$u \frac{\partial c}{\partial x} \;=\; \epsilon_y \frac{\partial^2 c}{\partial y^2} \;+\; w \frac{\partial c}{\partial y} \tag{3.5}$$

Since the method he presented to obtain a mathematical solution to this simplified equation is complex, he presented an alternative approximate method

as well to solve it numerically. However, the restricting assumptions made diminish the practical interest of the results obtained.

Dobbins (14), in 1944, presented a method to obtain a analytical solution to the simplified diffusion equation (equation 3.5) assuming a parabolic velocity distribution. The one dimensional case of the theory of turbulent sedimentation was verified by experimental work. However, the simplifying assumptions involved again introduce large errors when applied to the case of a natural stream.

Literature shows that several investigations have been carried out to study the simplified form of the diffusion equation (equation 3.4). Some key contributions are outlined below.

If the turbulence in a two-dimensional uniform flow is uniform from top to bottom the diffusion coefficient ϵ_s would be constant and equation 3.4 can be integrated to yield,

$$c = c_a \exp -\frac{w_s}{\epsilon_s}(y - a) \tag{3.6}$$

in which,

c_a = concentration at level $y = a$.

In practice the turbulence and hence the diffusion coefficient in streams is not constant over the depth. However, Hurst (23) and Rouse (42) achieved a uniform distribution of turbulence by mechanically agitating water in a small cylindrical tank. Measurements of the distribution of sediment concentration over the depth in these tanks showed agreement with equation 3.6, thus establishing the validity of the basic theory.

Assuming the sediment diffusion coefficient is linearly proportional to the kinetic eddy viscosity, or the diffusion coefficient of momentum, and the flow ve-

locity is represented by Prandtl-von Karman velocity law, Rouse (42) in 1937 presented a solution for equation 3.4 which is well-known as "Rouse Equation" for the distribution of suspended sediment in turbulent flow.

$$\frac{c}{c_a} = \left[\frac{(d-y)}{y}\frac{a}{(d-a)}\right]^z \tag{3.7}$$

in which, $z = \frac{w_s}{\beta k U_*}$

w_s = sediment fall velocity

d = the depth of flow,

β = a numerical constant,

k = von Karman's universal constant,

U_* = the bed shear velocity.

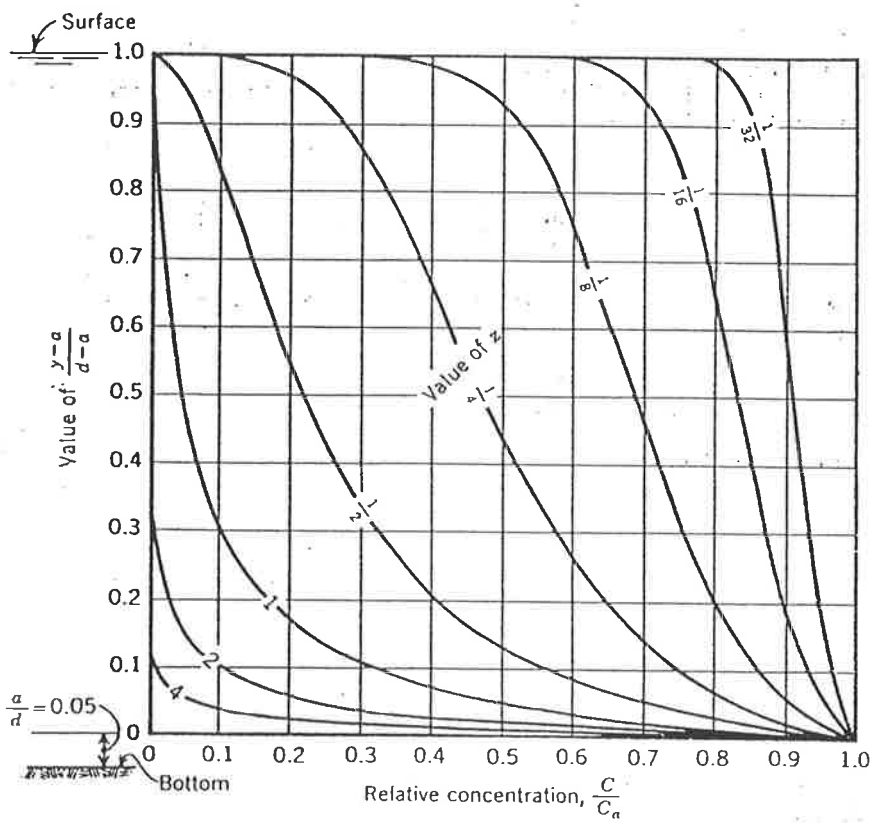

Figure 3.2: Graph of suspended load distribution equation for several values of z.

Figure 3.2 shows a graph of the equation 3.7 for several values of the exponent z. Equation 3.7 is seen to give unrealistic concentrations of zero at the surface, $y = d$, and infinite at the bed, $y = 0$. Despite these deficiencies, the Rouse equation has come into general use and has not been replaced by later ones.

Starting from the two-dimensional longitudinal equation of motion, Brian O'Connor (6) presented a method to represent the vertical distribution of sediment in a well mixed tidal estuary. The two-dimensional equation of motion for flow in a tidal estuary is:

$$\frac{1}{g}\frac{\partial U}{\partial t} + \frac{\partial}{\partial x}\left(\frac{U^2}{2g}\right) + \frac{H}{\rho}(1-\eta)\frac{\partial \rho}{\partial x} - \frac{1}{\rho g H}\frac{\partial \tau}{\partial \eta} = I \qquad (3.8)$$

in which,

U = horizontal flow velocity in the x-direction,
t = time,
H = water depth,
ρ = water density,
η = y/H,
y = elevation above the bed,
τ = horizontal shear stress,
I = water surface slope.

Assuming simple linear distribution for $\partial u/\partial t$ and $\partial u/\partial x$, and relating the shear stress to the velocity gradient by Prandtl's mixing length concept, expressions for the variation of the horizontal velocity, U, was obtained from the equation 3.8. Then he related the diffusion coefficient, ϵ_s, to the momentum transfer coefficient or eddy viscosity, ϵ_m, by $\epsilon_s = \beta\epsilon_m$ and solved the equation 3.4 analytically to yield a complex expression for distribution of suspended

sediment. He showed that this expression reduces to Rouse's equation, (equation 3.7), for the case of uni-directional flow.

J.N.Hunt in 1954 (22) developed the following differential equation for the distribution of suspended sediment in two-dimensional steady uniform flow,

$$\epsilon_s \frac{dc_v}{dz} + c_v \frac{dc_v}{dz}(\epsilon_w - \epsilon_s) + (1 - c_v)\, c_v w_s = 0 \qquad (3.9)$$

in which,

ϵ_w = diffusion coefficient for water,

c_v = sediment concentration by volume.

When $\epsilon_w = \epsilon_c$, equation 3.9 becomes,

$$\epsilon_s \frac{dc_v}{dz} + (1 - c_v)\, c_v w_s = 0 \qquad (3.10)$$

When c_v is negligible compared with unity, equation 3.10 becomes the same as equation 3.4.

To solve the equation 3.10, the diffusion coefficient ϵ_s used by Hunt was derived as was done for equation 3.7, except that U_* was obtained from,

$$\frac{U - U_{max}}{U_*} = \frac{1}{k}\left[\sqrt{1 - \frac{z}{d}} + B \ln \frac{B - \sqrt{1 - z/d}}{B}\right]$$

in which B is a constant to be determined from experimental data.

Introducing the expression for ϵ_s and integrating gives Hunt's equation for the distribution of suspended sediment,

$$\left(\frac{c_v}{1-c_v}\right)\left(\frac{1-c_a}{c_a}\right) = \left[\sqrt{\frac{1-z/d}{1-a/d}}\left(\frac{B_s-\sqrt{1-a/d}}{B_s-\sqrt{1-z/d}}\right)\right]^q \qquad (3.11)$$

in which,

$$q = \frac{w_s}{k_s\ B_s\ U_*}$$

and

B_s and k_s are constants similar to B and k, which are to be determined from measurements of sediment distribution. Hunt showed that equation 3.11 agreed more closely with measured concentrations than did equation 3.7. However, equation 3.11 has not come into use, probably because of its complicated form and the added difficulty of having two instead of one constant.

A model describing the distribution of sediment in unsteady, turbulent flow was presented by O'Connor (5) which was based upon a finite difference solution to the general diffusion equation. However, the model seems to have not come into use as the value of the model had not been tested using laboratory and field data.

Bechteler and Schrimpf (3) presented a relatively simple two-dimensional model for steady distribution of sediment, $dc/dt = 0$, neglecting vertical convection, $v = 0$, and horizontal diffusion, $\epsilon_x = 0$. For these assumptions, the general diffusion equation, equation 3.3, reduces to the form,

$$u\frac{\partial c}{\partial x} = w\frac{\partial c}{\partial y} + \epsilon_s\frac{\partial^2 c}{\partial y^2} + \frac{\partial \epsilon_s}{\partial y}\frac{\partial c}{\partial y} \qquad (3.12)$$

The numerical solution of the differential equation was presented by the finite

difference method. The numerical model was applied to four different combinations of velocity distributions; including parabolic and logarithmic distributions; and turbulent diffusion coefficients. Even though the predicted sediment distributions did not agree exactly with the test values, for practical sedimentation engineering, the results predicted were considered to be sufficiently accurate.

Smith and O'Connor (48) presented a two-dimensional mathematical model to predict longitudinal and vertical distributions of velocity and suspended sediment in estuarial type flows. Basic hydrodynamic equations of turbulent fluid motion are laterally integrated and then simplified by introducing the hydrostatic pressure approximations for long wave motion and neglecting correction factors for lateral velocity variations. The resulting equations, written in general cartesian co-ordinates are:

1. Momentum Equation

$$\frac{\partial u}{\partial t} + u\frac{\partial u}{\partial x} + w\frac{\partial w}{\partial z} = -\frac{1}{\rho}\frac{\partial p}{\partial x} - \frac{1}{b}\left[\frac{\partial}{\partial x}\left(b\overline{u'u'}\right) + \frac{\partial}{\partial z}\left(b\overline{u'w'}\right)\right] \quad (3.13)$$

$$\frac{\partial p}{\partial x} = \rho g \quad (3.14)$$

in which,

u, w = width averaged turbulent-mean velocity components in the x and z directions,

u', w' = turbulent fluctuation velocity components of u and w,

b = width of the channel; is a function of x and z,

p = width-averaged turbulent mean pressure.

2. Continuity Equation

$$\frac{\partial}{\partial x}(bu) + \frac{\partial}{\partial z}(bw) = 0 \tag{3.15}$$

Equations 3.13 to 3.15 are then closed by using equations:

$$\frac{\partial K}{\partial t} + u\frac{\partial K}{\partial x} + w\frac{\partial K}{\partial z} = \frac{\partial}{\partial z}\left(\frac{\mu_e}{\rho\sigma_K}\frac{\partial K}{\partial z}\right) + \frac{\mu_e}{\rho}\left(\frac{\partial u}{\partial z}\right)^2 - \epsilon + \frac{ga\mu_e}{\rho s_c}\frac{\partial c}{\partial z} \tag{3.16}$$

$$-\overline{u'w'} = \frac{\mu_e}{\rho}\frac{\partial w}{\partial z} \tag{3.17}$$

$$\mu_e = C_m\rho\frac{K^2}{\epsilon}; K = \frac{1}{2}\left(\overline{u'u'} + \overline{w'w'}\right); \epsilon = \frac{C_d K^{3/2}}{L_0} \tag{3.18}$$

$$\rho = \rho_0(1 + aC) \tag{3.19}$$

where,

a, C_m, C_d	=	numerical constants,
ρ_0	=	density of sediment-free water,
C	=	turbulent width-averaged concentration of sediment in suspension,
ϵ	=	turbulence energy dissipation rate,
σ_K	=	effective turbulent Prandtl number for turbulence energy,
S_c	=	effective turbulent Schmidt number,
L_0	=	dissipation length scale of the turbulence.

Equations 3.13 to 3.19 represent a "one equation" turbulence model for use in tidal estuaries.

Kerssens, Prins and Rijn (29) presented a two-dimensional vertical model assuming a steady and nearly uniform flow, a constant particle fall velocity, and

neglecting the longitudinal diffusion, and vertical convection. These assumptions simplify the general diffusion-convection equation to the form of equation 3.12. To solve the differential equation, a logarithmic distribution was applied for the local velocities and the vertical sediment mixing coefficients were represented by a parabolic-constant distribution. An implicit finite-difference method was used to solve the diffusion-convection equation.

In order to check the influence of the sediment diffusion coefficient on the sediment concentrations some test computations have been executed varying both the distribution and the magnitude of the diffusion coefficient and it was concluded that in the model the said influence is not large.

To verify the proposed model the siltation in a trench in a tidal estuary has been predicted and compared with the measured siltation rates. The method presented seems suitable for the computation of local sedimentation and erosion in sediment traps and dredged trenches, when the sediment transport is mainly in the form of suspended load.

3.5 Current Mathematical Models

In the field of suspended sediment transport extensive research work has been carried out by the Delft Hydraulic Laboratory in recent years to develop mathematical models to study the morphological processes. A two-dimensional vertical (SURTRENCH-2D) and a three-dimensional (SURTRENCH-3D) mathematical model have been developed, of which the two-dimensional model has been verified extensively using flume and field data and is widely accepted as the current method for suspended sediment predictions. The SURTRENCH-2D Model as developed by the Delft Hydraulic Laboratory (11) is presented in Section 3.6.

3.6 SURTRENCH-2D Model

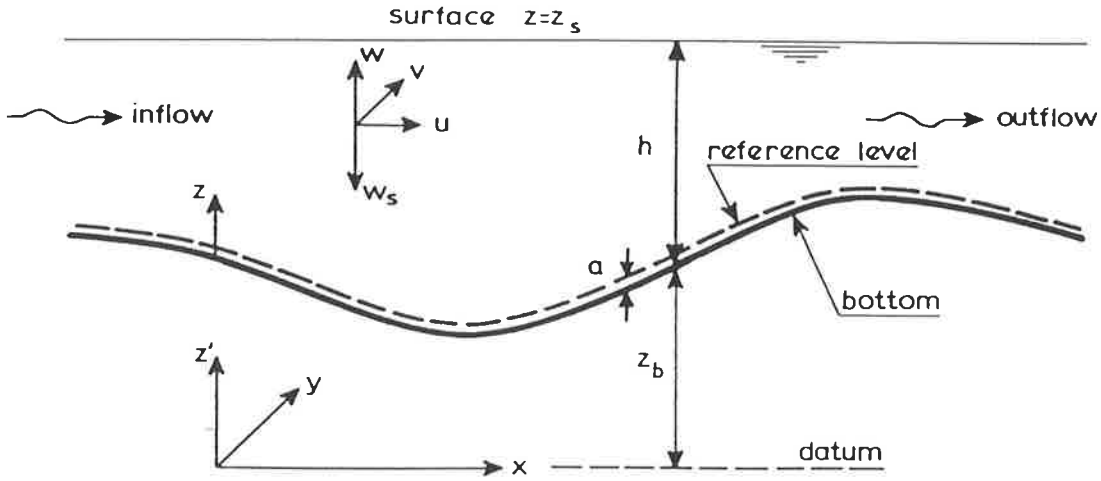

Figure 3.3: Definition Sketch

With reference to Figure 3.3, the Diffusion-Convection equation, equation 3.3, for time averaged variables in non-uniform flows can be written as follows (11) :

$$\frac{\partial c}{\partial t} + \frac{\partial}{\partial x}(uc) - \frac{\partial}{\partial x}\left(\epsilon_{s,x}\frac{\partial c}{\partial x}\right) + \frac{\partial}{\partial z}(w - w_s)\,c - \frac{\partial}{\partial z}\left(\epsilon_{s,z}\frac{\partial c}{\partial z}\right) = 0 \qquad (3.20)$$

in which,

c = local mean sediment concentration,

u, w = local mean flow velocities in longitudinal (x) and vertical (z) directions respectively,

w_s = particle fall velocity,

ϵ_s = sediment mixing coefficient,

t = time.

Assuming steady-state conditions and neglecting the longitudinal diffusive transport, which is shown to be in general an order of magnitude smaller

than the other terms (29), equation 3.20 reduces to:

$$\frac{\partial}{\partial x}(uc) + \frac{\partial}{\partial z}(w - w_c)\, c - \frac{\partial}{\partial z}\left(\epsilon_s \frac{\partial c}{\partial z}\right) = 0 \qquad (3.21)$$

Assuming the variables to be constant in lateral (y) direction, the sediment concentrations can be represented by integrating equation 3.21 over the (lateral) width of the flow, yielding:

$$\frac{\partial}{\partial x}(buc) + \frac{\partial}{\partial z} b\,(w - w_s)\, c - \frac{\partial}{\partial z}\left(b\epsilon_s \frac{\partial c}{\partial z}\right) = 0 \qquad (3.22)$$

in which,

b = width of the flow; is a function of x.

Equation 3.22, which is the basic equation of the SURTRENCH-2D model, can be solved numerically when the flow velocities (u, w), the sediment mixing coefficient (ϵ_s), the particle fall velocity (w_s) and the flow width (b) are known and appropriate boundary conditions are specified.

3.6.1 Flow Velocity Profiles.

Various models can be applied to describe the velocity field, depending on the complexity of the flow. In case of complicated flow conditions, the most widely used mathematical model is the K-EPSILON, K-E, model which is based on the equations of continuity and motion and two additional transport equations for the turbulence kinetic energy (K) and its dissipation rate (ϵ) to describe the turbulent fluid shear stress (41). A disadvantage of the application of the K-E model is the relatively large computation time needed to solve the complete set of equations. Consequently, the K-E model is not yet an attractive model for long term morphological computations. To reduce the computation time

and costs significantly, a simple model has been developed which is based on flexible profiles as suggested by Coles (9).

3.6.1.1 K-EPSILON Model.

Considering the flow in a channel of constant width (b) and a plane water surface, the equations of continuity and motion for steady state conditions in the vertical plane can be written as:

- Continuity:

$$\frac{\partial u}{\partial x} + \frac{\partial w}{\partial z} = 0 \tag{3.23}$$

- Motion:

$$\frac{\partial}{\partial x}\left(u^2\right) + \frac{\partial}{\partial z}\left(uw\right) + \frac{1}{\rho}\frac{\partial}{\partial x}\left(p - p_{R,x}\right) - \frac{1}{\rho}\left(\tau_{R,xz}\right) = 0 \tag{3.24}$$

$$\frac{\partial}{\partial z}\left(w^2\right) + \frac{\partial}{\partial x}\left(uw\right) + \frac{1}{\rho}\frac{\partial}{\partial z}\left(p - p_{R,z}\right) - \frac{1}{\rho}\left(\tau_{R,zx}\right) = 0 \tag{3.25}$$

in which,

u, w = time-averaged fluid velocity in x,z directions,
p = time-averaged static fluid pressure,
p_R = (Reynold's) turbulent fluid pressure,
τ_R = (Reynold's) turbulent fluid shear stress.

Basically, the Reynold's stresses represent a viscous part and a fluctuating (turbulence) part. Neglecting the viscous part, the fluctuating part can be approximated to (41):

$$p_{t,s} = 2\,\rho\,\epsilon_f\,\frac{\partial u}{\partial x} - \frac{2}{3}\rho K$$

$$p_{t,z} = 2\,\rho\,\epsilon_f\,\frac{\partial w}{\partial z} - \frac{2}{3}\rho K$$

$$\tau_{t,xz} = \rho\,\epsilon_f\left(\frac{\partial u}{\partial z} + \frac{\partial w}{\partial x}\right)$$

in which,

p_t = turbulence fluid pressure,

τ_t = turbulence fluid shear stress,

ϵ_f = fluid mixing coefficient (or eddy viscosity),

K = turbulence kinetic energy.

The K and its dissipation rate (ϵ) are defined as:

$$K = \frac{1}{2}\left[\overline{(u')^2} + \overline{(v')^2} + \overline{(w')^2}\right]$$

$$\epsilon = -\nu\left[\overline{\left(\frac{\partial u'}{\partial x}\right)^2} + \overline{\left(\frac{\partial u'}{\partial z}\right)^2} + \overline{\left(\frac{\partial w'}{\partial x}\right)^2} + \overline{\left(\frac{\partial w'}{\partial z}\right)^2}\right]$$

where,

u', v', w' = fluctuating components of the fluid velocity in x, y, z directions,

ν = kinematic viscosity.

over bars indicate time-averaged values.

The variables K and ϵ are related to the eddy viscosity (ϵ_f) by:

$$\epsilon_f = c_\mu \frac{K^2}{\epsilon} \tag{3.26}$$

in which,

c_μ = turbulence constant.

The transport equations for the turbulence energy (K) and the dissipation rate (ϵ) read:

$$\frac{\partial}{\partial x}(uK) + \frac{\partial}{\partial z}(wK) - \frac{p_{t,x}}{\rho}\frac{\partial u}{\partial x} - \frac{\tau_{t,xz}}{\rho}\frac{\partial u}{\partial z} - \frac{\partial}{\partial x}\left(\frac{\epsilon_f}{\sigma_K}\frac{\partial K}{\partial x}\right) - \frac{\partial}{\partial z}\left(\frac{\epsilon_f}{\sigma_K}\frac{\partial K}{\partial z}\right) + \epsilon = 0 \tag{3.27}$$

$$\frac{\partial}{\partial x}(u\epsilon) + \frac{\partial}{\partial z}(w\epsilon) - c_{1\epsilon}\frac{\epsilon}{K}\left(\frac{p_{t,x}}{\rho}\frac{\partial u}{\partial x} + \frac{\tau_{t,xz}}{\rho}\frac{\partial u}{\partial z}\right) - \frac{\partial}{\partial x}\left(\frac{\epsilon_f}{\sigma_\epsilon}\frac{\partial \epsilon}{\partial x}\right) - \frac{\partial}{\partial z}\left(\frac{\epsilon_f}{\sigma_\epsilon}\frac{\partial \epsilon}{\partial z}\right) + c_{2\epsilon}\frac{\epsilon^2}{K} = 0 \qquad (3.28)$$

in which $c_{1\epsilon}, c_{2\epsilon}, \sigma_K$ and σ_ϵ are universal constants.

Equations 3.23, 3.24, 3.25, 3.26, 3.27 and 3.28 represents a set of six equations with six unknowns (u, w, p, ϵ_f, K and ϵ) which can be solved numerically applying an appropriate set of boundary conditions.

Computation results for the flow in a trench are shown in Figure 3.6 (page 50).

3.6.1.2 PROFILE Model

Coles (9) showed that the velocity profiles in a non-uniform flow can be described by using a linear combination of a logarithmic profile representing the law of the wall and a perturbation profile representing the influence of pressure gradients. Used by Bijn (40) thus:

1. Longitudinal velocity.

   The velocity profile is described by:

$$u = A_1\, u_h\, \ln\left(\frac{Z}{Z_0}\right) + A_2\, u_h\, F\left(\frac{Z}{h}\right) \qquad (3.29)$$

where,

u	=	flow velocity at height Z above bed,
u_h	=	flow velocity at water surface ($Z = h$),
Z_0	=	zero-velocity level ($Z_0 = 0.03k_s$),
k_s	=	effective roughness height,
h	=	water depth,
A_1, A_2	=	dimensionless variables,
F	=	perturbation profile.

The perturbation profile (F) is represented by:

$$F\left(\frac{Z}{h}\right) = 2\left[\frac{Z-Z_0}{h-Z_0}\right]^t - \left[\frac{Z-Z_0}{h-Z_0}\right]^{2t} \tag{3.30}$$

in which,

$t =$ a coefficient.

Figure 3.4 shows the perturbation profiles for various values of t.

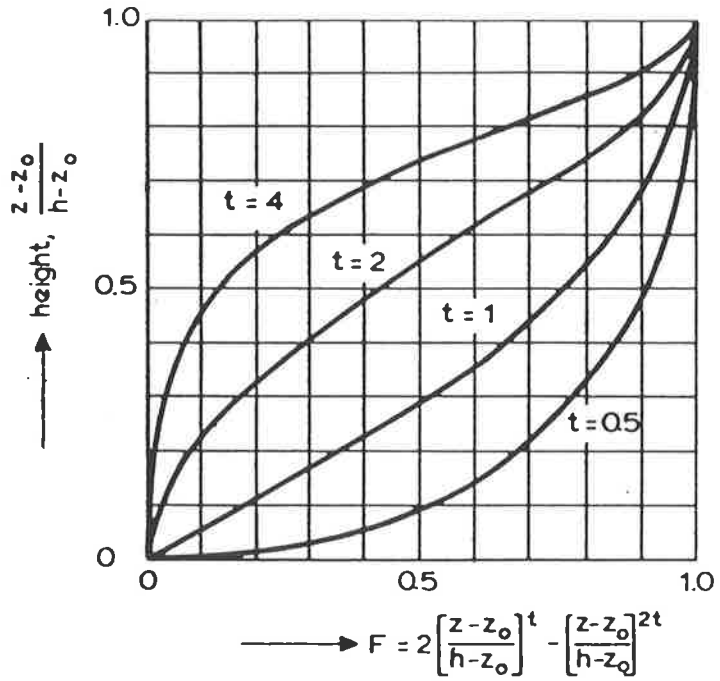

Figure 3.4: Perturbation profiles

The variable A_2 can be related to the variable A_1 by applying the boundary condition, $u = u_h$ for $Z = h$ resulting in:

$$A_2 = 1 - A_1 \ln\left(\frac{h}{Z_0}\right) \tag{3.31}$$

Combining equations 3.29, 3.30 and3.31 yields:

$$u = A_1 u_h \ln\left(\frac{Z}{Z_0}\right) + u_h\left[1 - A_1 \ln\left(\frac{h}{Z_0}\right)\right] \left[2\left(\frac{Z-Z_0}{h \quad Z_0}\right)^t - \left(\frac{Z-Z_0}{h-Z_0}\right)^{2t}\right] \tag{3.32}$$

The velocity profile, as described by equation 3.32, is completely defined when the unknown variables A_1, t and u_h are specified. Therefore, three additional equations must be specified, which are: Equation of continuity; equation for the t-parameter; and equation for the water-surface velocity, u_h.

(a) Continuity Equation:

The discharge Q can be represented by:

$$Q = b \int_{Z_0}^{h} u dz \tag{3.33}$$

in which, b = width.

Substitution of equation 3.32 in equation 3.33 and integration yields:

$$Q = \left[-1 + \ln\left(\frac{h}{Z_0}\right)\right] A_1 \; b \; h \; u_h + \left[1 - A_1 \; \ln\left(\frac{h}{Z_0}\right)\right] \left[\frac{3t+1}{2t^2+3t+1}\right] b \; h \; u_h \tag{3.34}$$

(b) t - Parameter Equation:

Analysis of velocity profiles measured in trenches situated perpendicular to the flow direction (40) showed that the measured mid-depth velocity at each location can be approximated by the mid-depth velocity computed from a logarithmic velocity profile at that location. The mid-depth velocity computed from the logarithmic velocity distribution is called the equilibrium mid-depth velocity. Thus:

$$u_{mid-depth} = u_{mid-depth \; equilibrium} \tag{3.35}$$

The mid-depth velocity according to equation 3.32, for $Z = 0.5h$, is:

$$u_m = A_1 \; u_h \; \ln\left(\frac{0.5h}{Z_0}\right) + u_h \left[1 - A_1 \; \ln\left(\frac{h}{Z_0}\right)\right] \left[2\,(0.5)^t - (0.5)^{2t}\right] \tag{3.36}$$

The equilibrium mid-depth velocity, $u_{m,e}$, using a logarithmic velocity distribution can be described by:

$$u_{m,e} = \frac{\ln(0.5h/Z_0)}{[-1 + \ln(h/Z_0)]} \frac{Q}{b\,h} \tag{3.37}$$

Substitution of equations 3.36 and 3.37 in equation 3.35 yields the t-parameter equation:

$$\frac{-1 + \ln(h/Z_0)}{\ln(0.5h/Z_0)} = \frac{3t+1}{(2t^2+3t+1)\left[2(0.5)^t - (0.5)^{2t}\right]} \simeq 0.16t^2 - 0.29t + 1.02 \tag{3.38}$$

(c) Water Surface Velocity Equation:

The surface velocity is described by a first order differential equation which yields an exponential adjustment of the surface velocity to the equilibrium surface velocity ($u_{h,e}$), as follows:

$$\frac{du_h}{dx} = \alpha_1 \frac{u_{h,e}}{h} - \alpha_2 \frac{u_h}{h} - \alpha_3 \frac{u_h}{b} \tag{3.39}$$

where,

h	=	water depth,
b	=	flow width,
$\alpha_1, \alpha_2, \alpha_3$	=	empirical coefficients to be determined by computer calibration using measured velocity profiles.

The equilibrium surface velocity is defined as the surface velocity from a logarithmic velocity distribution. Equation 3.39 can be solved numerically for a given value of the surface velocity at the inlet, $u_{h,0}$.

The complete set of equations 3.34, 3.38 and 3.39 is now defined and can be solved to determine the A_1, t and u_h variables. Using equation 3.32, the velocity profile can be

computed at each location. The coefficients α_1 and α_2 can be determined by calibrating the model using experimental data. The coefficient α_3 represents the adjustment of the surface velocity to variations in the transverse direction. Since experimental data were not available to calibrate α_3, the following expression has been applied that yields a gradual adjustment of the surface velocity.

$$\alpha_3 = 0.1 \tanh\left[10\left(\frac{db}{dx}\right)\right]$$

The input data for the PROFILE model are: discharge (Q), width (b) and depth (h), effective bed roughness (k_s), constant of Von Karman (k) and the surface velocity ($u_{h,0}$).

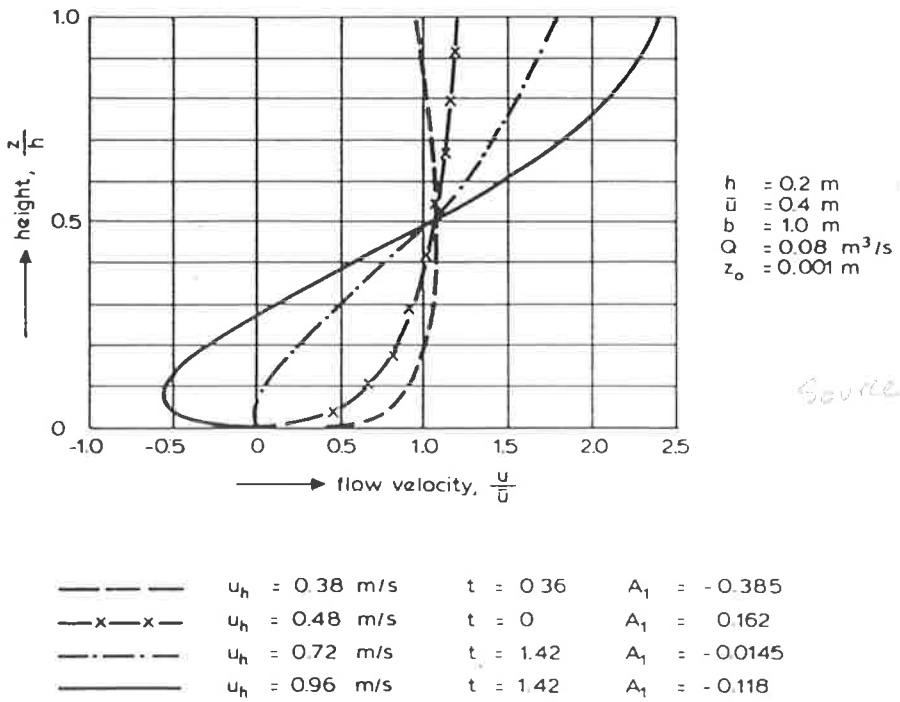

Figure 3.5: Velocity profiles according to PROFILE model.

Figure 3.5 shows some velocity profiles based on PROFILE model. As can be observed, the PROFILE model is capable

of representing a wide range of velocity profiles including those with flow reversal.

Computation results for the flow in a trench are shown in Figure 3.6 along with the velocity profiles computed by the sophisticated K-EPSILON model.

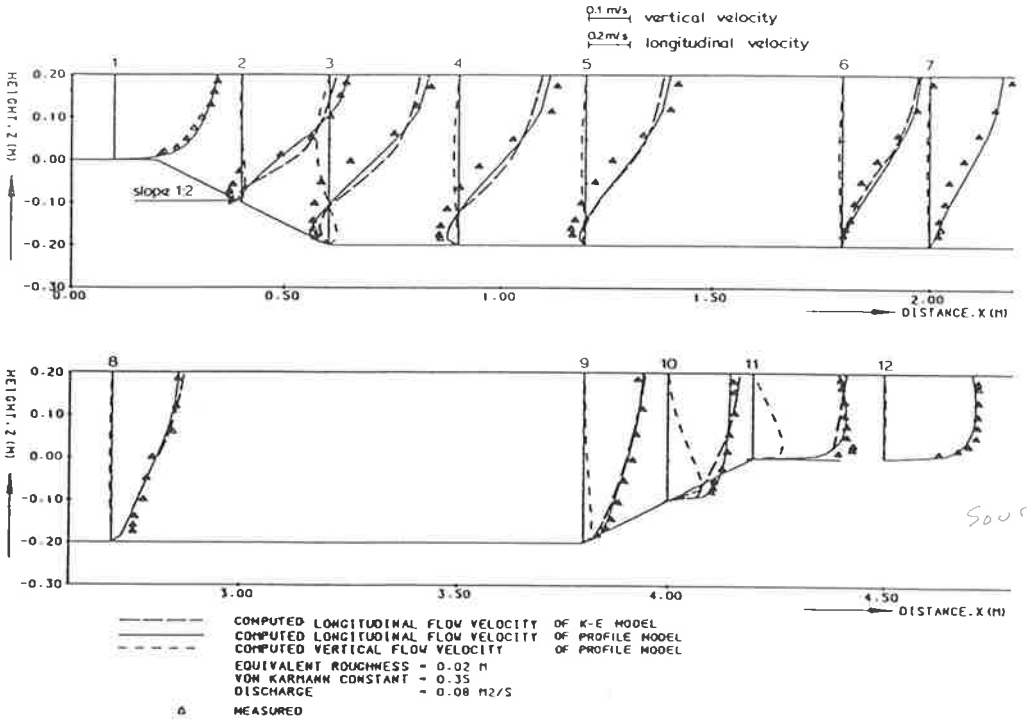

Figure 3.6: Measured and computed velocity profiles in a trench

(d) Vertical Flow Velocity:

The vertical flow velocity, w, can be computed from the width-integrated equation of continuity:

$$\frac{1}{b}\frac{\partial}{\partial x}(bu) + \frac{\partial}{\partial x}(w) = 0$$

$$yielding,\ w = -\int_{Z_b+Z_0}^{Z_b+Z} \frac{\partial u}{\partial x} dz - \frac{1}{b}\frac{db}{dx}\int_{Z_b+Z_0}^{Z_b+Z} u dz \quad (3.40)$$

Substitution of equation 3.32 in equation 3.40 and integration yields a (complicated) analytical expression for the vertical flow velocity.

(e) Bed-Shear Velocity:

The local bed-shear velocity, u_*, which is needed to determine the bed-boundary condition for the sediment concentrations, is computed from the flow velocity at height $Z = 0.05h$ above the mean bed level assuming a logarithmic velocity profile in the near-bed layer. This yields:

$$u_* = \frac{k\ u_b}{\ln(0.05h/Z_0)}$$

where,

u_b = flow velocity computed at $Z = 0.05h$ above the mean bed level,

k = von Karman constant,

h = water depth,

Z_0 = Zero-velocity level.

3.6.2 Sediment Mixing Coefficients.

The eddy viscosity concept is applied to represent the transfer of fluid momentum and sediment mass. The sediment mixing coefficient (ϵ_s) is related to the fluid mixing coefficient or eddy viscosity (ϵ_f) as follows:

$$\epsilon_s = \beta\ \phi\ \epsilon_f$$

where,

β = proportionality factor related to the difference in the transfer of fluid momentum and sediment mass,

ϕ = turbulence damping factor.

Based on the analysis of the data of Coleman (8), the following expression has been proposed for β-factor:

$$\beta = 1 + 2\left(\frac{w_s}{u_*}\right)^2; \quad for \;\; 0.1 < \frac{w_s}{u_*} < 1$$

Based on theoretical and experimental work, the following function has been proposed for the ϕ-factor:

$$\phi = 1 + \left(\frac{c}{c_0}\right)^{0.8} - 2\left(\frac{c}{c_0}\right)^{0.4}$$

in which,

$c_0 = 0.65$ = maximum volume concentration.

For smaller concentrations the influence of the ϕ-factor is relatively small and may, therefore, be neglected for most practical cases ($\phi = 1$).

3.6.2.1 K-EPSILON Model

At the present stage of research it appears that the best approach to compute the fluid mixing coefficient for complicated flow conditions is the application of the sophisticated K-E model. A detailed description of computation of fluid mixing coefficient using the K-E model is given in Section 3.6.1.1.

3.6.2.2 PROFILE Model

1. Vertical distribution of fluid mixing coefficient.

   Based on the experimental data of Coleman (8) showing almost constant mixing coefficients in the upper half of flow, Kerssens

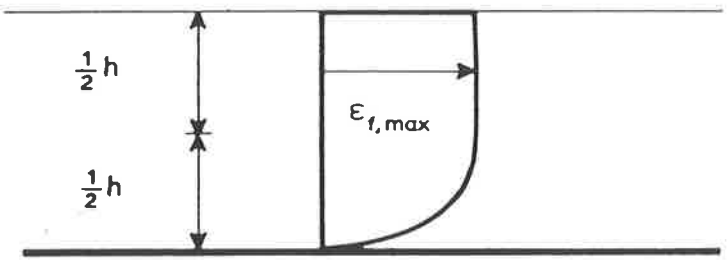

Figure 3.7: Vertical distribution of fluid mixing coefficient.

(29) introduced the parabolic-constant sediment mixing coefficient distribution, Figure 3.7, as follows:

$$\epsilon_f = \epsilon_{f,max} - \epsilon_{f,max}\left(1 - \frac{2Z}{h}\right)^2 ; \quad for \quad \frac{Z}{h} < 0.5$$

$$\epsilon_f = \epsilon_{f,max} ; \quad for \quad \frac{Z}{h} \geq 0.5$$

where,

$$\epsilon_{f,max} = 0.25\ k\ u_*\ h$$

= maximum value of fluid mixing coefficient.

2. Longitudinal distribution of fluid mixing coefficient.
   In longitudinal direction the variation of the mixing coefficient is effected by varying the $\epsilon_{f,max}$ value by use of a first order differential equation, as follows:

$$\frac{d}{dx}(\epsilon_{f,max}) = \left[\overbrace{\frac{\alpha_4}{h}(\epsilon_{f,max,e} - \epsilon_{f,max})}^{I} - \overbrace{\alpha_5 h \frac{d}{dx}(u_h - \overline{u})}^{II}\right]\left[\overbrace{e^{-15dh/dx}}^{III}\right]$$

in which,

$$\begin{aligned}
\epsilon_{f,max,e} &= 0.25\ k\ u_{*,e}\ h \\
&= \text{maximum fluid mixing coefficient} \\
&\quad \text{for equilibrium conditions,} \\
u_{*,e} &= \left(\frac{\sqrt{g}}{c}\right)\overline{u} \\
&= \text{equilibrium bed-shear velocity,} \\
\overline{u} &= \text{cross section averaged flow velocity,} \\
c &= \text{overall Chezy coefficient,} \\
\alpha_4, \alpha_5 &= \text{coefficients,} \\
h &= \text{water depth.}
\end{aligned}$$

In the above equation, Term I represents the decrease of the $\epsilon_{f,max}$ - value towards its equilibrium value. Term II represents the increase of the $\epsilon_{f,max}$ - value after a change of the flow velocity profile. Term III is a stabilizing term acting at steep sloping bottoms.

The coefficients α_4 and α_5 have been determined by calibrating with computation results of the sophisticated $K-E$ model for various conditions concerning the flow in trenches.

Figure 3.8 shows fluid mixing coefficients in a trench, computed using $K-E$ and PROFILE models.

3.6.3 Particle Fall Velocity

Usually, the representative particle fall velocity is determined from suspended sediment samples using laboratory, or in situ analysis methods. However, inaccuracies can occur due to; measuring errors related to the applied instruments, and schematization errors introduced by applying one particle fall velocity to represent the full range of the fall velocities from relatively large values close to the bed to relatively small values

close to the water surface. Test computations have shown an inaccuracy of the total sedimentation rate in a trench of about 25% for a variation of the fall velocity by 25%.

Generally, the vertical distribution of the suspended sediment size and fall velocity are not known, because of insufficient measurement data. In that case the fall velocity has to be predicted. This may lead to a considerably larger inaccuracy, and thus, stresses the importance of detailed field measurements.

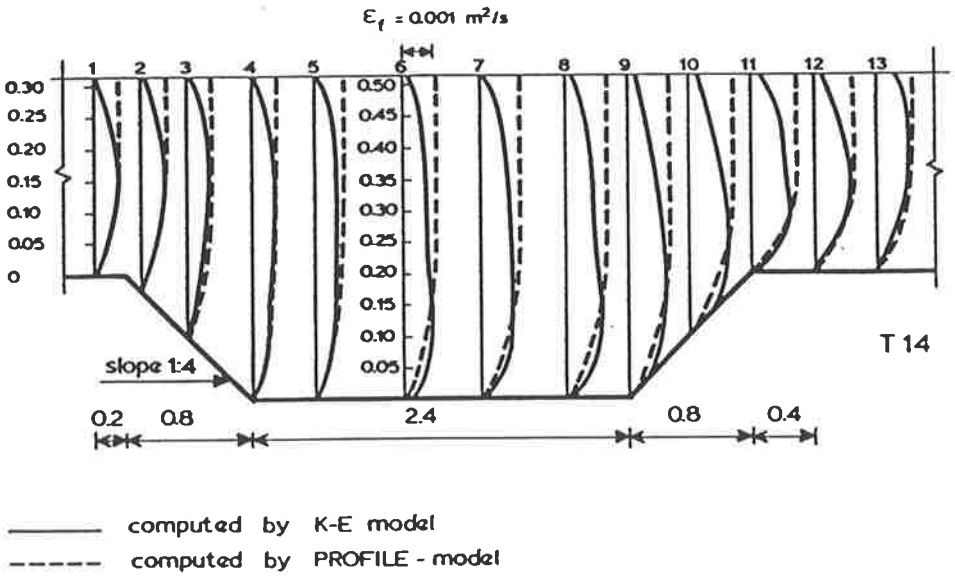

Figure 3.8: Computed fluid mixing coefficients in trench

The SURTRENCH-2D model presented in the foregoing sections has been developed as a tool for routine morphological computations in the daily engineering practice. For that purpose the fluid velocity and mixing coefficient distributions have been represented in as simple a form as possible. This inevitably means a compromise between the representation of the physics of the flow and sediment transport process, the overall accuracy of model and the computation cost. The model has been ver-

ified extensively using flume and field data. The verification results has shown that for suspended sediment transport in non-uniform conditions the model has produced reliable results in predicting sediment concentrations, transport rates and bed level changes in dredged trenches and channels. Taking into account the estimated errors of the basic parameters and boundary conditions, the measured bed levels are considered to be within the standard error range of the predicted values.

However, due to loss of accuracy because of a less sophisticated representation of the physics of the relevant processes, comparison of the depth-integrated sediment transport computed by the K-Epsilon model and the Profile model has shown a maximum relative error of about 30% for a steep-sided trench. For most situations such an error is considered to be sufficiently small considering the complexity of morphological processes. For specific problems when a higher accuracy is required, the use of the K-Epsilon model to compute the fluid mixing coefficients has been recommended.

Chapter 4

Physical Model

4.1 Introduction

In the experimental part of this research study a physical model of the entry to a dredged navigational channel through a shelving coastline was built to simulate siltation effects. The flow and siltation conditions which were obtained were used to verify the two numerical models which were under assessment.

4.2 Configuration of The Flow Domain

The plan view of the inlet area considered for study is the area enclosed by broken lines in Figure 4.1. The space available in the Hydraulic Laboratory to construct the physical model was taken into consideration when deciding the overall dimensions of the flow domain. Accordingly, the length and width of the model and of the computational domain, as shown in Figures 4.2 and 4.3, were selected as $7.75m$ and $1.2m$ respectively.

The slope of the bed in the transverse direction represents the gradient of the sea bed in the shore region. The depth of flow in the inlet and outlet areas was selected as $71mm$ at the shore boundary and $311mm$ at the offshore boundary. The width of the dredged section was 2.0m and the slope of the sides of the dredged channel was set to 1 : 3.75. The gradient of the bed in the longitudinal direction was 1 : 1000 and the depth of flow in the dredged section was $371mm$.

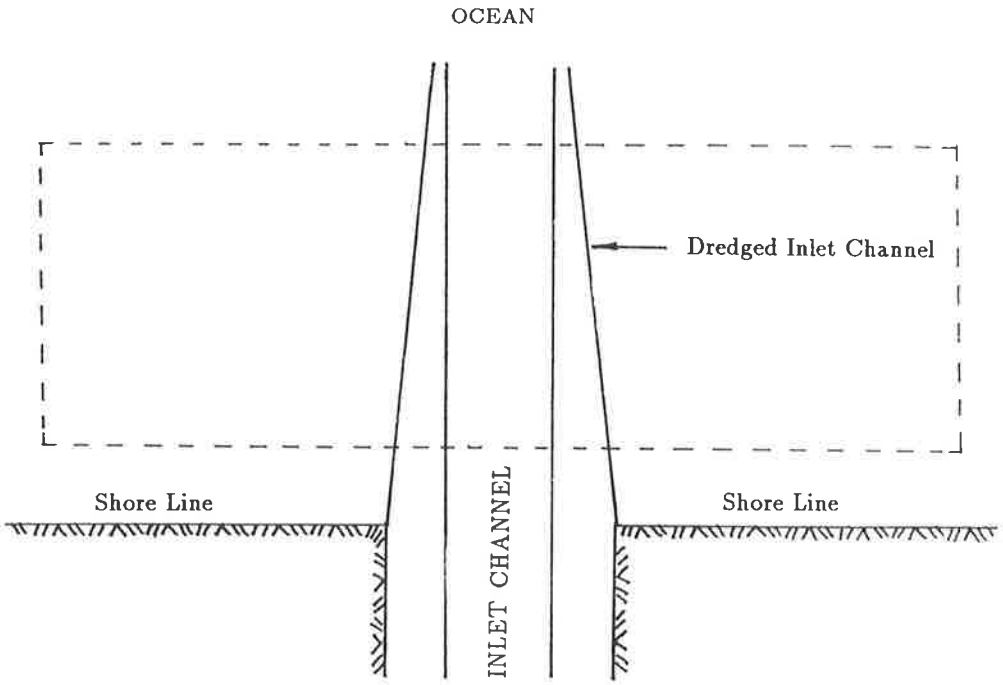

Figure 4.1: Area Considered for Detailed Study

The flow across the channel was assumed to be steady and flow through the inlet (or the dredged channel) was not taken into account.

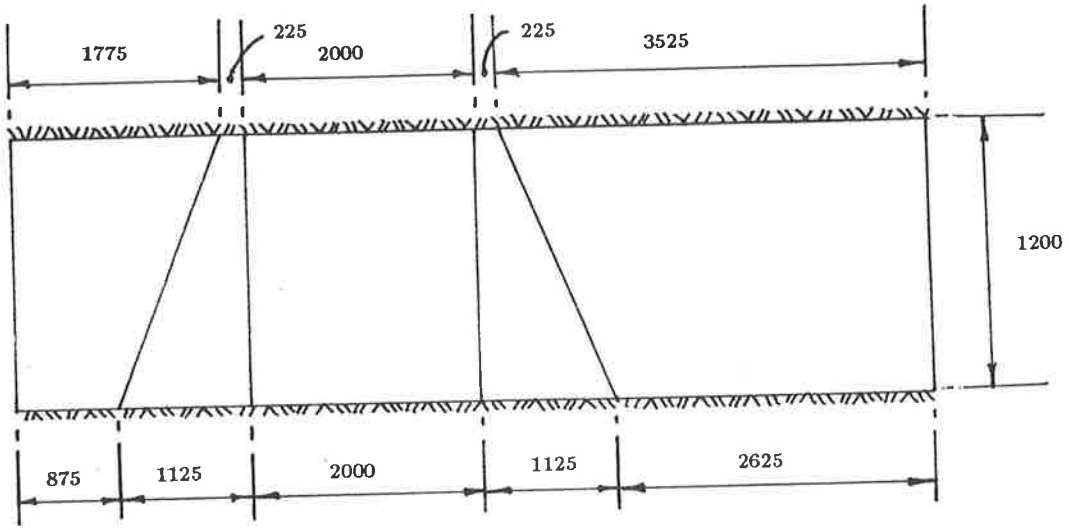

(a) Plan View

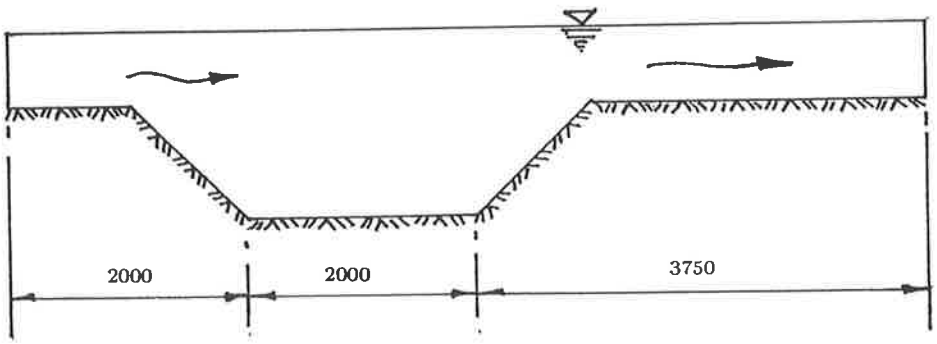

(b) Longitudinal Section

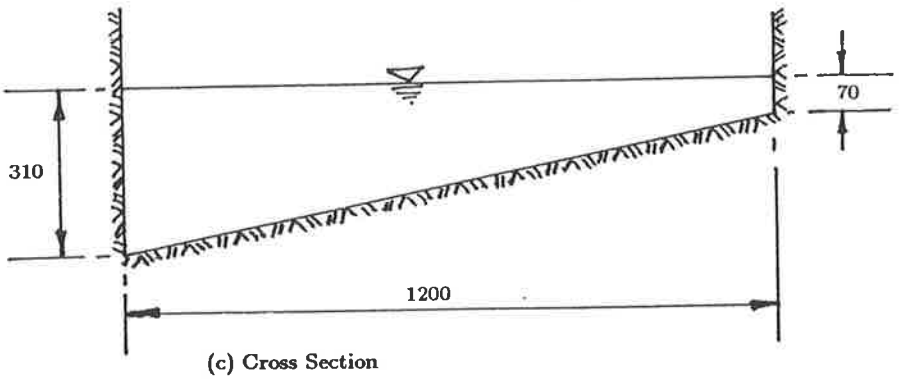

(c) Cross Section

Figure 4.2: Dimensions of the Flow Domain

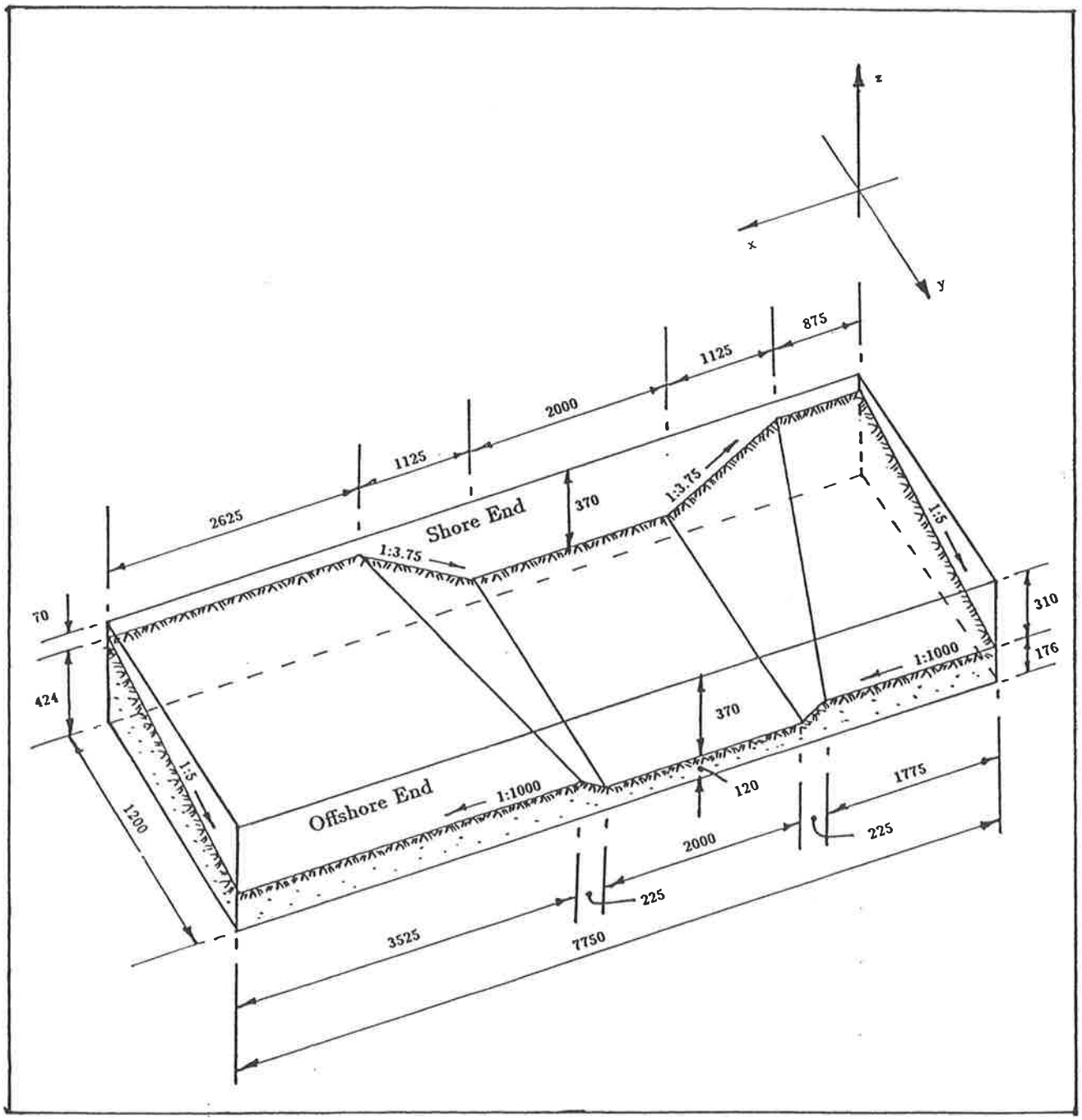

Figure 4.3: Isometric View of the Flow Domain

4.3 Physical Model

The experimental set up is indicated in Figure 4.4. Supply of water to the model was obtained from a constant head tank. The out-flow from the model was collected in a large sump and recirculated using a pump which had a discharge capacity bigger than the flow through the model so as to maintain a continuous overflow from the supply tank. The pump was kept running continuously during the experiment to maintain a constant head in the overhead tank and thereby to maintain a steady flow into the model. A weir box, with a sharp-crested V-notch was installed at the downstream end to carry out flow measurements.

Sieve analysis of the bed material used indicated (Figure 4.5) that the bed consisted of fine to medium sand of almost uniform size. The characteristic diameters of the bed material were: $d_{10} = 150\mu m$, $d_{50} = 240\mu m$ and $d_{90} = 380\mu m$.

In order to maintain a mean flow velocity of about 0.3 m/sec, which was considered to be large enough to initiate movement of the sediment used in the experiment, the discharge was maintained at about 2.45 cusecs. ($0.069\ m^3/sec$).

For validation of the flow simulation model, inlet and downstream flow velocity measurements should be carried out on a fixed bed model. Therefore, at the first instance, the entire bed of the physical model was covered with steel sheets to maintain a fixed bed until measurement of flow velocities were completed.

The experiment mainly consisted of extensive measurement of flow velocities. All flow velocity measurements were carried out using Laser-Doppler velocity measuring equipment.

In order to obtain input velocity boundary conditions for the flow simulation model, inlet velocity components in longshore and offshore directions

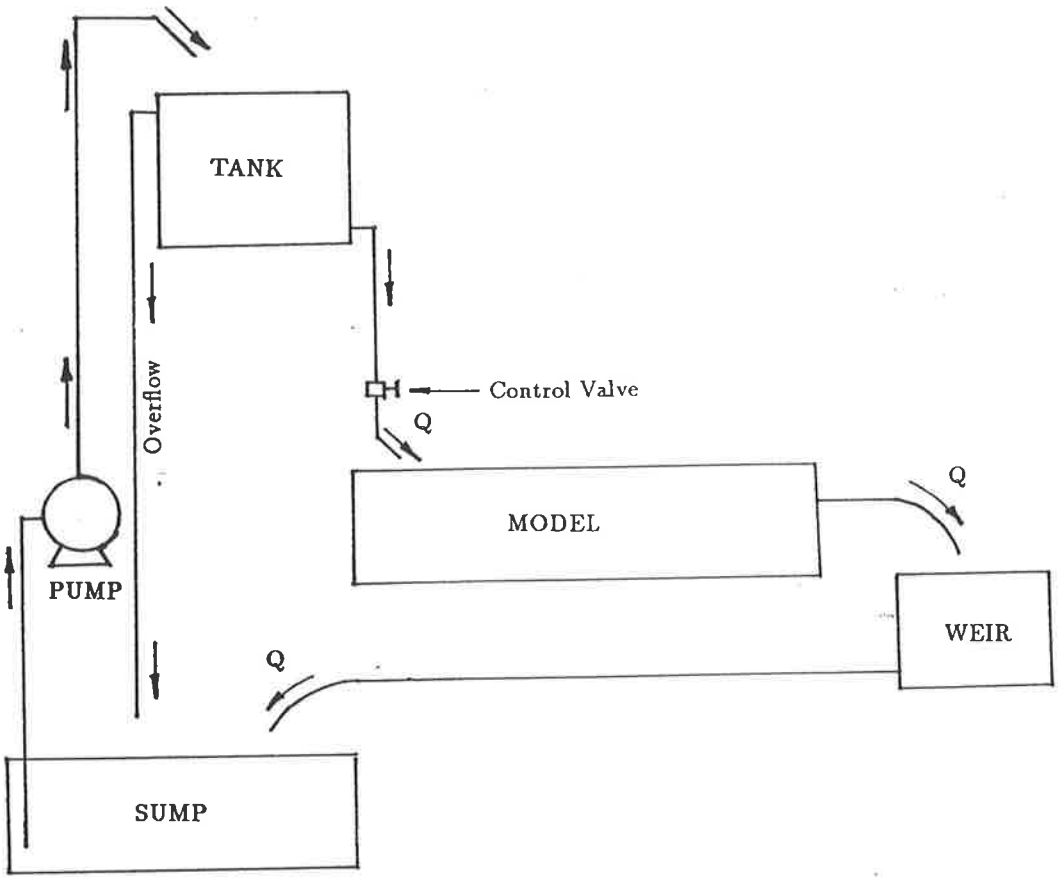

(a) Schematic Diagram of the Experimental Set Up

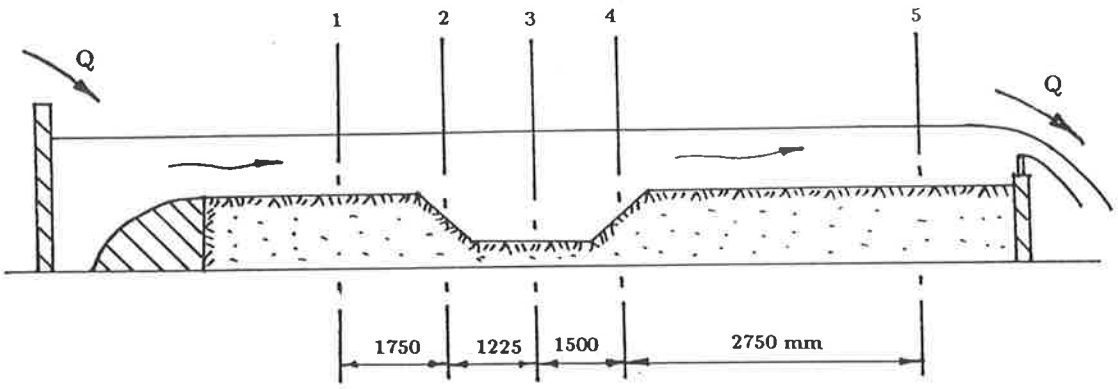

(b) Longitudinal Section and Velocity Measuring Stations

Figure 4.4: Experimental Set Up

were measured on all finite element grid lines as shown in Figure 4.6. For calibration of the flow simulation model, measurement of the longshore velocity components were carried out at four different downstream sections, at $x = 1.75$, 3.0, 4.5, and 7.25 meters, as shown in Figure 4.4.

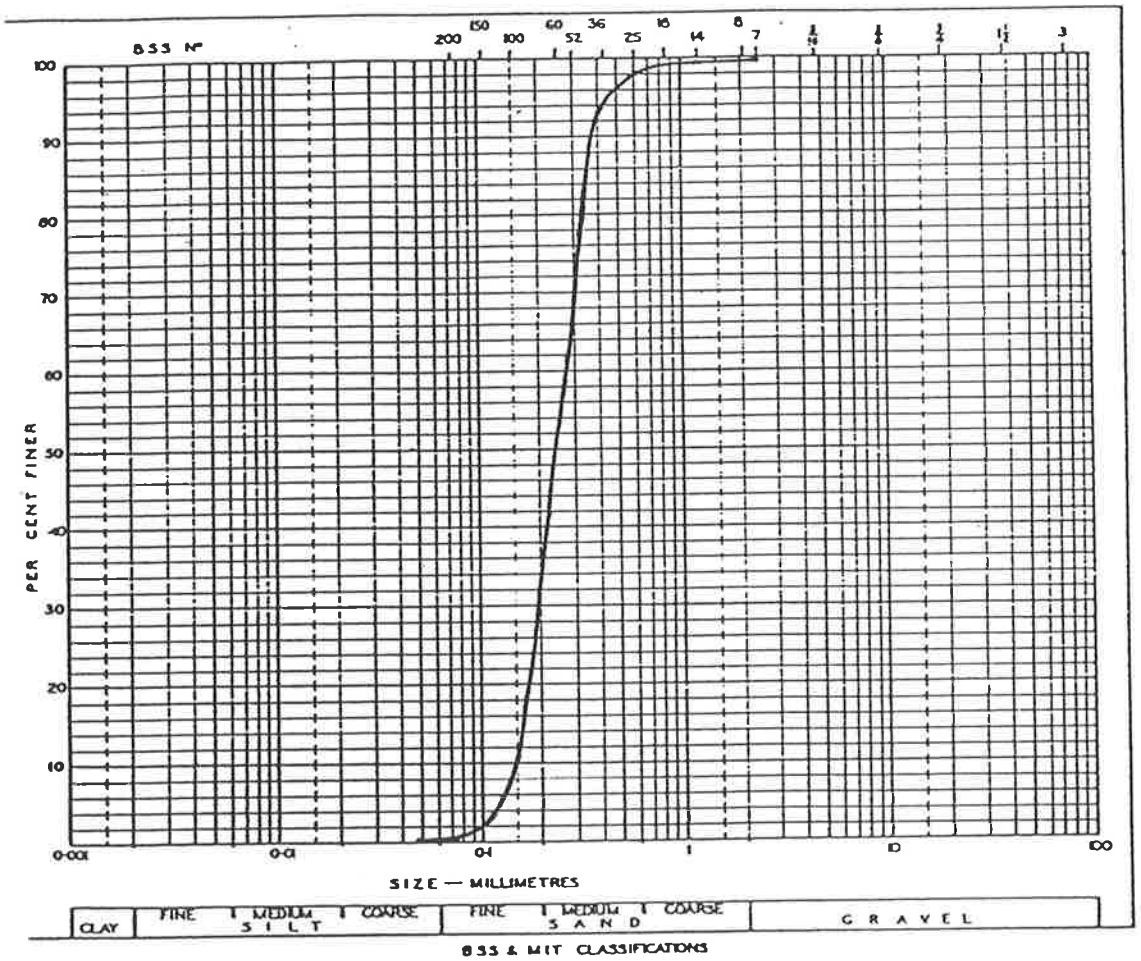

Figure 4.5: Particle Size Distribution of Bed Material

In addition to the measurement of inlet and downstream velocities turbulent kinetic energy (K) and its dissipation rate (ϵ) were also measured at the inlet, as described in Sections 4.3.2 and 4.3.3, to obtain input boundary conditions for the numerical models.

When calibration of the flow simulation model was completed, the metal sheets used to cover the bed were removed and the flow was restarted to

validate the sand transport model. After 3.0 hrs and 6.0 hrs of continuous steady flow, the flow was discontinued and the bed profiles of the entire area under consideration was measured.

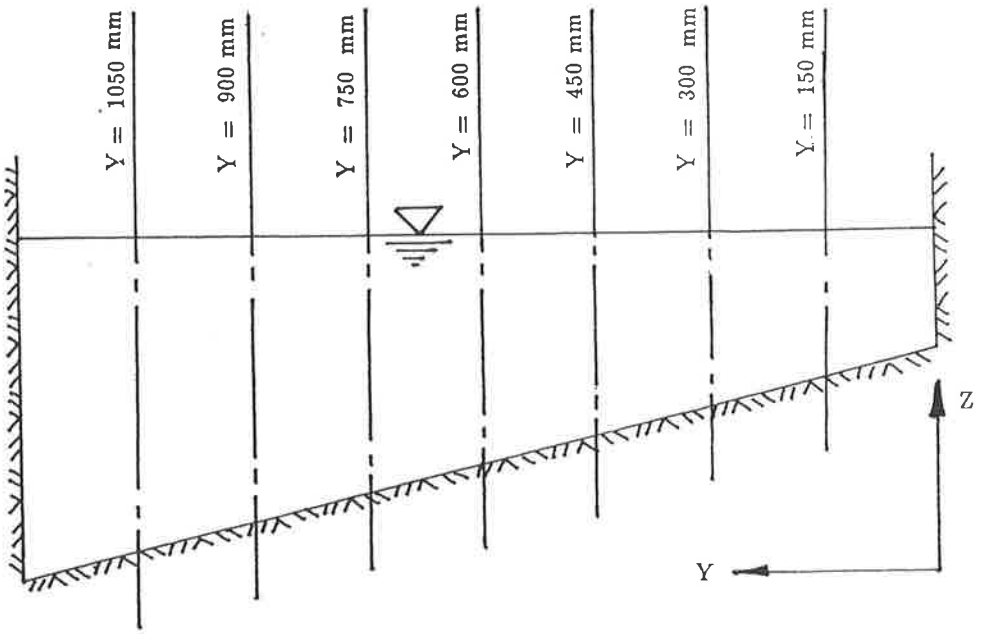

Figure 4.6: Flow Velocity Measuring Stations at the Inlet Cross Section

As the input velocity boundary conditions specified to the flow simulation model vary with the change of the bed profile at the inlet section, inlet velocity measurements were carried out at 2.5 hrs during the experiment to update the inlet boundary conditions.

4.3.1 Measurement of Inlet Velocities

Inlet velocities in the longshore and offshore directions were measured in the physical model, as described in Section 4.3, using Laser-Doppler velocity measuring equipment. In the Laser-Doppler processing programme the measured mean velocity at a point has been defined as:

$$Mean\ Velocity\ =\ \overline{X}\ =\ \frac{1}{N}\sum_{i=1}^{N} X\,(i)$$

where,

X(i) = velocity of each sample,

N = number of samples taken to calculate the mean.

The value of N was set to 256.

4.3.2 Measurement of Turbulent Kinetic Energy at the Inlet

In addition to calculation of mean velocities, the Laser-Doppler programme has been devised to measure the fluctuating components and to record the standard deviation of the velocity fluctuations for each measurement.

$$Standard\ Deviation\ =\ \sigma\ =\ \left[\frac{1}{N}\sum_{i=1}^{N}\left(X\,(i)^2\ -\ \overline{X}^2\right)\right]^{1/2}$$

Measured values of standard deviation in x and y directions were taken as the time-averaged values of the fluctuating components of the fluid velocity $\overline{u'}$ and $\overline{v'}$ in calculating the turbulent kinetic energy (K) at the inlet, using the formula presented in Section 3.6.1.1:

$$K\ =\ \frac{1}{2}\left[\overline{(u')^2}\ +\ \overline{(v')^2}\ +\ \overline{(w')^2}\right]$$

The prescribed initial values of K and ϵ at the inlet seems to exert little influence on the predictive accuracy of the flow simulation models (34). Therefore, as velocity measurements were not carried out in the vertical direction it was assumed that, $\overline{w'}\ =\ \overline{u'}$.

4.3.3 Measurement of Dissipation Rate of Turbulent Kinetic Energy at the Inlet

Dissipation rate of turbulent kinetic energy (ϵ) was evaluated from the following formula (33) using the values of measured turbulent kinetic energy (K).

$$\epsilon = \frac{C_\mu^{3/4} K^{3/2}}{l_m}$$

in which, l_m is a mixing length.

It was assumed that the value of mixing length is given by the well-known ramp function for wall boundary layers (32):

$$l_m = \lambda y_G$$

where,

λ = a constant in mixing length model,

y_G = effective width of shear flow.

The characteristic shear width of flow is defined by (32):

- For monotonically increasing/decreasing velocity profile,

$$y_G = y_2 - y_1$$

where at y_1,

$$\frac{u - u_b}{u_s - u_b} = 0.1$$

and at y_2,

$$\frac{u - u_b}{u_s - u_b} = 0.9$$

in which,

u_b = axial velocity at bed boundary,

u_s = axial velocity at free surface,

u = axial velocity.

– For velocity profiles without a maximum or minimum at either boundary,

$$y_G = y_2 - y_1$$

where at y_1,

$$\frac{u - u_b}{\overline{u} - u_b} = 0.1 \; ; \; for \; inner \; region \; of \; flow,$$

or at y_1,

$$\frac{u - \overline{u}}{u_s - u} = 0.9 \; ; \; for \; outer \; region \; of \; flow,$$

and at y_2,

$$u = \overline{u}$$

The inner region of flow is defined as the region between the bed boundary and the point of occurrence of the minimum/maximum velocity, $\overline{u}$.

Therefore, when the inlet velocity profiles are known the shear width can be calculated using above equations. A value of 0.125 was assumed for λ (32).

Measured inlet velocities in the longshore direction are presented in Figure 4.7.

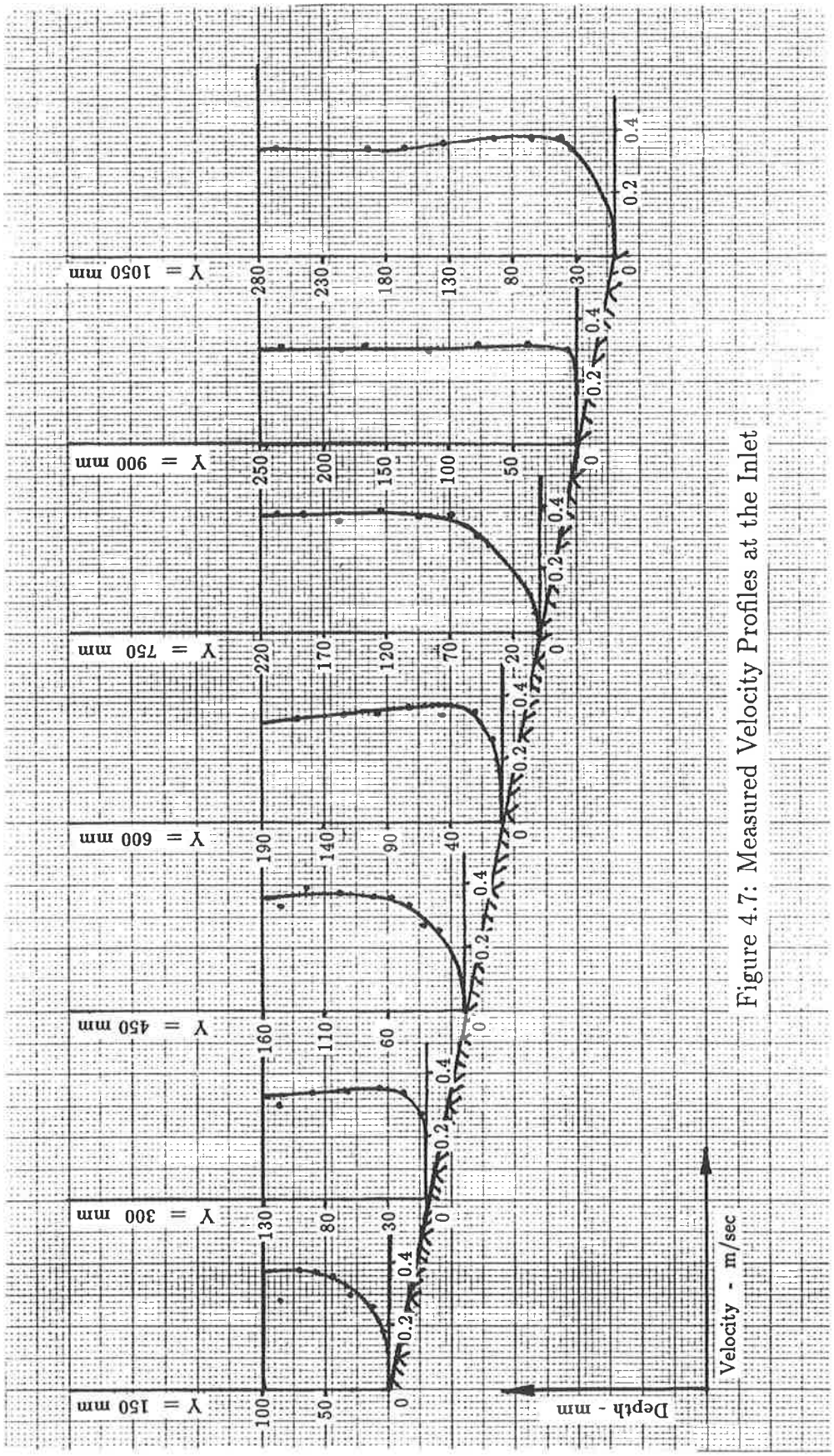

Figure 4.7: Measured Velocity Profiles at the Inlet

Chapter 5

Numerical Models

5.1 Introduction

In analysing flow across a dredged trench a comparatively simple profile model based on shape functions has been used to represent the vertical distribution of the velocities and mixing coefficients in the SURTRENCH-2D model presented in Section 3.6, because of excessive computation cost involved with the K-Epsilon model. Movement of sediment in suspension has been represented by a simplified version of the diffusion-convection equation and a bed-load formula has been used to describe the bed load.

An attempt was made in this research study to assess the computational feasibility of solving the complex problem of siltation in a dredged channel by using two numerical models, an advanced turbulent model coupled with a simple sand transport model, as described in the following sections.

5.2 Flow Simulation Models

A general purpose computer software package (FIDAP) which uses the finite element method to simulate many classes of incompressible fluid flows was used to simulate turbulent flow across the channel. In FIDAP the three-dimensional, steady, turbulent flow of an incompressible viscous fluid is represented by the following equations:

- Mass Conservation

$$\frac{\partial u_j}{\partial x_j} = 0 \tag{5.1}$$

- Momentum Conservation

$$u_j \frac{\partial u_i}{\partial x_j} = -\frac{\partial p}{\partial x_i} + \frac{\partial}{\partial x_j}\left[\mu\left(\frac{\partial u_i}{\partial x_j} + \frac{\partial u_j}{\partial x_i}\right)\right] \tag{5.2}$$

where,

u_i	=	mean fluid velocity component,
p	=	fluid pressure,
x_i	=	cartesian coordinates,
i	=	1,2,3
j	=	1,2,3
μ	=	total viscosity,
	=	$\mu_0 + \mu_t$
μ_0	=	laminar viscosity,
μ_t	=	turbulent viscosity.

Equation 5.1 together with equation 5.2 (three equations in three cartesian coordinate directions) forms a set of four equations which can be solved numerically for the three mean velocity components (u,v,w) and pressure when the turbulent viscosity (or eddy viscosity) is known.

Two possible turbulent models are available in FIDAP, a 'zero-equation' mixing length model and the 'two-equation' K-Epsilon model to deter-

mine the distribution of turbulent viscosity.

5.2.1 K-Epsilon Model

As already described in Section 3.6.1.1, the three-dimensional version of the K-Epsilon model comprises three additional equations as indicated below:

$$\rho\, u_j \frac{\partial K}{\partial x_j} = \frac{\partial}{\partial x_j}\left(\frac{\mu_t}{\sigma_K}\frac{\partial K}{\partial x_j}\right) - \rho\,\epsilon \tag{5.3}$$

$$\rho\, u_j \frac{\partial \epsilon}{\partial x_j} = \frac{\partial}{\partial x_j}\left(\frac{\mu_t}{\sigma_\epsilon}\frac{\partial \epsilon}{\partial x_j}\right) - \rho\, c_2 \frac{\epsilon^2}{K} \tag{5.4}$$

$$\mu_t = \rho\, c_\mu \frac{K^2}{\epsilon} \tag{5.5}$$

Equations 5.1, 5.2, 5.3, 5.4 and 5.5 represents a set of 7 equations with seven unknowns (u,v,w,p,μ_t, K and ϵ) which can be solved numerically. FIDAP adopts the Galerkin form of the weighted residuals method to solve these differential equations by the finite element method.

5.2.2 Mixing Length Model

As described in Section 6.3, relatively large computation time required to solve the equations in the K-Epsilon model made it unattractive for long term morphological computations. To reduce the computation time significantly, a relatively simple model, mixing length model, was used in the flow simulation model which is to be coupled with the Sand Transport Model in the Profile Model as described in Section 5.5.

In the mixing length model, the turbulent viscosity is represented by the Prandtl mixing length hypothesis.

$$\mu_t = \rho\, l_m^2 \left[\left(\frac{\partial u_i}{\partial x_j} + \frac{\partial u_j}{\partial x_i}\right)\frac{\partial u_i}{\partial x_j}\right]^{1/2} \tag{5.6}$$

where,

l_m = mixing length.

The distribution of the mixing length over the flow field can be prescribed with the aid of empirical information. The mixing length can be thought of as the mean free path for the collision or mixing of globules of turbulent fluid.

In FIDAP the mixing length values are computed based on Nikuradse's (41) Formula:

$$\frac{l_m}{R} = 0.14 - 0.08\left(1 - \frac{y}{R}\right)^2 - 0.06\left(1 - \frac{y}{R}\right)^4 \qquad (5.7)$$

where,

l_m = mixing length,

R = depth of flow,

y = normal distance from the wall.

5.2.3 Boundary Conditions for Flow Simulation Models

5.2.3.1 Inlet Boundary

It was assumed that the flow is fully developed by the time it reaches the inflow section. Inlet velocity components in the longshore and offshore directions measured in the physical model, as described in Section 4.3, were prescribed as input to the numerical model. Inlet velocity in the vertical direction was assumed to be zero.

Turbulent kinetic energy at the inlet was calculated, as described in Section 4.3.2, from the measured turbulent intensities in the physical model.

Dissipation rate of turbulent kinetic energy at the inlet was evaluated from the formula presented in Section 4.3.3 using the measured turbulent kinetic energy and velocity profiles.

5.2.3.2 Wall Boundaries

The standard K-Epsilon model which is employed in FIDAP is suitable for high Reynolds number flow and therefore cannot be used in the near-wall regions. The variation of the turbulent viscosity within the viscous sublayer in the near-wall region is modelled using van Driest's mixing length model with a transition to the standard high Reynolds number K-Epsilon model in flow regions beyond the viscous sublayer where the turbulence is fully developed.

In the van Driest mixing length approach, the eddy viscosity, as described in Section 5.2, is modelled as,

$$\mu_t = \rho\, l_m^2 \left[\left(\frac{\partial u_i}{\partial x_j} + \frac{\partial u_j}{\partial x_i} \right) \frac{\partial u_i}{\partial x_j} \right]^{\frac{1}{2}}$$

where,

μ_t = eddy viscosity,
l_m = van Driest mixing length,
i, j = 1,2,3

The van Driest mixing length is defined as,

$$l_m = k\, \delta \left(1 - e^{-y_u^+ / A} \right)$$

where,

A = an empirical constant,
k = von Karman constant,
δ = normal distance from the wall.

In this equation y_u^+ is the dimensionless normal distance from the wall defined in terms of the turbulent kinetic energy as,

$$y_u^+ = \rho\,\delta\frac{\left(c_\mu^{\frac{1}{2}}\,K\right)^{\frac{1}{2}}}{\mu}$$

where,

c_μ = a turbulence constant,

μ = dynamic viscosity,

K = turbulent kinetic energy.

While the computational domain for the mean flow equations encompasses the entire flow domain up to the solid boundary, the corresponding computational domain for the K & Epsilon equations of the K- Epsilon turbulent model only extends to near wall region. Appropriate boundary conditions are therefore needed at these locations for the K-Epsilon equations. As part of near-wall implementation, FIDAP applies the following boundary conditions for K and Epsilon.

$$\frac{\partial K}{\partial n} = 0$$

$$\epsilon = \frac{\left(c_\mu^{\frac{1}{2}}\,K\right)^{1.5}}{k\,\delta}$$

Where, n is the direction normal to the boundary.

If no-slip boundary condition is valid at the wall, then all the velocity components assume a zero value at the wall.

5.2.3.3 Outlet Boundary

The outlet boundary is located far away from the area of interest so as to allow the redevelopment of fully developed flow downstream. At the outflow no velocity boundary conditions are imposed, resulting in zero

normal and tangential stresses at the outflow boundary. Similarly, the turbulent kinetic energy and dissipation are not specified at the outflow boundary.

5.2.3.4 Water Surface

The position of the free water surface was assumed to be fixed and at the free water surface the velocity component in the vertical direction was assumed to be zero.

5.3 Creating Numerical Models Using FIDAP

FIDAP is a general purpose finite element program for simulating viscous incompressible fluid flows. The finite element method has a long and successful history in the solution of structural analysis problems. Over recent years the finite element approach has been applied to a wide range of computational fluid dynamics problems. FIDAP is a well supported commercially available general purpose computational fluid dynamics package based on the finite element method which was selected for use in this study. (Fluid Dynamics Intl Illinois)

In finite element method the flow domain is divided into a number of simply shaped regions called finite elements. The definition of the element is accomplished by identifying the locations of the element corners in space. The application of the Galerkin finite element procedure to the Navier-Stokes equations results in a set of non-linear algebraic equations. This non-linear system of equations is then solved to determine the velocity components, pressure or other degree of freedom included in the problem statement at each node in every element.

In FIDAP, two different solution methodologies are utilized for solving the non-linear equation system mentioned above. The first approach solves all conservation equations in a simultaneous manner, while the second approach solves each equation separately in a sequential segregated manner.

Experience has shown that the fully coupled approach is the most cost-effective for the majority of two-dimensional problems. However, for unusually large two-dimensional problems and a majority of three-dimensional problems, the computer resources required can become prohibitively expensive.

The segregated approach is guaranteed to have substantially reduced disk storage requirements compared to the fully coupled solver. However, due to the sequential and uncoupled nature, the segregated solver requires more iterations than the coupled solver.

In the fully coupled approach various iterative procedures are available in FIDAP including, a simple fixed point iteration scheme known as successive substitution (or Picard Iteration), several Newton-type methods (Newton-Raphson method, Modified Newton-Raphson method also known as the secant or chord method and Quasi-Newton Updates Method), Matrix Free solver, and combination strategies (to combine any two of the above described methods).

The fully coupled solution approach requires the formation of the global system matrix which includes all the unknown degrees of freedom. The segregated solution algorithm, which is based on the implicit approach, avoids the direct formation of a global system matrix. Instead, this matrix is decomposed into smaller sub-matrices each governing the nodal unknowns associated with only one conservation. These smaller sub-matrices are then solved in a sequential manner using direct Gaussian elimination.

As described in Section 6.3, the disk space required for the successive substitution solver became very excessive, and hence the segregated solver was used in all simulations carried out in this project.

FIDAP consists of three program modules known as FIPREP, FIDAP and FIPOST. The three modules correspond to the three phases associated with solving a flow problem using a finite element programme. These phases are:

1. Creating the data that define the problem to be solved. This is called pre-processing.
2. Performing the numerical simulation. This is the processing (or number-crunching) phase.
3. Reviewing and analyzing the solution, or the post-processing phase.

The basic flow of information is from FIPREP to FIDAP to FIPOST.

5.3.1 Creating FIPREP Input

The FIPREP module requires basic data to create the geometry, boundary conditions, initial conditions, fluid properties and program control specifications. The FIPREP input file, known as FIINP, contains all these information requires to define the problem which is to be simulated. The FIINP files used for K-Epsilon and Mixing Length models are given in Appendices A and B respectively.

5.3.1.1 Input Files for Defining the Geometry

While finite element computer codes are powerful tools for the simulation of physical phenomena such as fluid flow, the accuracy and cost-effectiveness of the solution are, to a large extent, depend on the mesh employed. Typically, the data preparation of a finite element analysis is the most labour consuming stage.

The FIDAP simulation package has automated mesh generation capability in the sub-module known as FIMESH for the cases of fixed boundaries and a limited cases of movable boundaries such as flow with moving surface, solidification and melting, and mass transport due to chemical reactions.

As the FIMESH sub-module does not support generation of finite element mesh for movable bed boundaries, two subroutines were provided to generate coordinates of the nodal points and to define nodal connectivities in the three-dimensional computation domain. The subroutine USRNOD is used to generate nodal coordinates of the finite element mesh. In the first cycle of the Profile Model (see Section 5.5) all nodal coordinates were generated using analytical formulae. In all other cycles the bed coordinates were generated using the subroutine SEDIM which returns the new bed profile, after time Δt, according to the method described in Section 5.5.

In FIDAP the finite elements are input in groups. In any element group, all elements are by definition of the same type (fluid, solid, boundary etc.) and the same geometry (Quadrilateral, Brick, etc.) with the same velocity-pressure approximation.

The three-dimensional flow domain was first divided into a set of 8 node brick elements. Boundary elements are used to impose boundary conditions such as law of the wall boundary conditions in the case of the K-Epsilon model. All wall boundaries were divided into quadrilaterals with 4 nodes.

In order to decide an optimum size for elements, flow simulation was carried out initially for several mesh configurations, starting from a coarse mesh with 620 elements to a finer mesh with 3968 elements. As the computation time needed to solve the equations is relatively large for a finer mesh, a compromise had to be made between the accuracy and the

computation time before selecting the following dimensions. The longitudinal direction was divided into 31 elements of length 250 mm each and the transverse direction consisted of 8 elements of width 150 mm each. The vertical direction was divided into 8 elements, the dimensions of which were decreased towards the bed to provide a greater resolution in the zone where large velocity gradients exist. The solution domain, as shown in Figure 5.1, thus consisted of 1984 brick-elements of 8 nodes each and 2592 nodal points.

The details about how the elements are connected in each element group is provided in the subroutine USRELM. To minimize the size of the global system matrix formed in solution phase, FIDAP adopts the convention of numbering in the directions starting from minimum mesh dimension to the maximum mesh dimension. Accordingly, numbering of the elements and nodes started from the origin and proceeded along the vertical(z), offshore(y), and longshore(x) directions respectively.

The user supplied subroutines USRNOD and USRELM are given in Appendices C and D.

5.3.1.2 Boundary Conditions

The boundary conditions applied to the fluid include:

- specified velocities.
- specified turbulent kinetic energies(K).
- specified dissipations(ϵ).

Details about specified boundary conditions have been described in Section 5.2.3.

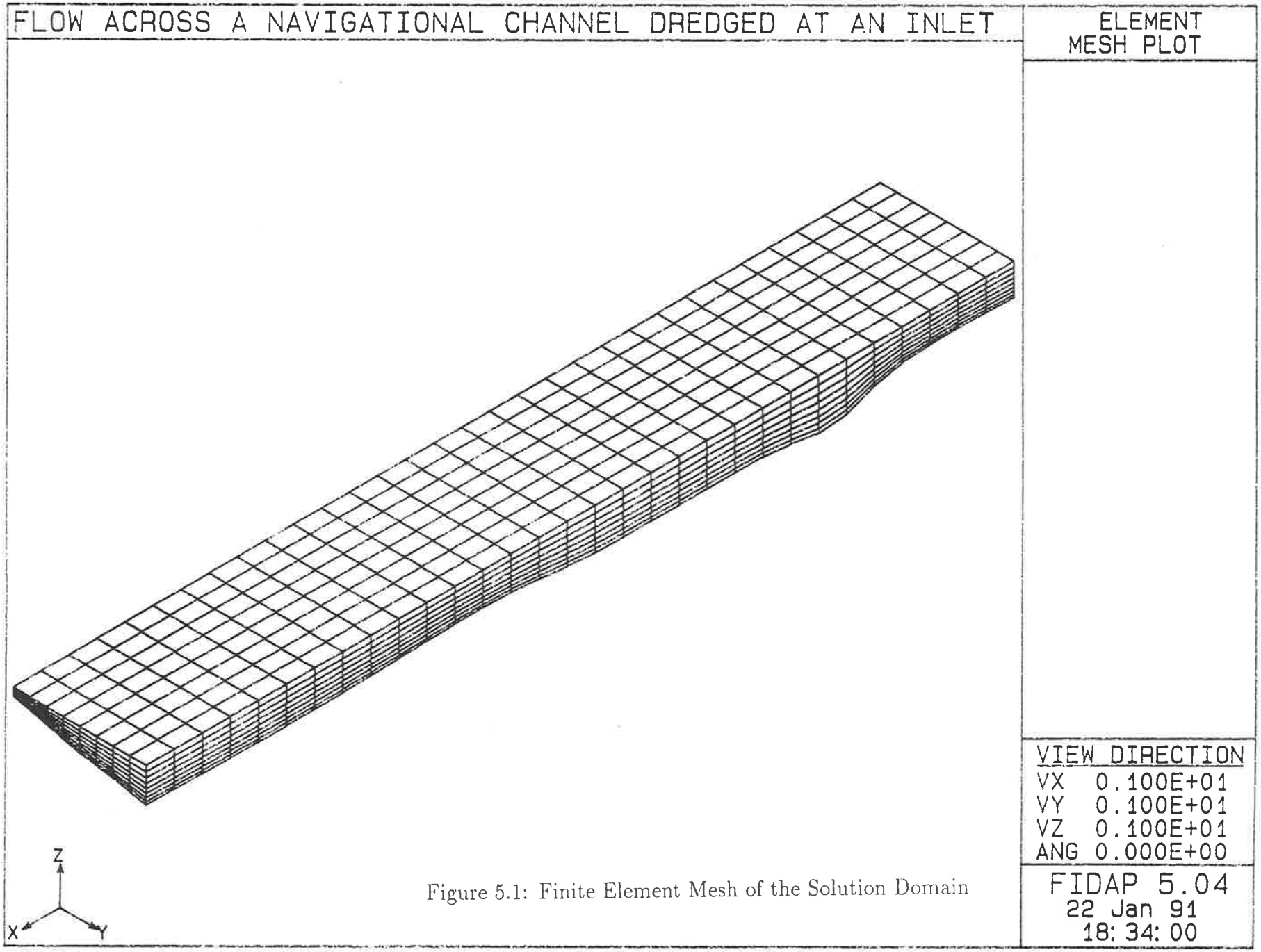

Figure 5.1: Finite Element Mesh of the Solution Domain

5.3.1.3 Initial Conditions

Initial conditions should be specified for velocities, turbulent kinetic energies and dissipations. These values serve as initial guesses for the iterative solution procedure. It was observed that a good estimates of initial values are very important for convergence to be achieved. FIDAP has a complete restart capability; that is, the initial conditions for a run can be the values obtained as the output of a previous run. Therefore, once the solution converged for a set of initial values, the restart capability was used for all subsequent runs.

5.3.1.4 Fluid Properties

The user is required to supply numerical values of the physical properties that relate to the problem being studied. Following data is used in the flow simulation models.

fluid density,	γ	=	1000.0 kg/m^3
kinematic viscosity,	ν	=	1×10^{-6} m^2/sec
turbulence constant,	c_μ	=	0.09
empirical constant,	$c_{1\epsilon}$	=	1.44
empirical constant,	$c_{2\epsilon}$	=	1.92
empirical constant,	σ_K	=	1.00
empirical constant,	σ_ϵ	=	1.30
von Karman constant,	k	=	0.41
van Driest's constant,	A	=	26.00

5.3.1.5 Programme Control Specification

The information given in programme control specification is referred to as commands or control cards. The FIPREP control cards specify infor-

mation for the execution of the FIDAP module. The control cards can be divided into a number of different functional sections, each of which specifies a particular type of data.

- Master Control Cards

  The Master Control Cards determine the type of analysis to be performed by FIDAP. The options selected in this section completely determine the mode of execution of FIDAP. The Master Control Cards include: *DATAPRINT, *EXECUTION, *PRESSURE, *PROBLEM, *SOLUTION, etc.

- Solution Detail Control Cards

  These control cards, such as *ITERATION, *PRINTOUT, control functions of the program which needs to be performed at selected time steps of the solution process.

- Nodal Data Control Cards

  These control cards, such as *NODES, *RENUMBER, *ORIGIN, are used to input the coordinates of the nodal points in the mesh discretization.

- Boundary Condition Data Control Cards

  The control cards in this section are used to specify the various boundary conditions for the model. The Boundary Condition Control Cards include: *BCNODE, *BCSYSTEM, etc.

- Fluid Properties Data Control Cards

  These control cards, such as *DENSITY, *VISCOSITY, etc., are used to input the values of various fluid properties.

- Element Group Data Control Cards

  The control cards in this section, such as *ELEMENTS, are used to specify the element type and to input nodal connectivity for the elements.

5.3.2 Creating FIDAP Input

The FIDAP program module uses the least number of files of the three modules. For the mixing length model the user has to supply the subroutine, USRMXL, which returns the values of mixing length, as described in Section 5.2.2, for each element.

The user supplied subroutine USRMXL is given in Appendix-E .

5.3.3 Convergence Criteria

If a solution based on a particular non-linear iterative method is to be effective, appropriate criteria must be used to terminate the iteration. At the end of each iteration, the solution obtained should be checked to see whether it has converged within preset tolerances or whether the iteration is diverging.

In FIDAP, in the case of segregated solver, iteration is terminated when the following convergence criteria is satisfied:

$$\frac{\|U_i - U_{i-1}\|}{\|U_i\|} \leq DTOL$$

where,

U_i = solution vector for iteration i,

U_{i-1} = solution vector for iteration i-1,

DTOL= convergence tolerance.

The norm $\|.\|$ is a root mean square norm summed over all the equations for the model. The above convergence criteria is computed separately for each degree of freedom being solved for, i.e., the vector U comprises all the nodal values of a particular degree of freedom. Convergence is considered to be obtained when all of these norms are simultaneously less

than the specified tolerance, DTOL. The recommended value for DTOL for the segregated solver is 0.001.

5.4 Sand Transport Model

When the velocity field is obtained from the flow simulation model, FIDAP, the sand transport is calculated using the Sand Transport Model. The model considered is basically similar to what was used by Hillier and Jenkins (21).

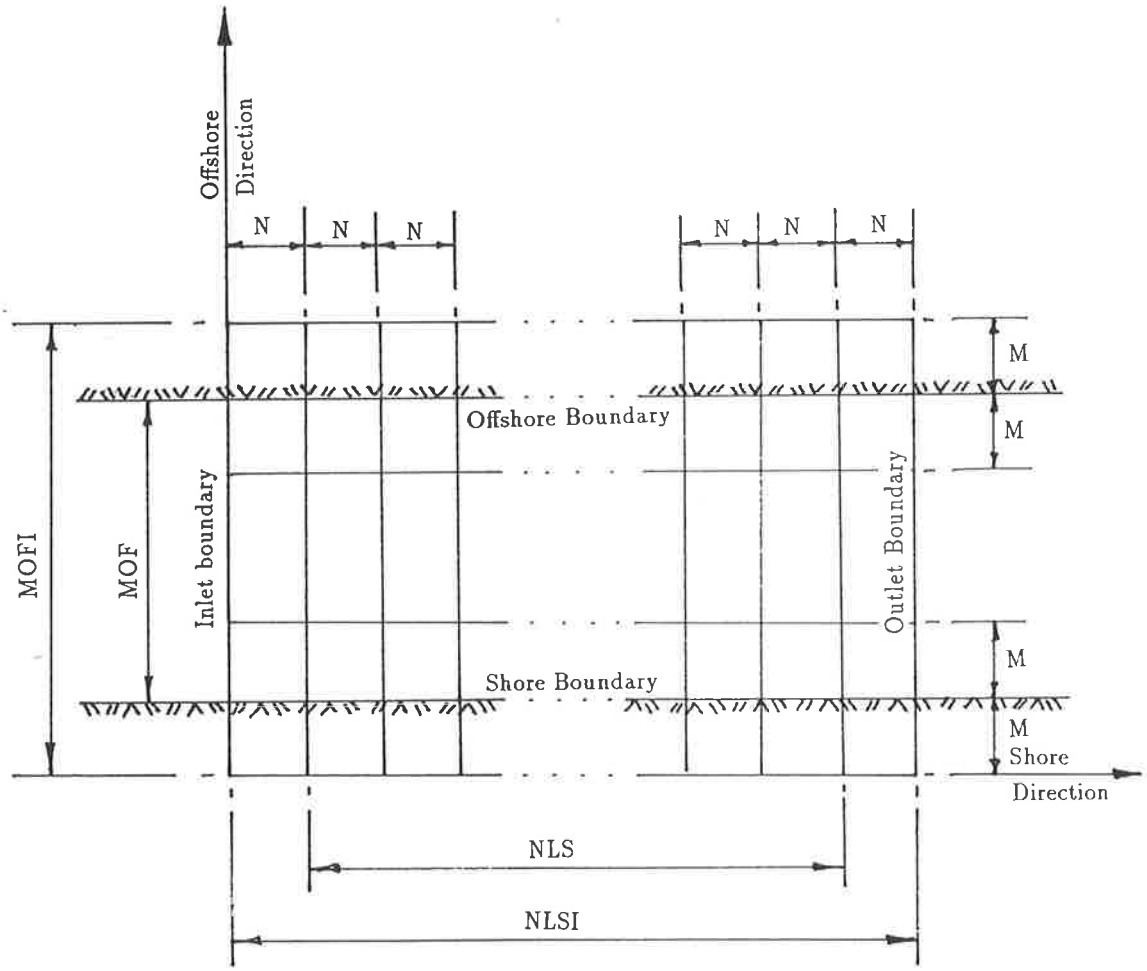

Figure 5.2: Grid System of the Sand Transport Model

As shown in Figure 5.2, the model zone was divided into a grid system on the horizontal plane, the longshore and offshore directions being divided into equal number of sections as used in the mesh for FIDAP.

MOF = number of cells in the offshore direction,
= 8
MOFI = MOF + 2
NLS = number of cells in the longshore direction,
= 31
NLSI = NLS + 2

The nodal velocities obtained from FIDAP are then used to calculate the sand movement in each cell. The program was devised to distribute these sand movements throughout the grid and produce a new bottom profile.

For the purpose of comparison, two different formulae were used to calculate the sand transport. In the first method, Shield's (46) bedload formula and in the second method a new approach to calculate sediment transport proposed by Ackers and White (1) was used.

5.4.1 Shield's Formula

Shield's Bedload Formula for calculation of sand transport, is based on the assumption that shear stress is the main parameter defining sediment transporting power, and can be written as follows:

$$\frac{q_s\,\gamma_s}{q\,S\,\gamma} = 10\frac{\tau_0 - (\tau_0)_{cr}}{(\gamma_s - \gamma)\,d} \tag{5.8}$$

where,

q_s = bedload rate in volume per unit time and unit width,

q = rate of liquid in volume per unit time and unit width,

S = slope of the energy grade line,
γ = specific weight of liquid,
γ_s = specific weight of sediment,
τ_0 = shear stress,
$(\tau_0)_{cr}$ = critical shear stress at which sediment particles are about to move,
d = d_{50} = mean particle diameter.

The rate of liquid flow can be related to the mean flow velocity as,

$$q = UT \times H \tag{5.9}$$

in which,

UT = mean flow velocity,
H = depth of flow.

The bed shear stress can be calculated from (20),

$$\tau_0 = \gamma\, H\, S \tag{5.10}$$

The critical bed shear stress, (kg/m^2), can be related to the mean particle diameter(meters) as (28),

$$(\tau_0)_{cr} = 192.65\ d \tag{5.11}$$

When equations 5.9, 5.10 and 5.11 are substituted, equation 5.8 will be reduced to the form,

$$q_s = 10\frac{UT.H.S.\gamma}{\gamma_s}\left[\frac{\gamma.H.S - 192.65\ d}{(\gamma_s - \gamma)\, d}\right] \tag{5.12}$$

Substitution of known values for γ, γ_s and d in equation 5.12 will yield:

$$q_s = 9.573\ UT.H.S\,(995.38\ H.S - 0.04624) \tag{5.13}$$

in which,

$$\begin{aligned} \gamma &= 1000.0\ kg/m^3 \\ \gamma_s &= 2650.0\ kg/m^3 \\ \mathrm{d} &= d_{50} = 2.4 \times 10^{-4}\ meters \end{aligned}$$

The slope of the energy grade line can be expressed in metric units (for Manning's $n = 0.025$) as (20),

$$S = \frac{0.0006 \times UT^2}{H^{\frac{4}{3}}} \tag{5.14}$$

Therefore when the values of UT and H are known, the sediment transport can be calculated using equations 5.13 and 5.14.

5.4.2 Method Proposed by Ackers and White

There has been an academic preference for shear stress as the main parameter defining the sediment transporting power. However, the total shear on a deformed bed (rippled or duned) is in part composed of the along-stream components of the normal pressure on the irregular bed profile. Although these normal pressures may contribute indirectly to sediment motion through suspension, many methods separate the bed shear into the nontransporting form loss and the shear on the grains. As the rate of transport is very sensitive to transporting power, inaccuracy in this separation procedure may give large errors of prediction. In engineering practice, this factor is important because few natural streams have a plane bed. Based on this criteria Ackers and White (1) has proposed a method, that use average stream velocity in preference to shear stress, to calculate transport of noncohesive sediment by a steady uniform flow. This method can be summarized as follows:

A dimensionless expression for grain diameter has been derived by elim-

inating shear stress from the two Shields parameters (46) as,

$$D_{gr} = D\left[\frac{g\,(s-1)}{\nu^2}\right]^{\frac{1}{3}} \tag{5.15}$$

in which,

D_{gr} = Dimensionless grain diameter,
D = D_{50} = Sediment diameter,
ν = kinematic viscosity,
g = acceleration of gravity.

A sediment mobility number has been defined by assuming the sediment mobility is given by the ratio of the appropriate shear force on unit area of the bed to the immersed weight of a layer of grains.

$$F_{gr} = \frac{v_*^n}{\sqrt{gD\,(s-1)}}\left[\frac{v}{\sqrt{32}\log\left(\frac{\alpha H}{D}\right)}\right]^{1-n} \tag{5.16}$$

where,

F_{gr} = sediment mobility number,
v_* = shear velocity,
v = mean velocity of flow,
H = mean depth of flow,
n = a constant the value of which depends on sediment size,
α = a constant relating the grain roughness to the median sediment diameter, D.

A dimensionless expression for sediment transport rate has been derived as,

$$G_{gr} = C\left(\frac{F_{gr}}{A} - 1\right)^m \tag{5.17}$$

where,

G_{gr} = dimensionless sediment transport rate,

C = a constant,

A = initial motion parameter,

= value of F_{gr} at initial motion,

m = a constant.

The sediment transport rate has been related to G_{gr} by,

$$X = G_{gr}\, s\, \frac{D}{H} \left(\frac{v}{v_*}\right)^n \tag{5.18}$$

where,

X = sediment transport, mass flux per unit mass flow rate,

s = mass density of sediment relative to that of fluid.

When transformed to volume rate per unit time per unit width,

$$q_s = \frac{X}{s}\, v\, H \tag{5.19}$$

where,

q_s = sediment transport rate; in $m^3/sec/m$,

Based on analysis carried out using extensive experiments a value of 10 has been suggested for the constant α and the parameters n, m, A and C used in the equations 5.16 & 5.17 have been related to the dimensionless grain diameter as,

$$n = 1.00 - 0.56 \log D_{gr}$$

$$A = \frac{0.23}{\sqrt{D_{gr}}} + 0.14$$

$$m = \frac{9.66}{D_{gr}} + 1.34$$

$$\log C = 2.86 \log D_{gr} - (\log D_{gr})^2 - 3.53$$

Substitution of known values for D ($240\mu m$), s (2.65), g ($9.753\ m/sec^2$) and ν ($1 \times 10^{-6}\ m^2/sec$) in equation 5.15 will yield:

$$D_{gr} = 6.0593$$

Substitution of the value of D_{gr} in the equations for parameters of n, A, m and C will yield:

n = 0.5618
A = 0.2334
m = 2.9343
C = 0.0125

The shear velocity can be defined as,

$$v_* = \sqrt{g\ H\ S} \tag{5.20}$$

where,

S = slope of the energy grade line,
H = mean depth of flow.

The slope of the energy grade line can be expressed in metric units (for Manning's $n = 0.025$) as (20),

$$S = \frac{0.0006 \times v^2}{H^{4/3}} \tag{5.21}$$

Substitution of equation 5.21 in 5.20 will yield:

$$v_* = \frac{0.0781 \times v}{H^{1/6}} \tag{5.22}$$

Substitution of the values of n, A, m, C, v_* and α in equations 5.16, 5.17, 5.18 and 5.19 will finally yield:

$$q_s = 1.2567\times10^{-5}.v.H^{0.0936}\left[\frac{7.7019\ v}{H^{0.0936}\left[\log 10\left(4.1667\times10^{-4}H\right)\right]^{0.4382}}-1\right]^{2.9343} \quad (5.23)$$

Therefore, when the values of the mean velocity (v) and the mean depth of flow (H) are known the sediment transport can be calculated using equation 5.23.

For calculation of sediment transport rate, depth averaged velocities were used in the Sand Transport formula. Therefore, the nodal velocities obtained from the FIDAP were first converted to depth averaged nodal velocities. These depth averaged nodal velocities were then converted to cell velocities in longshore and offshore directions. Using the Sand Transport formula, the rate of sediment transport was calculated in longshore and offshore directions for each cell.

Thus, if just one cell is considered, (figure 5.3) its sediment transport components can be averaged with those of the surrounding cells, as described in Section 5.4.4, to obtian the boundary flow.

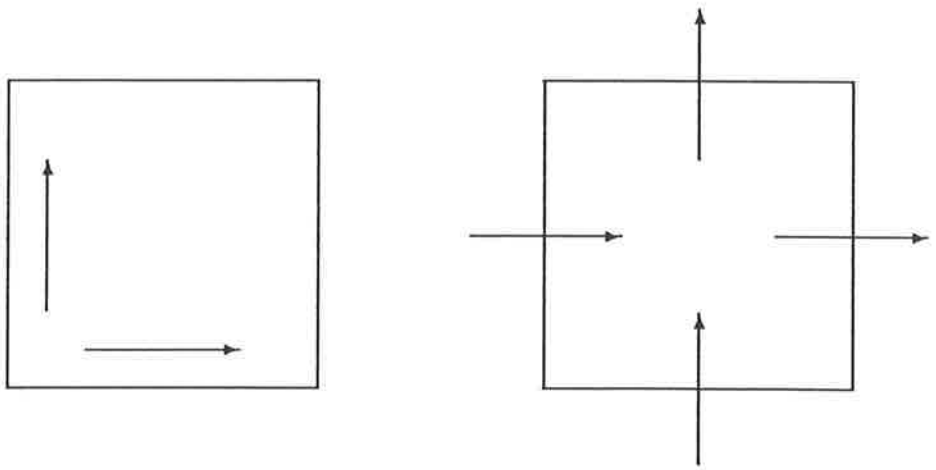

Figure 5.3: Sediment Transport Components in a Cell

The sand movement within the cell is then the difference between the

transport rates into the cell and the transport rates out of the cell. Thus, if the nett movement is positive, the cell is accreting and the negative net movement means the cell is eroding.

The sediment movement is actually a volume rate per unit time per unit width. Therefore, multiplication by the cell width and an appropriate time interval will yield the volume change of sand. Then simply dividing by the cell area will give the change in depth of the cell.

5.4.3 Boundary Conditions for the Sand Transport Model

Following boundary conditions were used in the Sand Transport model.

5.4.3.1 Inflow Boundary

At the inflow boundary it was assumed that the rate of sediment transport in longshore direction was equal to the rate of sediment transport in the first cell in the same direction (figure 5.4).

$$SANDX(1,J) = SANDX(2,J)$$

$$H(1,J) = H(2,J)$$

where,

$SANDX(I,J)$ = sediment transport in cell(I,J) in longshore direction,

H = depth of the cell,

J = 2 to MOF+1.

5.4.3.2 Outflow Boundary

Similar to the inflow boundary, at the outflow boundary the rate of sediment transport in longshore direction was assumed to be equal to

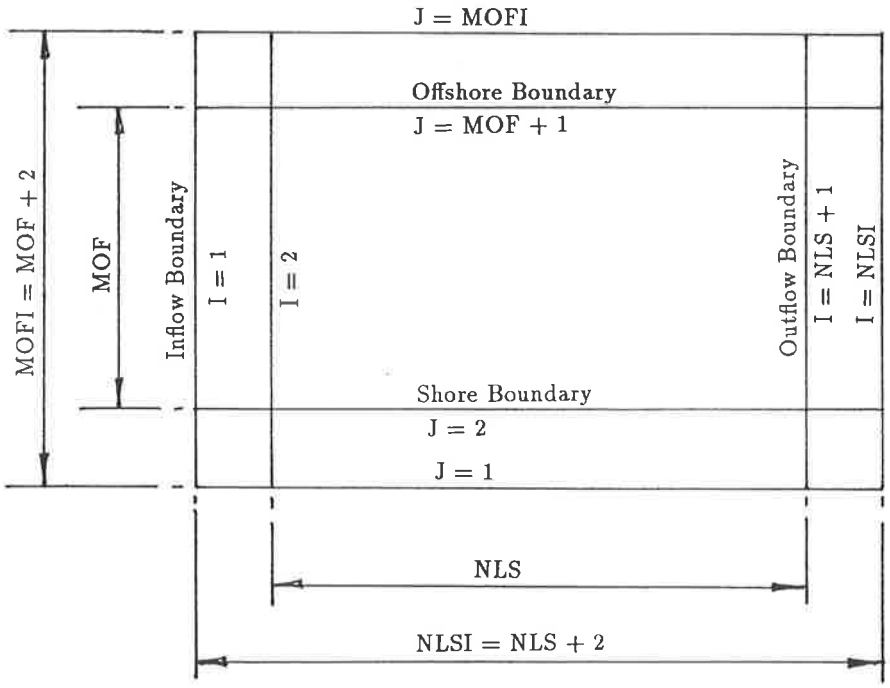

Figure 5.4: Boundaries of the Sand transport Model

the rate of sediment transport in the last cell in the same direction.

$$SANDX(NLSI, J) = SANDX(NLS + 1, J)$$

$$H(NLSI, J) = H(NLS + 1, J)$$

in which,

J = 2 to MOF+1

5.4.3.3 Shore Boundary

At the shore boundary, the rate of sediment transport in the offshore direction was assumed to be zero.

$$SANDY(I, 1) = 0.0$$

$$H(I,1) = H(I,2)$$

where,

$SANDY(I,J)$ = sediment transport in the cell(I,J) in offshore direction,

I = 2 to NLS+1

5.4.3.4 Offshore Boundary

Similar to the shore boundary, the rate of sediment transport in the offshore direction was assumed to be zero.

$$SANDY(I,MOFI) = 0.0$$

$$H(I,MOFI) = H(I,MOF+1)$$

in which,

I = 2 to NLS+1

5.4.4 Calculation of Sediment Transport Rate

With reference to the Figure 5.5 following variables are defined:

$U(I,J)$ = cell velocity in longshore direction,

$V(I,J)$ = cell velocity in offshore direction,

$UT(I,J)$ = total cell velocity,

$SAND(I,J)$ = total cell sand transport rate,

$THETA$ = $\tan^{-1}[V(I,J)/U(I,J)]$

$SANDX(I,J)$ = $SAND(I,J)\cos(THETA)$,

$SANDY(I,J)$ = $SAND(I,J)\sin(THETA)$.

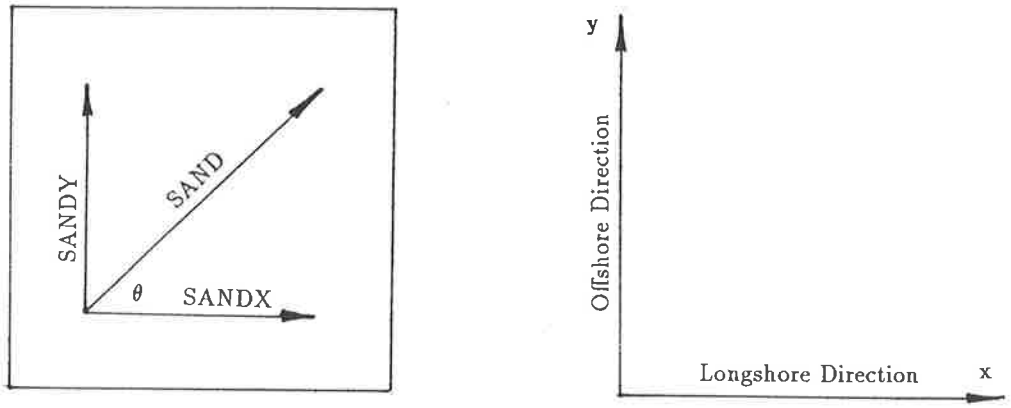

Figure 5.5: Sediment Transport in a Cell

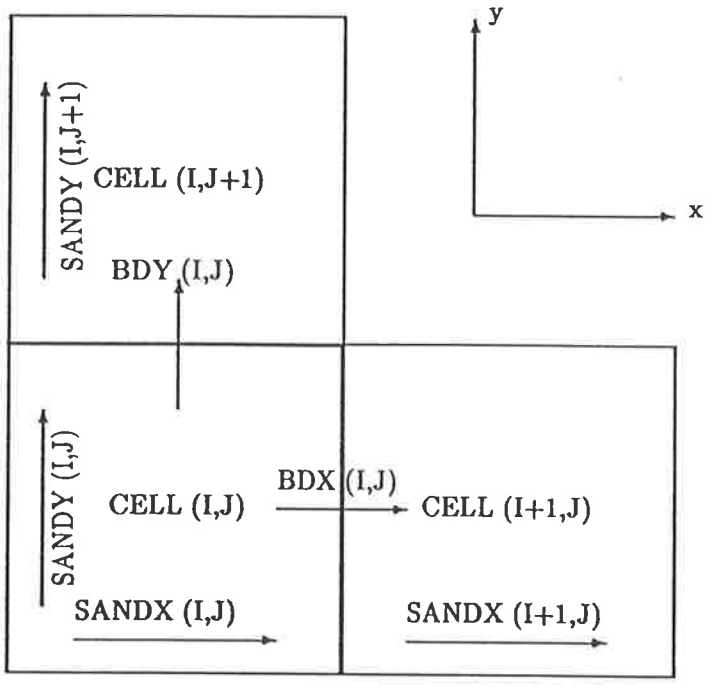

Figure 5.6: Cell Edge Flow

With reference to Figure 5.6:

Cell edge flow in longshore direction $= BDX(I,J)$

$= \frac{1}{2}.[SANDX(I,J) + SANDX(I+1,J)]$

Cell edge flow in offshore direction $= BDY(I,J)$

$= \frac{1}{2}.[SANDY(I,J) + SANDY(I,J+1)]$

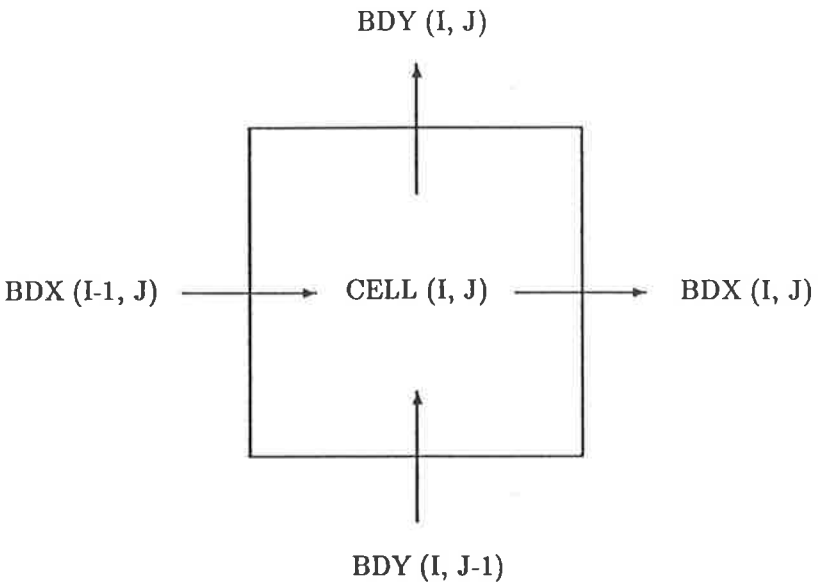

Figure 5.7: Nett Sand Transport in a Cell

With reference to Figure 5.7:

Net longshore sand transport in cell(I,J) $= XMOVE(I,J)$

$= BDX(I-1,J) - BDX(I,J)$

Net offshore sand transport in Cell(I,J) $= YMOVE(I,J)$

$= BDY(I,J-1) - BDY(I,J)$

The amount of Erosion or Deposition in Cell(I,J) = RISE

$= [M.XMOVE(I,J) + N.YMOVE(I,J)].MTA/AREA$

where,

M,N = width of cell(I,J) in longshore and offshore directions respectively,

AREA = M . N ,

MTA = time period for which the sand transport is calculated.

New Depth of Cell(I, J) = $H(I, J)$ - RISE

5.5 Profile Model

Using a flow simulation model (FIDAP) described in Section 5.2 and a Sand Transport Model described in Section 5.4 a Profile Model, as shown in the Flow Chart in Figure 5.8, was developed for morphological evolution of the shore area. The constituents of the Profile Model are as follows:

- The initial bed profile of the area under consideration is measured or decided.
- A known flow field is established over the area under consideration.
- The velocity field in the computation domain is numerically simulated using Mixing Length model, FIDAP.
- Rate of transport of sediment due to known velocity field is calculated using the Sand Transport Model.
- Change of bed profile due to transport of sediment for a time period Δt is calculated and the new bed profile is obtained.

The steps mentioned above constitutes a complete cycle of the Profile Model. The new bed profile obtained after time Δt is then used as the initial profile for the next cycle. This procedure is continued until sufficient number of cycles are completed over the required time period for which morphological evolution of the shore area is to be determined.

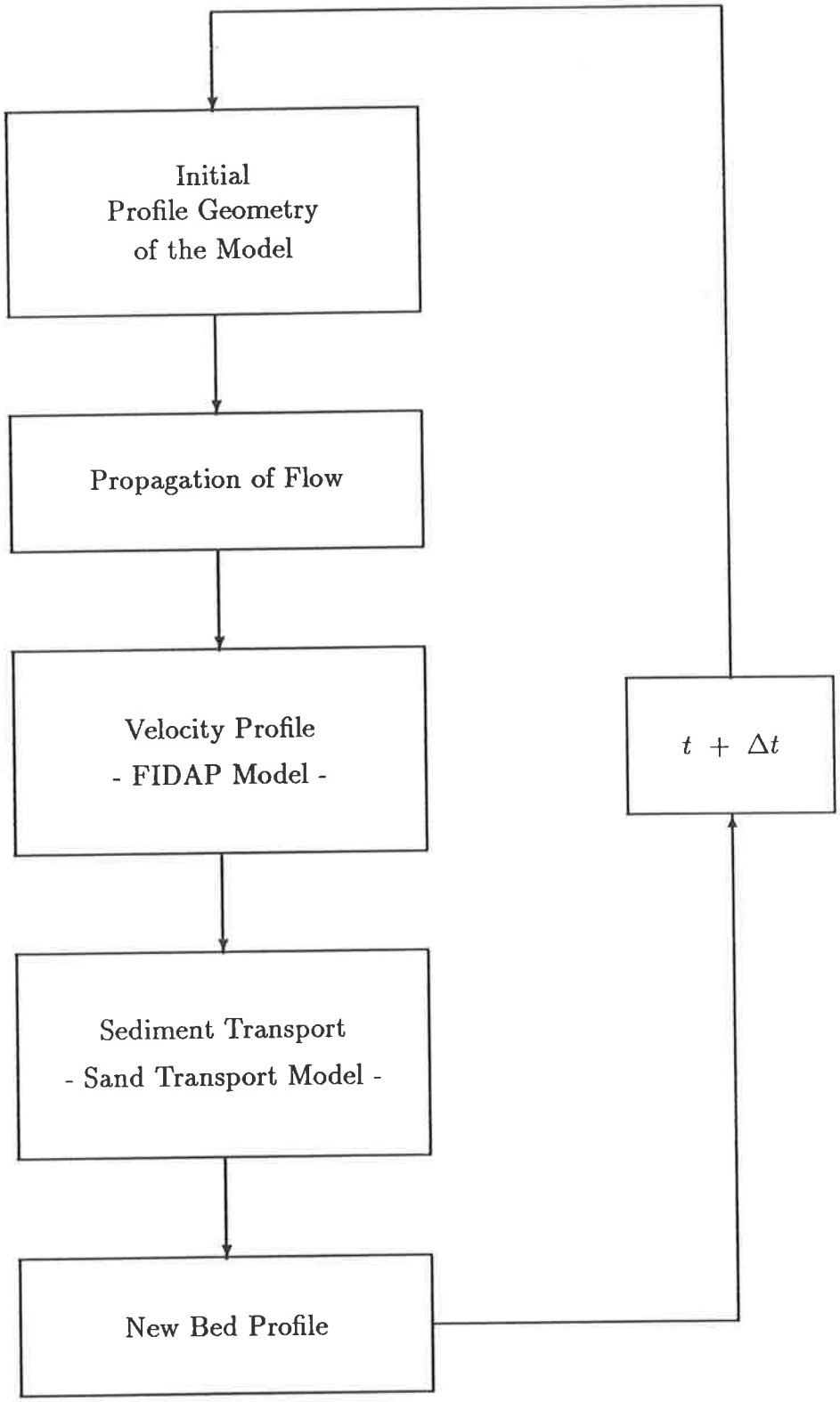

Figure 5.8: Flow Chart of the Profile Model

In the flow simulation model of this study, for the sake of simplicity, it was assumed that the flow across the channel is steady, even though it will never be steady in actual practice.

However, when the flow details are known sediment transport caused by any arbitrary flow, such as tidal flow, could still be modelled using the profile model by approximating the actual flow to be equivalent to a set of steady currents as shown in Figure 5.9. In the example shown in

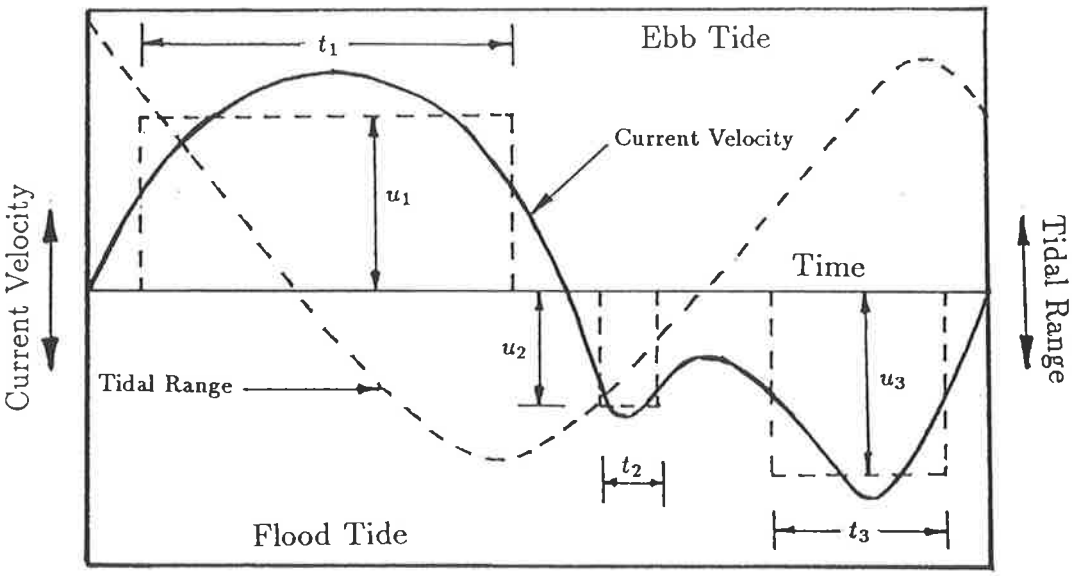

Figure 5.9: Representation of the Tidal Flow by a set of Steady Currents

Figure 5.9, the mean tidal cycle has been schematized to 3 quasi-steady flow periods of t_1, t_2 *and* t_3 hours each. The periods with small velocities below initiation of sediment motion near slack tide can be neglected.

The Fortran program written to read the velocity components from the output file, FDOUT, of the flow simulation model, FIDAP, and to calculate the sand movement and the new bed profile is shown in Appendix-C.

Chapter 6

Results and Discussion

6.1 Introduction

When a littoral current on a coastline passes over a dredged channel, the sediment transport capacity decreases and a certain amount of the transported sediment in motion will be deposited in the channel. An accurate sedimentation prediction can be obtained from a detailed mathematical approach modelling all relevant phenomena such as the increased turbulence generated by the decelerated flow, the current and wave-related mixing process and the intensified pick-up of bed material by the re-accelerated flow.

An attempt to set up a mathematical theory of sedimentation should take into account both the character of the sediment and the character of the fluid motion. The K-Epsilon model is considered as the best mathematical model available at present to represent turbulent flow. Any mathematical model to represent sediment transport should take into account the movement of sedi-

ment by both suspension and bed load. As discussed in Chapter 3 the movement of sediment in suspension is best described by the complicated diffusion-convection equation. Therefore, if the K-Epsilon model can be coupled with the diffusion-convection equation and a bed load formula, one can expect a very good mathematical model to represent sediment transport in turbulent flow. However, for long term morphological computations implying the successive computation of the flow field, the use of K-Epsilon model or the complicated diffusion-convection equation is still not attractive because of the limitations of available computer resources. To overcome this problem various mathematical models have been proposed by combining the simplified diffusion-convection equation with comparatively simple flow models. The SURTRENCH model presented in Section 3.6 is one such model which has been tested and verified extensively.

An important factor of this study was to assess the computational feasibility of attempting to solve this complex problem by using two discrete numerical models, an advanced turbulent flow model coupled with a simple (compared to the diffusion-convection equation) sand transport model, as described in Chapter 5. For comparison two turbulent models, the sophisticated K-Epsilon model and the Mixing Length model, were used to represent turbulent flow in the channel. To solve the differential equations in these models a powerful and fast computer software package (FIDAP) was used.

The flow and connected transport process was discretized into a number of cycles of duration Δt and in each cycle the flow model was coupled with a sand transport model, as described in Section 5.5, to simulate sand transport. For comparison two numerical models, a simple bed load formula and a total load formula, were used to represent sand transport. Computed flow velocities and sand transport in the channel have been compared against measured values in Sections 6.4 and 6.5 respectively.

6.2 Accuracy of the Velocity Measurements

As transport rates are critically dependent upon velocity it was felt desirable to check flow and velocity measurements with due care. Accuracy of the velocity measurements carried out using Laser-Doppler velocity measuring equipment and the measured flow at the weir box could be verified by comparing the flow through the model measured at the weir with the flow computed using measured velocities deduced from laser doppler equipment.

For measurement of flow through the model a weir box was installed at the downstream end as shown in Figure 4.4 (page 62). The flow over the Triangular sharp-crested weir was computed using the following formula (18):

$$Q = \frac{8}{15} C_e \sqrt{2g} \tan\left(\frac{1}{2}\theta\right) h_e^{2.5} \tag{6.1}$$

in which,

Q	=	discharge (cusecs),
C_e	=	effective discharge coefficient,
θ	=	notch angle,
h_e	=	effective head at the weir (ft),
	=	$h_1 + K_h$
h_1	=	head at the weir,
K_h	=	a constant,
g	=	acceleration of gravity.

The coefficients C_e and K_h are related to the notch angle θ and has been presented in graphical form in (18). For $\theta = 90^0$ the corresponding values can be obtained from these graphs as, $K_h = 0.0027$ ft and $C_e = 0.578$.

Substitution of the known values (h_1=303mm) in equation 6.1 will yield,

$$Q = 2.45 \text{ cusec} = 0.069\ m^3/sec$$

In evaluation of the flow using measured velocities, depth integrated flow velocities were used.

Flow computed using measured velocities at the inlet boundary = 0.072 m^3/sec (only 4.3% more than the measured flow)

Flow computed using measured velocities at the outlet boundary = 0.068 m^3/sec (only 1.4% less than the measured flow)

The flow through the model computed using measured velocity profiles at the inlet and outlet boundaries agreed quite well with the flow measured at the weir indicating that there was reasonable consistency between flows measured by these two methods. While the laser doppler velocities as measured at a point are very accurate, the problem of resolving these velocity components and integrating over the flow areas, can allow errors to creep into the evaluation of the total flow.

6.3 Convergence of the Flow Simulation Models

The solution of the nonlinear system of discrete equations arising from the steady-state Navier-Stokes equations represents the most time-consuming stage of the analysis and for medium to large problems can account for up to 80% of the total computer resources used. Therefore, the decision as to which solution algorithm to employ for this phase can govern and ultimately limit the size of the finite element model that can be treated.

It was observed that convergence of both turbulent models, K-Epsilon and Mixing Length, by the segregated method of solution were very sensitive to the prescribed initial conditions. Convergence could not be achieved unless the prescribed initial conditions were within the radius of convergence. Depending upon the solution strategy used, this radius of convergence can sometimes be quite small and care must be exercised in the choice of the initial conditions.

The fully coupled (successive substitution) solution approach described in Section 5.3 has a better radius of convergence. However, for the size of the finite element mesh used in the simulations (3-D, 1984 brick elements) the peripheral storage required for the global system matrix exceeded the available disk storage. Therefore, the segregated algorithm which is guaranteed to have substantially lower storage requirement compared to the fully coupled solver was used in the numerical simulations. The actual execution time will, in general, depend on the size and nature of the problem being solved and how close are the prescribed initial conditions to the actual solution within the radius of convergence. The solution obtained at a previous run often appears as a suitable set of initial conditions for these trials.

Because of two additional degrees of freedom (K and ϵ) involved, the K-Epsilon model required more iterations to converge to a solution than the Mixing Length model. Also, the CPU time required to perform one iteration in the K-Epsilon model was substantially higher compared to the Mixing Length model.

Starting from a set of estimated initial values the K-Epsilon model needed, for convergence to a convergence tolerance of 0.001, more than 70 iterations and about 1200 minutes (20 hours) of CPU time on a SUN-4 computer compared to 45 iterations and 230 minutes (less than 4.0 hours) of CPU time needed for the Mixing Length model. Therefore, on average the K-Epsilon model required more than 5 times computation time for convergence compared to the Mixing

Length model. As such, the K-Epsilon model would not be attractive for use in long term morphological computations.

As the number of iterations taken for convergence depend upon how close are the prescribed initial conditions to the actual solution, for the 36 runs of the FIDAP model completed to simulate 6.0 hrs of flow in the Profile Model, the number of iterations the Mixing Length model needed for convergence, with the restarting facility, varied from 69 to 4. The corresponding CPU time taken was 361 and 21 minutes respectively. To complete all 36 runs of the flow simulation model in the Profile Model, the total CPU time needed was 2763 minutes (46.0 hrs).

6.4 Computed Velocity Profiles

As the Laser-Doppler velocity measuring programme installed on the processing P.C. did not indicate the direction of the velocity, (the Bragg cell was not used), movement of dye particles were observed in order to determine the directions of the offshore velocity components at the inlet. However, as the inlet velocity components in the offshore direction were relatively small compared to the longshore components, dye particles moved rapidly in the downstream direction making a determination difficult. Therefore, in the first simulation, all offshore velocity components at the inlet were assumed to be in the offshore direction (positive y-direction). The computed velocity profiles using the mixing length model showed high velocities at the offshore end and negative or small velocities at the shore end which was caused by a strong secondary recirculation in the horizontal plane, as shown in Figure 6.1. Examination of the velocities in the inlet region indicated that the flow from the offshore region at the inlet drags into the shore region of the dredged channel to "fill" the space created in sudden increase in the depth of flow at the shore end from 70mm to

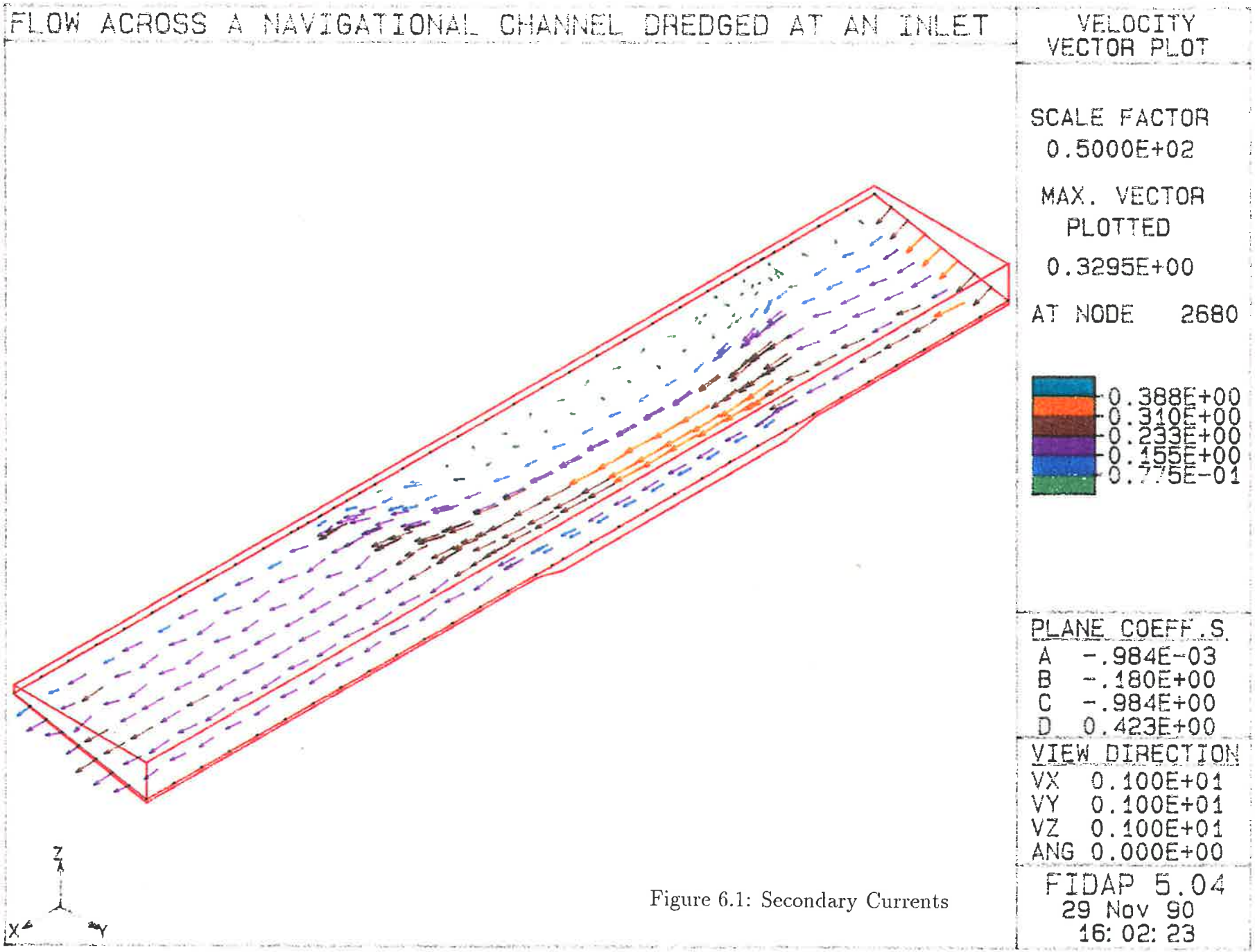

Figure 6.1: Secondary Currents

370mm. This shows that the inlet section is too close to the dredged channel and hence the flow velocities at the inlet are affected by the sudden increase in flow area at the shore end.

However, limitation of the space available in the hydraulic laboratory made it impossible to shift the inlet section any further upstream. As such, the directions of the measured offshore velocity components at the inlet were adjusted until the best agreement between the measured and computed velocity profiles were obtained at all four downstream velocity measuring sections.

Computed velocity profiles using the K-Epsilon and Mixing Length models have been compared against the measured velocities, at four downstream sections, in Figures 6.2 and 6.3.

6.5 Sand Transport Models

As mentioned already, the use of K-Epsilon model would not be attractive for long term morphological computations because of the relatively large computation time needed to solve the equations. Therefore, the Mixing Length Model was used to simulate flow in the flow simulation model which was coupled with the sand transport model in the Profile Model.

In the physical model the bed contours were recorded after 3.0 and 6.0 hrs. of continuous flow. The 6.0 hrs. time period was divided into 36 cycles of 10 minutes duration each and the Profile Model was executed as described in Section 5.5 for 36 cycles using Shield's formula and the method proposed by Ackers and White.

After 3.0 hrs. of flow new input velocities, as measured from the physical model, were prescribed to the flow simulation model.

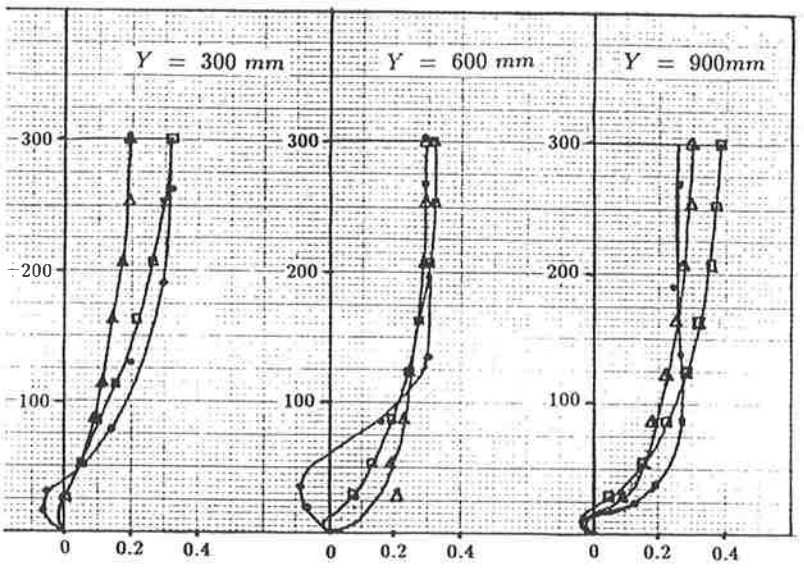

(a) At $X = 1.75m$

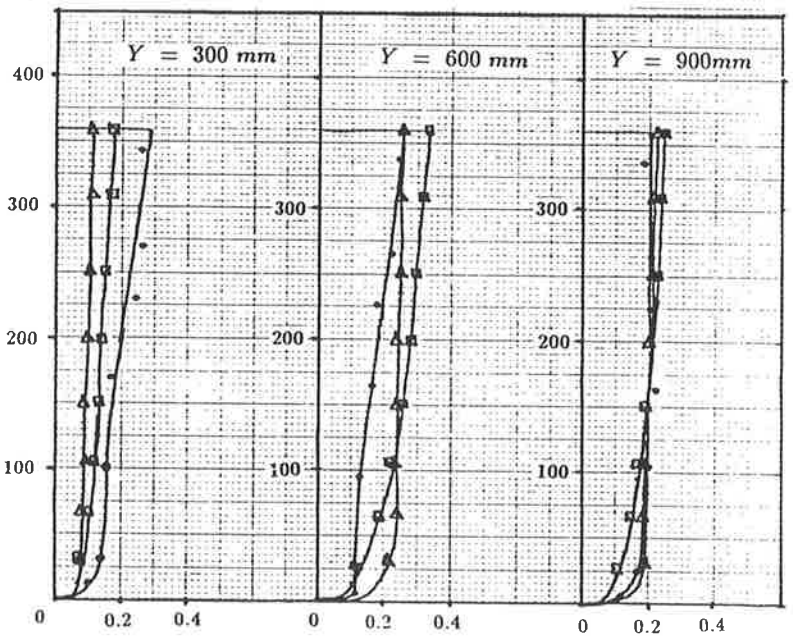

(b) At $X = 3.00m$

Measured

Computed Using K-E Model

Computed Using Mixing-Length Model

Figure 6.2: Measured and Computed Velocities

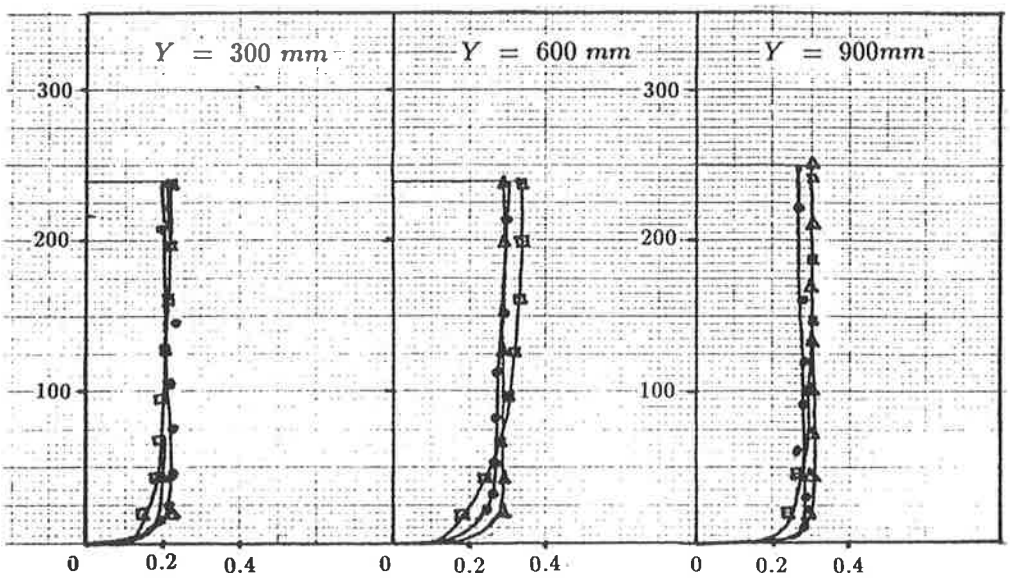

(a) At $X = 4.50m$

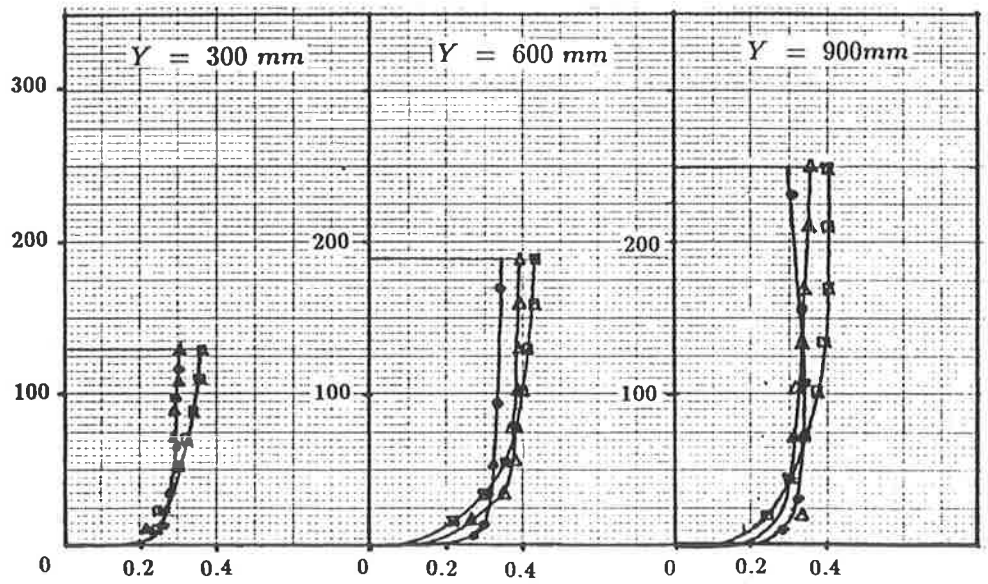

(b) At $X = 7.25m$

Measured

Computed Using K-E Model

Computed Using Mixing-Length Model

Figure 6.3: Measured and Computed Velocities(Continued)

As the source code for the FIDAP Module was not accessible to the user, it was not possible to couple the Sand Transport Model with the Flow Simulation Model to complete all 36 cycles continuously. Therefore, at the end of each cycle in FIDAP Module, the nodal velocities in the output file were used to create the new bed profile after the time interval MTA (10 minutes)and FIDAP Module was initiated manually again for the next cycle. As such all 36 cycles in FIDAP Module had to be initiated manually calculating the new bed profiles in between every two cycles. Since this was a very labour consuming exercise, reduction of the time interval, MTA, any further to improve accuracy would be at the expense of increased labour hours and also more computation time for running increased number of cycles.

Shield's formula over predicted sand movement and the simulation had to be stopped as the finite element mesh was distorted, as shown in Figure 6.4, after few cycles.

The bed profiles computed using Ackers and White method, after 3.0 and 6.0 hrs, have been compared against the measured values in Figures 6.5 and 6.6.

6.6 Discussion

Flow at an inlet is a very complex phenomena which cannot be represented in hydraulic terms without making suitable simplifications. In this study, the problem has been simplified by examining the flow and transport effects of a littoral current passing over the inlet channel. The following assumptions are made in this study:

- the transporting flow is assumed to be steady and across the dredged channel.

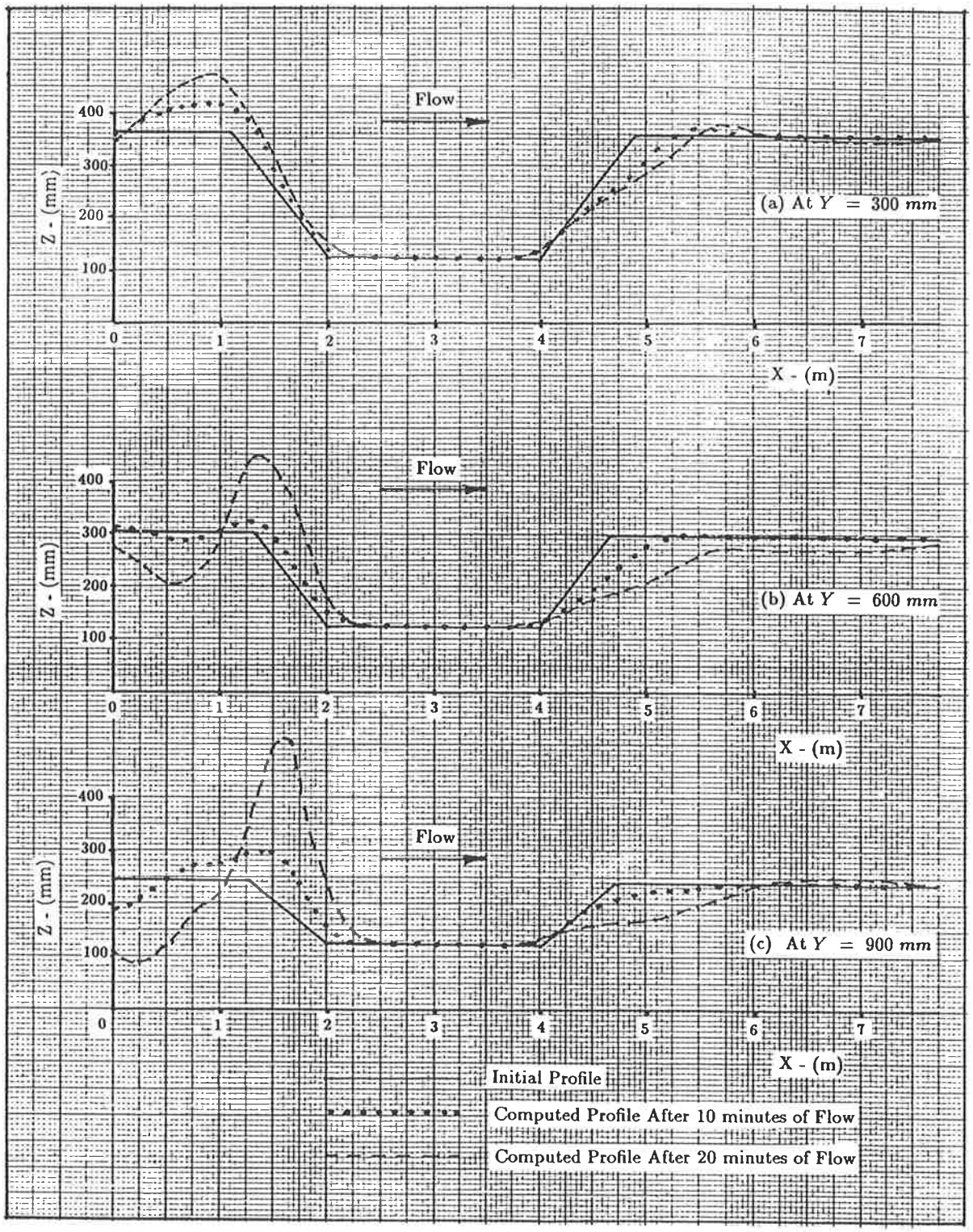

Figure 6.4: Longitudinal Bed Profiles Computed Using Shield's Formula

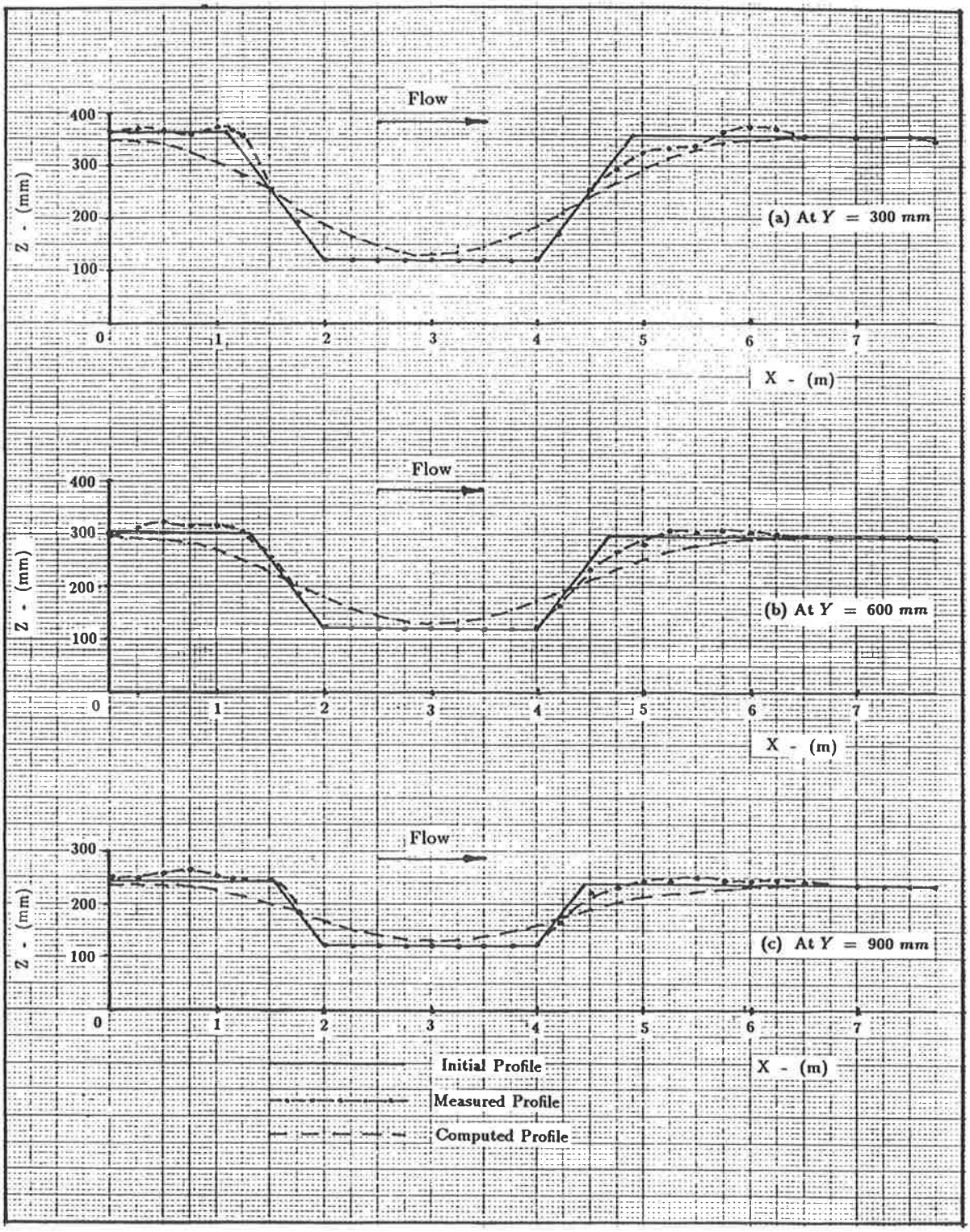

Figure 6.5: Longitudinal Bed Profiles Computed Using Ackers and White Method After 3.0 hours of Flow

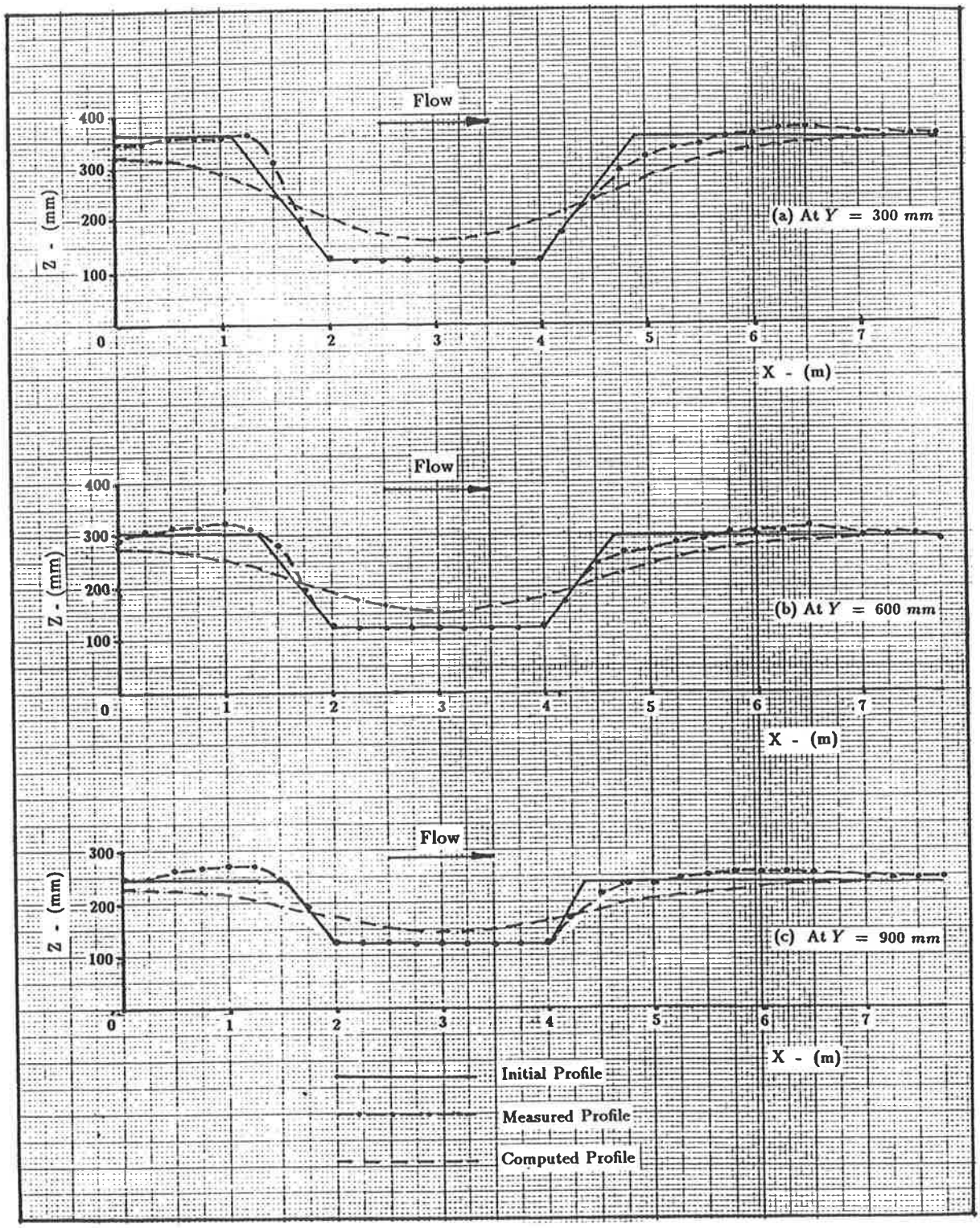

Figure 6.6: Longitudinal Bed Profiles Computed Using Ackers and White Method After 6.0 hours of Flow

- flow through the inlet has not been taken into account.
- wave action and connected parameters, such as wave refraction and defraction have not been considered.
- A wall boundary has been introduced at the shore-boundary to be able to divide the flow domain into a mesh of brick elements.
- a wall boundary has been introduced at the offshore-boundary to simplify the offshore problem.

Two turbulent models, the sophisticated K-Epsilon Model and the Mixing Length Model, were used to simulate the 3-dimensional flow across the channel.

In the sand transport models, the flow domain has been reduced to a 2-dimensional area on the horizontal plane, which has been divided into a set of cells. Sand transport within each cell was computed using depth averaged velocity in each cell. Therefore, the sand transport models are two-dimensional depth averaged models.

In both models, Shield's bedload formula and the method proposed by Ackers and White, when the other parameters are constant the rate of sand transport is a function of depth of flow and mean flow velocity. Therefore, accurate prediction of nodal velocities in the flow simulation model will govern the accuracy of the outcome of the sand transport models.

Given more time for this project it would have been interesting to attach more sophisticated transport models to match the excellence of the flow models and to integrate both flow and transport effects in a major combined simulation.

6.6.1 Flow Simulation Models

Measured and computed velocity profiles at four different downstream sections of the channel have been shown in Figures 6.2 and 6.3.

- (a) At X=1.75 m

  This section is located on the side slope of the dredged channel on the inlet side, Figure 4.4(b). As can be seen in Figure 6.2(a) an important observation that can be made is all computed and measured velocity profiles at all three transverse sections (y=300, 600 and 900 mm), except the computed profile of the K-Epsilon model at y=600 mm, clearly showed recirculation (reverse flow) closer to the bed. However, computed negative velocities were less than the measured values.

  Even though computed velocity profiles deviated from the measured values at certain locations, the performance of the numerical models, in general, were reasonably good compared to the computed velocities at a similar section of the trench in the flow simulation model used in the SURTRENCH- 2D model, Figure 3.6 (page 50).

- (b) At X=3.0 m

  This section is located at the center of the dredged channel. As can be seen in Figure 6.2(b), compared to the velocity at the section X=1.75 m, no reverse flow was shown by any of the profiles. In the measured velocity profiles at y=300 and 600 mm, a sudden change of the curvature was observed in the region of about 150 mm from the bed which is an indication of the influence of the nearby recirculation region. This is comparable with the measured velocities at a similar location of the SURTRENCH-2D model, Figure 3.6. However, both flow simulation models, K-E and Mixing Length, did not show such an influence indicating that in the numerical models the recirculation region is not close to this section.

At the section y=900 mm, the computed velocities of the K-E model were almost equal to the measured values.

- (c) At X=4.5 m

  This section is located on the side slope of the dredged channel on the downstream side, Figure 4.4(b). As this section is well away from the re-circulation region, all computed velocities were in reasonably good agreement with the measured values with the K-E model being more accurate than the Mixing length model.

- (c) At X=7.25 m

  This section is located on the downstream end of the flow domain very close to the outlet. Similar to the section at X=4.5 m, all computed velocities were in good agreement with the measured values with the K-E model being again more accurate.

In general, it was observed that at sections X=4.5 m and X=7.25 m the flow simulation models over predicted velocities.

Based on above mentioned observations it could be concluded that velocities predicted by both turbulent models agreed reasonably well with all measured velocities at four downstream sections, with the exception of a few sections in the recirculation region.

The K-Epsilon model, in general, predicted velocities closer to the measured values when compared to the Mixing Length Model. Specially, in the flow velocity measuring stations downstream of the dredged channel (i.e. at $x = 4.5$ and $x = 7.5m$) the K-Epsilon Model predicted velocities to a fairly good accuracy. Therefore, in cases where the calculated velocity field serves as an input for the modelling of sediment transport, the use of a refined turbulence model, such as K-E, seems more appropriate.

However, examination of computed velocities elsewhere in the flow domain revealed that the numerical models predicted higher velocities in the regions $y = 300$ to $y = 450$ mm and $y = 750$ to $y = 900$ mm from the inlet up to the dredged channel.

When the directions of the specified offshore velocity components were adjusted at the inlet until best agreement is obtained between measured and computed velocity profiles at all four downstream sections, it was observed that predicted velocities in the region from the inlet up to the dredged channel were very sensitive to the direction of inlet velocities in the offshore direction. However, it was also observed that change of the directions of offshore velocity components at the inlet did not have a significant effect on the computed velocities downstream of the dredged channel (i.e. $x = 4.5$ & $x = 7.25$ m).

As such, any inaccuracy caused by adjustment of inlet velocities in the offshore direction could have been avoided by shifting the inlet further upstream of the dredged channel.

Since computer resources required to solve the non-linear equations in the sophisticated K-E model are excessive, the use of K-E model still seems to be not very popular in the analysis of complicated 3-dimensional problems. Being one of the first commercially available three dimensional finite element fluid analysis computer software packages, it seems that the the K-E model in FIDAP is still being improved. The FIDAP package used at the beginning of this project had to be returned to the supplier in the USA in order to obtain the upgraded latest version of the package as problems were encountered initially in running the 3-dimensional K-Epsilon version. Due to this reason a considerable amount of time (some three months) was lost in attempts made to get the model running with the older version of FIDAP. When the latest version (version 5.04) of FIDAP was received, in which the problems encountered for 3-dimensional K-E model had been rectified, very limited time was left for numerical simulations

and completion of this project. As a result, the time factor did not allow detailed calibration of the numerical models, specially the K-E model which should have been calibrated for empirical constants used to improve model predictions. It has been experienced in previous research in this field that length of the recirculation region is very sensitive to certain empirical constants used in the equations of the K-E turbulent model.

The following assumptions made in making the numerical models would also have affected the accuracy of the predicted results.

- All wall boundaries, including the bed boundary, have been assumed to be fully rough (no-slip boundary condition).
- For specification of normal and tangential boundary conditions, the bed boundary has been assumed to be horizontal.

It is also expected that accuracy of computed velocities could be increased by having a finer mesh discretization, specially in the recirculation region.

After an investigation carried out at the Delft Hydraulic Laboratory (51) for the 2-dimensional SURTRENCH model, Section 3.6, to determine the influence of element size on the numerical accuracy, it has been recommended that;

- The grid has to be refined, as shown in Figure 6.7, in the horizontal direction around the expected point of separation.
- The length of the side slope of the dredged channel should be divided into at least 10 elements.
- The number of grid points in the vertical direction, with coordinates stretching towards the free surface, should not be smaller than about 10.

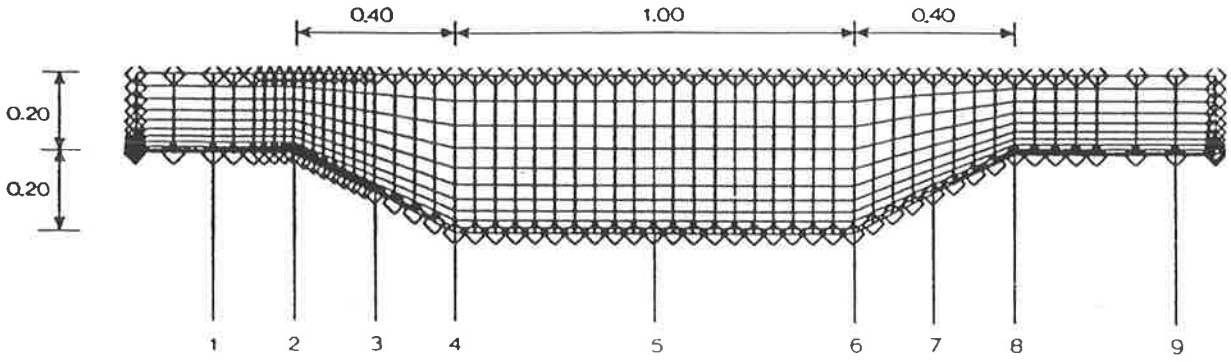

Figure 6.7: Trench dimensions (m) and grid size

However, in this experiment for the ease of calculating sand transport, the 2-dimensional element mesh in the sand transport model was divided into equal size elements (cells) in longitudinal (x) and transverse (y) directions. Further, in order to read directly from the FIDAP output file the flow velocities at the corners of these elements (cells) to calculate depth averaged cell velocities, the same mesh discretization was used in the horizontal plane of the flow simulation model. As such, the element grid in the flow simulation model did not have finer elements in horizontal directions in the recirculation region and the length of the side slope of the dredged channel had been divided into only 5 elements at the shore end and one element at the offshore end, Figure 6.8

Therefore, it can be concluded that when the assumptions made are considered along with the mesh discretization used and non-calibration of the models, the flow simulation models gave reasonable to good accuracy except for a few sections in the recirculation and inlet regions which in retrospect would have been expected.

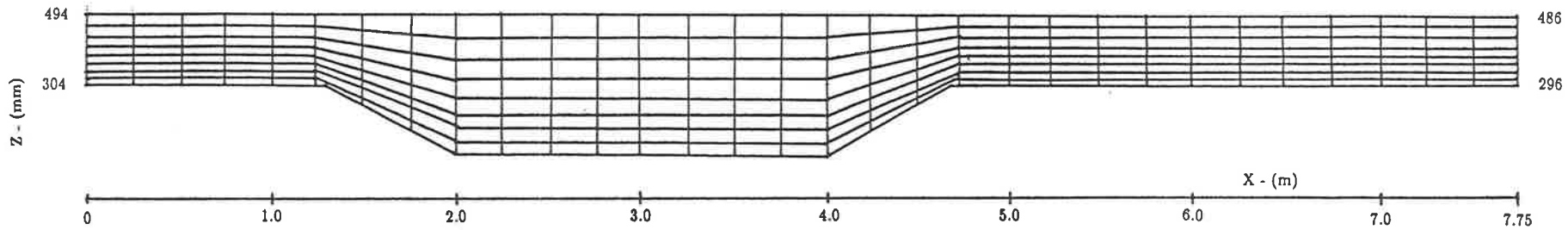

(a) Vertical section of the finite element mesh at Y = 600 mm

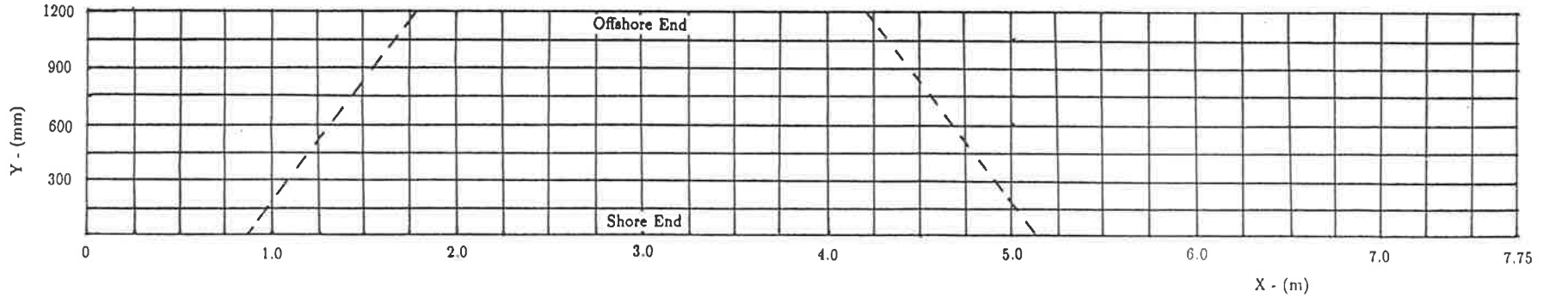

(b) Plan view of the finite element mesh

Figure 6.8: Mesh Discretization in horizontal and vertical planes

6.6.2 Sand Transport Models

6.6.2.1 Shield's Formula

The transport of sediment particles by a flow of water can be in the form of bed-load and suspended load, depending on the size of the bed material particles and the flow conditions. Usually, three modes of particle motion are distinguished:

1. Rolling and sliding motion or both.
2. Saltation motion.
3. Suspended particle motion.

When the value of bed-shear velocity just exceeds the critical value for initiation of motion, the particles will begin rolling and sliding or both, in continuous contact with bed. For increasing values of the bed-shear velocity, the particles will be moving along the bed in more or less regular jumps, the process known as saltation. When the value of the bed-shear velocity exceeds the fall velocity of the particles, the sediment particles can be lifted to a level at which the upward turbulent forces will be comparable with or of higher order than the submerged weight of the particles and as a result the particles may go in suspension.

Usually, the combined transport of particles by rolling, sliding and saltating is referred to as the bed-load transport.

Shield's formula, equation 5.8, which is essentially a bed load formula is based on the assumption that shear stress is the main parameter defining sediment transporting power. Transport of sediment by suspension at high shear velocities has not been taken into account and at all velocities sediment is assumed to

be transported as bed load. Further, the resistance to sand movement caused by the bed forms on the deformed bed has not been considered in the formula.

Further, the velocity field existing at the granular surface determines the shear stress on the grains. Therefore, as described in the SURTRENCH Model, Section 3.6.1.2, it is more realistic to relate the bed shear velocity to the flow velocity at the bed level. But in this experiment, the bed shear stress, hence the bed shear velocity, in the Shield's formula has been related to the depth averaged mean flow velocity which could be higher than the near bed velocity.

As a result of the reasons mentioned above and also since the sand transport is a function to the fifth power of the mean fluid velocity (equation 5.13) exaggerated sand movement can be expected in areas where the velocity is high relative to the depth.

As described in Section 6.6.1, the flow simulation model predicted higher velocities in the regions $Y = 300mm$ to $Y = 450mm$ and $Y = 750mm$ to $Y = 900mm$ in the area between the inlet and the dredged channel. Examination of bed profiles at the inlet region, Figure 6.9, shows that these higher velocities have caused exaggerated erosion of the cells in the region from $Y = 600mm$ to $Y = 1050mm$ and consequent abnormal deposition in the adjacent cells in the region from $Y = 150mm$ to $Y = 450mm$. After few iterations, the depth difference between these cells became large and resulted in corresponding large velocities (Figure 6.10) which further increased the depth differentials and caused distortion in the finite element mesh. Therefore, the sand transport model became unstable after few iterations.

It is expected that performance of the sand transport model using the Shield's bed-load formula can be improved by taking the following steps;

1. Shift the inlet further upstream of the dredged channel and calibrate the flow simulation model to improve accuracy of the predicted velocities.

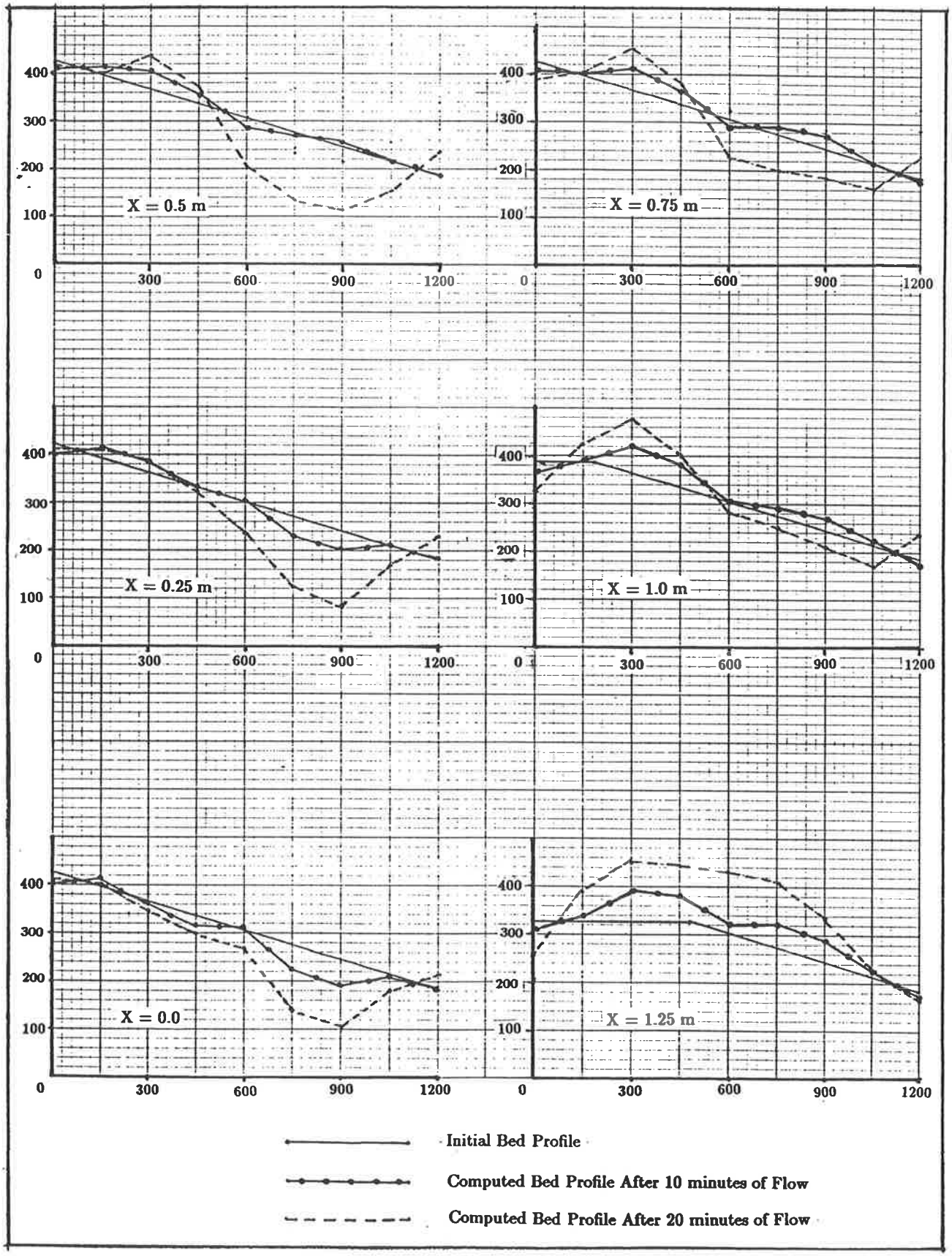

Figure 6.9: Transverse Bed Profiles Computed Using Shield's Formula

Computed Depth Averaged Cell Velocities After 20 Minutes of Flow

I	J=1	J=2	J=3	J=4	J=5	J=6	J=7	J=8
1	0.132	0.327	0.374	0.303	0.324	0.377	0.322	0.145
2	0.129	0.319	0.382	0.313	0.344	0.434	0.353	0.142
3	0.163	0.316	0.333	0.345	0.389	0.439	0.388	0.174
4	0.186	0.330	0.315	0.349	0.402	0.438	0.405	0.193
5	0.181	0.302	0.294	0.365	0.417	0.436	0.422	0.208
6	0.135	0.223	0.231	0.329	0.403	0.430	0.431	0.216
7	0.089	0.155	0.169	0.247	0.319	0.370	0.389	0.194
8	0.057	0.115	0.138	0.189	0.245	0.300	0.313	0.148
9	0.040	0.093	0.125	0.169	0.222	0.273	0.262	0.114
10	0.031	0.082	0.124	0.171	0.225	0.270	0.244	0.101
11	0.027	0.078	0.126	0.176	0.232	0.271	0.237	0.096
12	0.025	0.077	0.128	0.181	0.236	0.269	0.231	0.094
13	0.025	0.077	0.130	0.185	0.239	0.266	0.225	0.091
14	0.026	0.079	0.133	0.188	0.241	0.263	0.219	0.089
15	0.029	0.082	0.135	0.191	0.241	0.258	0.214	0.087
16	0.033	0.089	0.140	0.194	0.243	0.257	0.213	0.088
17	0.042	0.105	0.152	0.206	0.253	0.265	0.225	0.096
18	0.056	0.130	0.174	0.225	0.271	0.285	0.249	0.110
19	0.073	0.161	0.200	0.248	0.295	0.309	0.276	0.125
20	0.097	0.200	0.233	0.281	0.325	0.337	0.301	0.137
21	0.129	0.252	0.273	0.318	0.353	0.361	0.321	0.146
22	0.149	0.282	0.294	0.336	0.370	0.378	0.335	0.151
23	0.141	0.273	0.287	0.336	0.380	0.389	0.341	0.151
24	0.128	0.255	0.280	0.337	0.388	0.396	0.341	0.149
25	0.122	0.250	0.282	0.341	0.394	0.399	0.337	0.144
26	0.120	0.250	0.287	0.347	0.399	0.399	0.330	0.139
27	0.120	0.253	0.292	0.354	0.404	0.398	0.322	0.134
28	0.122	0.257	0.298	0.361	0.408	0.396	0.315	0.130
29	0.123	0.261	0.303	0.366	0.412	0.394	0.309	0.126
30	0.125	0.264	0.308	0.372	0.415	0.393	0.304	0.123
31	0.127	0.267	0.312	0.377	0.417	0.391	0.301	0.121

Figure 6.10: Cell Velocities Computed Using Shield's Formula After 20 minutes of Flow

2. Bed shear stress to be related to the near bed velocity.

3. The time interval (MTA) for calculation of sand transport for a cycle to be lowered.

However, as Shield's formula is purely a bed load formula, errors in predicted results can be expected at higher shear velocities relative to the critical shear velocity. Therefore, Shield's formula was not considered as suitable for long term morphological computations and an alternative simple model was tried.

6.6.2.2 Ackers and White Method

The method proposed by Ackers and White predicts the total load and not the bed-load transport only. In this method, average stream velocity has been used in preference to shear stress as the basis of sediment transport function. The grain roughness has been taken into account in equation 5.16 by relating it to the median sediment diameter. As such this method can be expected to perform better than the Shield's formula. However, in the formula for calculation of sand transport, equation 5.23, when the other parameters are constant the rate of sand transport is a function to the power four of the mean flow velocity. Therefore, the computed sand transport would be very sensitive to the mean flow velocity. As a result of this and also since the bed shear velocity was related to the depth averaged mean flow velocity, equation 5.20, the model could be expected, in general, to over predict sand movement.

Review of measured bed contours in the Physical Model, as shown in Figure 6.11, and measured bed profiles in Figures 6.5 and 6.6 reveal the following:

1. The sand moving in the longshore direction in the region upstream of the dredged channel has deposited on the upstream side slope of the dredged

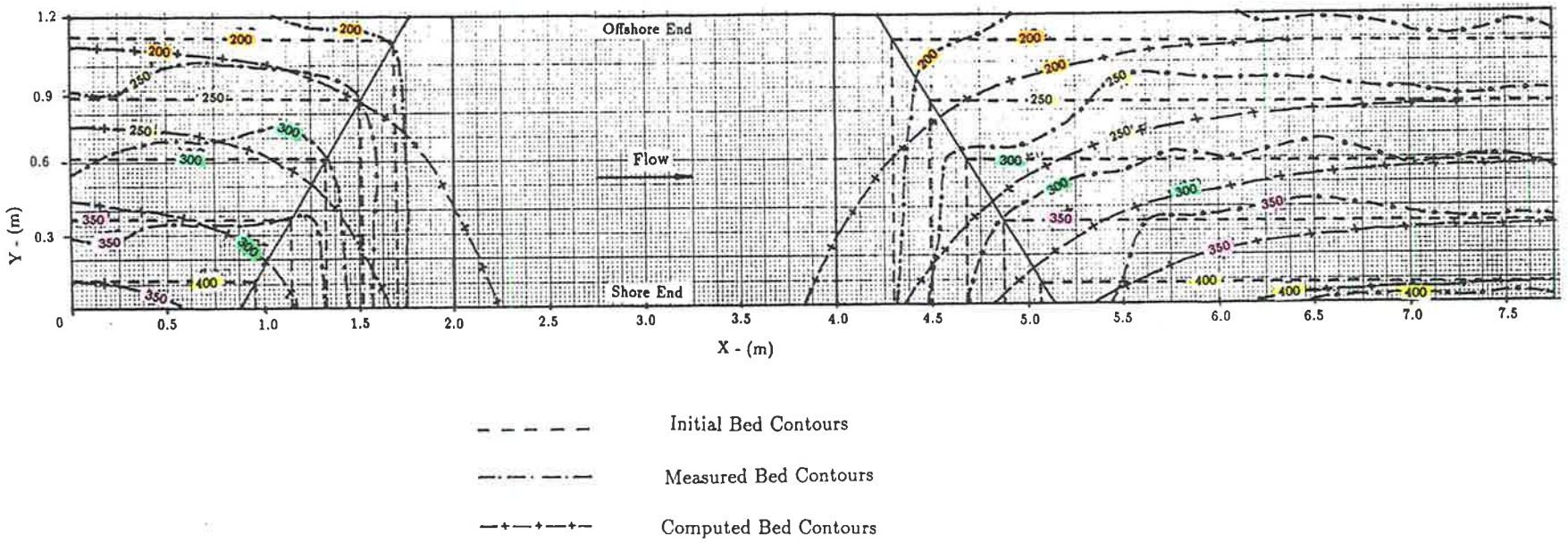

Figure 6.11: Measured and Computed Bed Contours After 6.0 Hrs of Flow

channel, when the flow velocity, and hence the transport capacity, decreases due to increase in the depth of flow.

2. In the area immediately downstream of the dredged channel erosion of sand has taken place due to increase in the flow velocity, hence the transport capacity, when the depth of flow decreases along the side slope.

3. At the downstream end of the flow domain closer to the outlet section, measured bed contours were almost parallel to the original bed contours and the contours had moved prominently in the transverse direction. This indicates that very little sand movement has taken place in the longitudinal direction.

4. No sand movement has taken place in the dredged channel, from $X = 2.0\ m$ to $X = 4.0\ m$, due to low velocity caused by the increased depth. In this area, the flow velocity seems to be not large enough to initiate movement of sand.

5. An interesting observation made was a definite movement of sand in the off-shore (transverse) direction in all areas upstream and downstream of the dredged channel. As both measured and computed flow velocity components in the off-shore direction were small compared to the longitudinal components, the movement of sand in the off-shore direction cannot be explained in terms of flow velocities. As the bed has a large gradient (1:5) in the off-shore direction compared to the longshore direction (1:1000) the gravity seems to have played a role in movement of sand in the transverse direction. A number of factors contribute to establishing a natural submerged 'angle of repose' under flow conditions.

6. As the mean flow velocity was low compared to the size of the bed material, very little movement of sand by suspension was observed.

The following observations can be made when the bed contours, as shown in

Figure 6.11 and bed profiles shown in Figures 6.5 and 6.6, computed using Ackers and White method are reviewed.

1. A prominent movement of sand in the longshore direction can be seen throughout the flow domain, which is a clear over prediction compared to the Physical Model.

2. The sand moving along the longitudinal (longshore) direction upstream of the dredged channel has deposited in the dredged channel when the flow velocities drop due to increase in the depth of flow.

3. Erosion has taken place on the downstream slope of the dredged channel as the flow velocities increase due to decrease of depth.

4. In the area downstream of the dredged channel where the computed flow velocities have a better match with the measured velocities, measured and computed bed profiles, Figures 6.5 and 6.6, have similar shapes and are almost parallel. Similarly, in this region measured bed contours are almost parallel to the computed bed contours (Figure 6.11). Therefore if not for the over prediction of sand in the longitudinal direction by the numerical model, the measured and computed bed profiles would have agreed reasonably well. Moreover, the computed bed contours in this region were very close to the initial bed contours. As such, if not for this over predicted long shore sand transport in the numerical model, the computed bed contours would have matched very well with the initial bed contours indicating that very little sand movement has taken place in the longshore direction in complete agreement with observations made in the physical model.

5. The movement of sand in the offshore direction observed in the Physical Model was not seen in the numerical model. It should be noted here that the effect of gravity has not been taken into consideration in the numerical model. As such it will be interesting to examine whether the

gravity has played a role in the movement of sand along the steep gradient in the offshore direction.

6. In the upstream region of the dredged channel where the computed (Mixing Length Model) velocities did not show good agreement with the measured velocities, the computed bed profiles deviated from the measured profiles as would be expected.

An important factor that would have affected the predictions of the sand transport model is the changing bed profile and hence the flow velocities at the inlet which has not been taken into consideration. It was assumed that the prescribed inlet velocities remain unchanged throughout the experiment even though the bed profile is allowed to vary. With the continuous changing of the bed profile at the inlet and in the region upstream of the dredged channel, the inlet flow velocities both in the longitudinal and transverse directions should be expected to vary to maintain a constant discharge. As the computed flow velocities upstream of the dredged channel were found to be very sensitive specially to the direction and the magnitude of transverse velocities, this would have had a direct effect on the model predictions.

The performance of the sand transport model can be expected to improve by taking the same measures as mentioned in Section 6.6.2.1.

6.7 Conclusions

The 3-dimensional turbulent flow across a channel dredged at an inlet was simulated using two different advanced turbulent models. These numerical models, in general, performed reasonably well with the sophisticated K-Epsilon model being more accurate than the Mixing Length model. When the empirical constants are calibrated and a finer mesh discretization is used the models can

be expected to perform even better. Recommendations for improvement of the flow simulation models have been presented in Section 6.8.

Two different numerical models were used to simulate sand transport across the dredged channel. The Shield's bed load formula seems to overpredict unusually high sand transport at higher velocities and as such would not be suitable for long term morphological computations.

The sand transport model which used the Ackers and White method performed reasonably well in the areas where the computed velocities were in agreement with the measured velocities. It has been assumed in this method that mean flow velocity is the main factor that influence the transport capacity. As the sand transport is a function of the fourth power of the mean velocity (equation 5.23), when the other parameters are constant a 10% increase of mean velocity could increase the sand transport by 45% . Therefore, a small error in the predicted flow velocities could accumulate to create a major error in the predictions of the sand transport model when a simulation is carried out over a large number of cycles for long term morphological computations. Thus, the accuracy of predictions of such a long term model will depend critically upon the accuracy of the predicted velocities in the flow simulation model.

In the region downstream of the dredged channel where the computed velocities were in good agreement with the measured velocities, if not for the over-predicted longshore sand transport in the numerical model and the sand transport observed in the transverse direction in the physical model, the computed bed profiles (Figures 6.5 and 6.6) and contours (Figure 6.11) would have shown better agreement with the measured bed profiles and contours.

The Mixing length model over-predicted velocities in the region down stream of the dredged channel compared to the K-E model. As such, provided the required computer resources are available, the use of K-E model to couple with the sand transport model would have enabled more accurate results to

be obtained than those from the Mixing length model.

One of the important factors of this study was to assess the computational feasibility of attempting to solve a complex problem by using two numerical models as explained in this thesis. It can be concluded that, once calibrated and validated using measured data, an advanced flow simulation model coupled with a simple sand transport model, as used in this experiment, appears feasible at this stage to predict long term morphological computations to a reasonable accuracy.

It is expected that the numerical models used in this project could be improved by taking the steps presented in Section 6.8 as future work.

6.8 Future Work

As described in the previous sections of this chapter, several important factors that would have affected the accuracy of predictions of the flow simulation and sand transport models should have been checked to improve the models. However, the loss of time, as mentioned already, did not allow many improvement and refinement runs to be carried out on numerical models. However, since the numerical models performed reasonably well even without improvement, it would be worthwhile to investigate the influence of the following factors on the performance of the models.

1. It was observed that the inlet section used in the experiment was too close to the dredged channel and also the velocities in the inlet region were very sensitive to the prescribed inlet velocities in the transverse direction. Therefore, inlet section should be shifted further upstream well away from the dredged channel to reduce the influence of flow in the dredged channel on the inlet.

2. As it was assumed that prescribed inlet flow velocities remain unchanged during the total period of time for which the sand transport was calculated, suitable measures should be taken to maintain a constant cross-section at the inlet.

3. The coarse mesh discretization used, specially in the recirculation region, as described in Section 6.6.1, would have had an effect on the accuracy of the flow simulation models. Therefore, element mesh should be refined to satisfy the requirements mentioned in Section 6.6.1.

4. Use of depth averaged velocities to calculate shear velocities could, in general, cause over prediction in the sand transport models. Therefore, the mesh discretization in the vertical direction should be made in such a way that near bed velocities could be obtained directly from the FIDAP output file to calculate the shear velocities instead of depth average velocities.

5. In the Profile Model, Section 5.5, the time period for which the sand transport is to be calculated has been discretized to a number of cycles of duration Δt (MTA) each. The accuracy of this discretization will increase with the decrease of the time Δt. Therefore, the time interval, Δt, used to calculate sand transport for a cycle should be reduced as small as practically possible. However, decrease of Δt would result in increase of total number of runs by FIDAP and hence would increase total CPU time.

6. As described already, numerical models should be calibrated for empirical constants used.

7. It was observed that strong gradient (1:5) present in the transverse direction added more complications, such as influence of gravity, on the already complicated 3-dimensional model. Therefore, for validation of the model and to reduce the complexity of the problem the 3-dimensional

model should be run initially without any gradient in the offshore (transverse) direction. This will avoid the necessity of prescribing transverse velocities at the inlet and calibration of the models would be comparatively easier. If the numerical models perform well after calibration, transverse gradient should be introduced and increased gradually to check the influence of the gravity in movement of sand in the transverse direction.

Appendix-A

FIDAP input file FIINP for the K-Epsilon Model

```
/FIPREP INPUT FILE FOR THE K-EPSILON MODEL
*TITLE
FLOW ACROSS A NAVIGATIONAL CHANNEL DREDGED AT AN INLET
/ELEMENTS=1984(31X8X8), NODES=2592(32X9X9)
/SPECIFY THE NODAL COORDINATES
*NODES(CARTESIAN,SUBROUTINE=11)
/SPECIFY THE NODAL CONNECTIVITIES OF THE 3-D ELEMENTS
*ELEMENTS(GROUP=1,BRICK,NODES=8,SUBROUTINE=12,MVISC=1)
/SPECIFY THE NODAL CONNECTINITIES OF THE WALL BOUNDARY ELEMENTS
/SHORE WALL BOUNDARY
*ELEMENTS(GROUP=2,WALL,QUADRILATERAL,NODES=4,SUBROUTINE=12,MDENS=1,
MVISC=1)
/OFFSHORE WALL BOUNDARY
*ELEMENTS(GROUP=3,WALL,QUADRILATERAL,NODES=4,SUBROUTINE=12,MDENS=1,
MVISC=1)
/BED WALL BOUNDARY
*ELEMENTS(GROUP=4,WALL,QUADRILATERAL,NODES=4,SUBROUTINE=12,MDENS=1,
MVISC=1)
*RENUMBER
*PROBLEM(NONLINEAR,3-D,TURBULENT)
*EXECUTION(NEWJOB)
*DATAPRINT(CONTROL,NODES=3,ELEMENTS=2,CONSTRAINED=2,FLUX=2,
INITIAL=3,SPINES=1)
*SOLUTION(SEGREGATED=80,VELCONV=0.001)
*DENSITY(SET=1,CONSTANT=1.0E3)
*VISCOSITY(SET=1,K.E.=1)
1.0E-3,1.44,1.92,0.09,1.0,1.3,0.9,0.41,26.0,0.8,0.9,0.9
*OPTIONS(UPWINDING)
*ICNODE(UX,READ)
*ICNODE(UY,READ)
*ICNODE(UZ,READ)
*ICNODE(KINETIC,CONSTANT=0.008)
*ICNODE(DISSIPATION,CONSTANT=0.001)
/INLET VELOCITY IN THE X-DIRECTION
*BCNODE(UX)
1    1    0.00
9    0    0.00
10   0    0.00
11   0    0.18
12   0    0.22
13   0    0.28
14   0    0.31
15   0    0.34
16   0    0.36
17   0    0.37
18   0    0.38
19   0    0.00
20   0    0.24
21   0    0.30
22   0    0.34
23   0    0.35
24   0    0.36
25   0    0.36
26   0    0.35
```

```
27    0     0.32
28    0     0.00
29    0     0.12
30    0     0.22
31    0     0.30
32    0     0.34
33    0     0.36
34    0     0.37
35    0     0.38
36    0     0.39
37    0     0.00
38    0     0.24
39    0     0.31
40    0     0.35
41    0     0.36
42    0     0.36
43    0     0.35
44    0     0.34
45    0     0.32
46    0     0.00
47    0     0.06
48    0     0.18
49    0     0.29
50    0     0.35
51    0     0.37
52    0     0.38
53    0     0.38
54    0     0.38
55    0     0.00
56    0     0.24
57    0     0.30
58    0     0.31
59    0     0.31
60    0     0.31
61    0     0.31
62    0     0.31
63    0     0.31
64    0     0.00
65    0     0.09
66    0     0.30
67    0     0.38
68    0     0.38
69    0     0.37
70    0     0.35
71    0     0.34
72    0     0.32
73    1     0.00
81    0     0.00
/INLET VELOCITY IN THE Y-DIRECTION
*BCNODE(UY)
10    0     0.000
11    0     0.070
12    0     0.090
13    0     0.100
14    0     0.120
15    0     0.124
16    0     0.136
17    0     0.140
18    0     0.140
19    0     0.000
20    0     0.070
21    0     0.090
```

```
22    0     0.100
23    0     0.120
24    0     0.124
25    0     0.136
26    0     0.140
27    0     0.140
28    0     0.000
29    0    -0.065
30    0    -0.086
31    0    -0.100
32    0    -0.115
33    0    -0.122
34    0    -0.137
35    0    -0.145
36    0    -0.160
37    0     0.000
38    0     0.060
39    0     0.082
40    0     0.100
41    0     0.110
42    0     0.120
43    0     0.138
44    0     0.150
45    0     0.180
46    0     0.000
47    0     0.060
48    0     0.082
49    0     0.095
50    0     0.100
51    0     0.105
52    0     0.114
53    0     0.120
54    0     0.135
55    0     0.000
56    0    -0.060
57    0    -0.082
58    0    -0.090
59    0    -0.090
60    0    -0.090
61    0    -0.090
62    0    -0.090
63    0    -0.090
64    0     0.000
65    0    -0.060
66    0    -0.082
67    0    -0.090
68    0    -0.090
69    0    -0.090
70    0    -0.090
71    0    -0.090
72    0    -0.090
/INLET VELOCITY IN THE Z-DIRECTION EQUALS ZERO
*BCNODE(UZ)
1     1     0.0
81    0     0.0
/VELOCITY IN THE X-DIRECTION ON THE SHORELINE BOUNDARY SHOULD BE ZERO
*BCNODE(UX)
1     81    0.0
2512  0     0.0
2     81    0.0
2513  0     0.0
```

```
3      81    0.0
2514   0     0.0
4      81    0.0
2515   0     0.0
5      81    0.0
2516   0     0.0
6      81    0.0
2517   0     0.0
7      81    0.0
2518   0     0.0
8      81    0.0
2519   0     0.0
9      81    0.0
2520   0     0.0
/VELOCITY IN THE Y-DIRECTION ON THE SHORELINE BOUNDARY SHOULD BE ZERO
*BCNODE(UY)
1      81    0.0
2512   0     0.0
2      81    0.0
2513   0     0.0
3      81    0.0
2514   0     0.0
4      81    0.0
2515   0     0.0
5      81    0.0
2516   0     0.0
6      81    0.0
2517   0     0.0
7      81    0.0
2518   0     0.0
8      81    0.0
2519   0     0.0
9      81    0.0
2520   0     0.0
/VELOCITY IN THE Z-DIRECTION ON THE SHORELINE BOUNDARY SHOULD BE ZERO
*BCNODE(UZ)
1      81    0.0
2512   0     0.0
2      81    0.0
2513   0     0.0
3      81    0.0
2514   0     0.0
4      81    0.0
2515   0     0.0
5      81    0.0
2516   0     0.0
6      81    0.0
2517   0     0.0
7      81    0.0
2518   0     0.0
8      81    0.0
2519   0     0.0
9      81    0.0
2520   0     0.0
/VELOCITY IN THE X-DIRECTION ON THE OFFSHORE BOUNDARY SHOULD BE ZERO
*BCNODE(UX)
73     81    0.0
2584   0     0.0
74     81    0.0
2585   0     0.0
```

```
75    81   0.0
2586  0    0.0
76    81   0.0
2587  0    0.0
77    81   0.0
2588  0    0.0
78    81   0.0
2589  0    0.0
79    81   0.0
2590  0    0.0
80    81   0.0
2591  0    0.0
81    81   0.0
2592  0    0.0
/VELOCITY IN THE Y-DIRECTION ON THE OFFSHORE BOUNDARY SHOULD BE ZERO
*BCNODE(UY)
73    81   0.0
2584  0    0.0
74    81   0.0
2585  0    0.0
75    81   0.0
2586  0    0.0
76    81   0.0
2587  0    0.0
77    81   0.0
2588  0    0.0
78    81   0.0
2589  0    0.0
79    81   0.0
2590  0    0.0
80    81   0.0
2591  0    0.0
81    81   0.0
2592  0    0.0
/VELOCITY IN THE Z-DIRECTION ON THE OFFSHORE BOUNDARY SHOULD BE ZERO
*BCNODE(UZ)
73    81   0.0
2584  0    0.0
74    81   0.0
2585  0    0.0
75    81   0.0
2586  0    0.0
76    81   0.0
2587  0    0.0
77    81   0.0
2588  0    0.0
78    81   0.0
2589  0    0.0
79    81   0.0
2590  0    0.0
80    81   0.0
2591  0    0.0
81    81   0.0
2592  0    0.0
/VELOCITY IN THE X-DIRECTION ON THE BED BOUNDARY SHOULD BE ZERO
*BCNODE(UX)
1     81   0.0
2512  0    0.0
10    81   0.0
2521  0    0.0
```

```
19    81   0.0
2530  0    0.0
28    81   0.0
2539  0    0.0
37    81   0.0
2548  0    0.0
46    81   0.0
2557  0    0.0
55    81   0.0
2566  0    0.0
64    81   0.0
2575  0    0.0
73    81   0.0
2584  0    0.0
/VELOCITY IN THE Y-DIRECTION ON THE BED BOUNDARY SHOULD BE ZERO
*BCNODE(UY)
1     81   0.0
2512  0    0.0
10    81   0.0
2521  0    0.0
19    81   0.0
2530  0    0.0
28    81   0.0
2539  0    0.0
37    81   0.0
2548  0    0.0
46    81   0.0
2557  0    0.0
55    81   0.0
2566  0    0.0
64    81   0.0
2575  0    0.0
73    81   0.0
2584  0    0.0
/VELOCITY IN THE Z-DIRECTION ON THE BED BOUNDARY SHOULD BE ZERO
*BCNODE(UZ)
1     81   0.0
2512  0    0.0
10    81   0.0
2521  0    0.0
19    81   0.0
2530  0    0.0
28    81   0.0
2539  0    0.0
37    81   0.0
2548  0    0.0
46    81   0.0
2557  0    0.0
55    81   0.0
2566  0    0.0
64    81   0.0
2575  0    0.0
73    81   0.0
2584  0    0.0
/FREE SURFACE NORMAL VELOCITY SHOULD BE ZERO
*BCNODE(UZ)
9     81   0.0
2520  0    0.0
18    81   0.0
2529  0    0.0
```

```
27    81   0.0
2538  0    0.0
36    81   0.0
2547  0    0.0
45    81   0.0
2556  0    0.0
54    81   0.0
2565  0    0.0
63    81   0.0
2574  0    0.0
72    81   0.0
2583  0    0.0
81    81   0.0
2592  0    0.0
/TURBULENT KINETIC ENERGY AT THE INLET
*BCNODE(KINETIC)
1    1    0.0000
9    0    0.0000
10   0    0.0000
11   0    0.0024
12   0    0.0029
13   0    0.0035
14   0    0.0036
15   0    0.0035
16   0    0.0033
17   0    0.0030
18   0    0.0022
19   0    0.0000
20   0    0.0024
21   0    0.0029
22   0    0.0035
23   0    0.0036
24   0    0.0035
25   0    0.0033
26   0    0.0030
27   0    0.0022
28   0    0.0000
29   0    0.0017
30   0    0.0024
31   0    0.0031
32   0    0.0038
33   0    0.0042
34   0    0.0044
35   0    0.0038
36   0    0.0015
37   0    0.0000
38   0    0.0010
39   0    0.0018
40   0    0.0027
41   0    0.0039
42   0    0.0049
43   0    0.0054
44   0    0.0045
45   0    0.0008
46   0    0.0000
47   0    0.0014
48   0    0.0020
49   0    0.0025
50   0    0.0030
51   0    0.0035
52   0    0.0034
53   0    0.0027
54   0    0.0005
```

```
55    0     0.0000
56    0     0.0018
57    0     0.0021
58    0     0.0023
59    0     0.0021
60    0     0.0020
61    0     0.0014
62    0     0.0009
63    0     0.0001
64    0     0.0000
65    0     0.0018
66    0     0.0021
67    0     0.0023
68    0     0.0021
69    0     0.0020
70    0     0.0014
71    0     0.0009
72    0     0.0001
73    1     0.0000
81    0     0.0000
/DISSIPATION RATE OF TURBULENT KINETIC ENERGY AT THE INLET
*BCNODE(DISSIPATION)
1     1     0.0000
9     0     0.0000
10    0     0.0000
11    0     0.0117
12    0     0.0058
13    0     0.0039
14    0     0.0027
15    0     0.0020
16    0     0.0016
17    0     0.0013
18    0     0.0000
19    0     0.0000
20    0     0.0117
21    0     0.0058
22    0     0.0039
23    0     0.0027
24    0     0.0020
25    0     0.0016
26    0     0.0013
27    0     0.0000
28    0     0.0000
29    0     0.0074
30    0     0.0039
31    0     0.0029
32    0     0.0024
33    0     0.0022
34    0     0.0019
35    0     0.0015
36    0     0.0000
37    0     0.0000
38    0     0.0031
39    0     0.0019
40    0     0.0018
41    0     0.0021
42    0     0.0023
43    0     0.0022
44    0     0.0016
45    0     0.0000
46    0     0.0000
47    0     0.0053
```

```
48    0     0.0019
49    0     0.0015
50    0     0.0014
51    0     0.0014
52    0     0.0011
53    0     0.0014
54    0     0.0000
55    0     0.0000
56    0     0.0075
57    0     0.0019
58    0     0.0011
59    0     0.0006
60    0     0.0004
61    0     0.0002
62    0     0.00011
63    0     0.0000
64    0     0.0000
65    0     0.0075
66    0     0.0019
67    0     0.0011
68    0     0.0006
69    0     0.0004
70    0     0.0002
71    0     0.00011
72    0     0.0000
73    1     0.0000
81    0     0.0000
/NORMAL & TANGENTIAL DIRECTIONS ON THE SHORELINE BOUNDARY EDGES
*BCNODE(COORDINATE)
1     81    1
2512  0     1
9     81    1
2520  0     1
1     1     1
9     0     1
73    1     1
81    0     1
*BCSYSTEM(SET=1,EDGE,1TANGENTIAL)
0,0,0,1,0,0,0,0,0
/NORMAL & TANGENTIAL DIRECTIONS ON THE OFFSHORE BOUNDARY EDGES
*BCNODE(COORDINATE)
73    81    2
2584  0     2
81    81    2
2592  0     2
73    1     2
81    0     2
2584  1     2
2592  0     2
*BCSYSTEM(SET=2,EDGE,1TANGENTIAL)
0,0,0,1,0,0,0,0,0
/NORMAL & TANGENTIAL DIRECTIONS ON THE BED BOUNDARY NODES
*BCNODE(COORDINATE)
1     81    3
2512  0     3
73    81    3
2584  0     3
1     9     3
73    0     3
2512  9     3
2584  0     3
*BCSYSTEM(SET=3,EDGE,1TANGENTIAL)
0,0,0,1,0,0,0,0,0
*END
```

Appendix-B

FIDAP input file for the Mixing Length Model

```
/FIPREP INPUT FILE FOR THE MIXING LENGTH MODEL
*TITLE
FLOW ACROSS A NAVIGATIONAL CHANNEL DREDGED AT AN INLET
/ELEMENTS=1984(31X8X8), NODES=2592(32X9X9)
/SPECIFY THE NODAL COORDINATES
*NODES(CARTESIAN,SUBROUTINE=11)
/SPECIFY THE NODAL CONNECTIVITIES OF THE 3-D ELEMENTS
*ELEMENTS(GROUP=1,BRICK,NODES=8,SUBROUTINE=12,MVISC=1)
*RENUMBER
*PROBLEM(NONLINEAR,3-D,TURBULENT)
*EXECUTION(NEWJOB)
*DATAPRINT(CONTROL,NODES=3,ELEMENTS=2,CONSTRAINED=2,FLUX=2,
INITIAL=3,SPINES=1)
*SOLUTION(SEGREGATED=80,VELCONV=0.001)
*DENSITY(SET=1,CONSTANT=1.0E3)
*VISCOSITY(SET=1,MIXING=1)
1.0E-3
*OPTIONS(UPWINDING)
*ICNODE(UX,READ)
*ICNODE(UY,READ)
*ICNODE(UZ,READ)
/INLET VELOCITY IN THE X-DIRECTION
*BCNODE(UX)
1    1    0.00
9    0    0.00
10   0    0.00
11   0    0.22
12   0    0.28
13   0    0.31
14   0    0.34
15   0    0.36
16   0    0.37
17   0    0.38
18   0    0.38
19   0    0.00
20   0    0.30
21   0    0.34
22   0    0.35
23   0    0.36
24   0    0.36
25   0    0.35
26   0    0.34
27   0    0.32
28   0    0.00
29   0    0.22
30   0    0.30
31   0    0.34
32   0    0.36
33   0    0.37
34   0    0.38
35   0    0.39
36   0    0.39
37   0    0.00
38   0    0.31
39   0    0.35
40   0    0.36
```

```
41   0    0.36
42   0    0.35
43   0    0.34
44   0    0.33
45   0    0.32
46   0    0.00
47   0    0.18
48   0    0.29
49   0    0.35
50   0    0.37
51   0    0.38
52   0    0.38
53   0    0.38
54   0    0.38
55   0    0.00
56   0    0.30
57   0    0.31
58   0    0.31
59   0    0.31
60   0    0.31
61   0    0.31
62   0    0.31
63   0    0.31
64   0    0.00
65   0    0.30
66   0    0.38
67   0    0.38
68   0    0.37
69   0    0.35
70   0    0.34
71   0    0.33
72   0    0.32
73   1    0.00
81   0    0.00
/INLET VELOCITY IN THE Y-DIRECTION
*BCNODE(UY)
10   0    0.000
11   0    0.090
12   0    0.100
13   0    0.120
14   0    0.124
15   0    0.136
16   0    0.140
17   0    0.140
18   0    0.140
19   0    0.000
20   0    0.090
21   0    0.100
22   0    0.120
23   0    0.124
24   0    0.136
25   0    0.140
26   0    0.140
27   0    0.140
28   0    0.000
29   0   -0.086
30   0   -0.100
31   0   -0.115
32   0   -0.122
33   0   -0.137
34   0   -0.145
35   0   -0.150
```

```
36    0    -0.160
37    0     0.000
38    0     0.082
39    0     0.100
40    0     0.110
41    0     0.120
42    0     0.138
43    0     0.150
44    0     0.160
45    0     0.180
46    0     0.000
47    0     0.082
48    0     0.095
49    0     0.100
50    0     0.105
51    0     0.114
52    0     0.120
53    0     0.125
54    0     0.135
55    0     0.000
56    0    -0.082
57    0    -0.090
58    0    -0.090
59    0    -0.090
60    0    -0.090
61    0    -0.090
62    0    -0.090
63    0    -0.090
64    0     0.000
65    0    -0.082
66    0    -0.090
67    0    -0.090
68    0    -0.090
69    0    -0.090
70    0    -0.090
71    0    -0.090
72    0    -0.090
/INLET VELOCITY IN THE VERTICAL (Z) DIRECTION EQUALS ZERO
*BCNODE(UZ)
1     1     0.0
81    0     0.0
/VELOCITY IN THE LONGSHORE (X) DIRECTION ON THE SHORELINE BOUNDARY
/SHOULD BE ZERO
*BCNODE(UX)
1     81    0.0
2512  0     0.0
2     81    0.0
2513  0     0.0
3     81    0.0
2514  0     0.0
4     81    0.0
2515  0     0.0
5     81    0.0
2516  0     0.0
6     81    0.0
2517  0     0.0
7     81    0.0
2518  0     0.0
8     81    0.0
2519  0     0.0
9     81    0.0
2520  0     0.0
```

```
/VELOCITY IN THE OFFSHORE (Y) DIRECTION ON THE SHORELINE BOUNDARY
/SHOULD BE ZERO
*BCNODE(UY)
1     81   0.0
2512  0    0.0
2     81   0.0
2513  0    0.0
3     81   0.0
2514  0    0.0
4     81   0.0
2515  0    0.0
5     81   0.0
2516  0    0.0
6     81   0.0
2517  0    0.0
7     81   0.0
2518  0    0.0
8     81   0.0
2519  0    0.0
9     81   0.0
2520  0    0.0
/VELOCITY IN THE VERTICAL (Z) DIRECTION ON THE SHORELINE BOUNDARY
/SHOULD BE ZERO
*BCNODE(UZ)
1     81   0.0
2512  0    0.0
2     81   0.0
2513  0    0.0
3     81   0.0
2514  0    0.0
4     81   0.0
2515  0    0.0
5     81   0.0
2516  0    0.0
6     81   0.0
2517  0    0.0
7     81   0.0
2518  0    0.0
8     81   0.0
2519  0    0.0
9     81   0.0
2520  0    0.0
/VELOCITY IN THE LONGSHORE (X) DIRECTION ON THE OFFSHORE BOUNDARY
/SHOULD BE ZERO
*BCNODE(UX)
73    81   0.0
2584  0    0.0
74    81   0.0
2585  0    0.0
75    81   0.0
2586  0    0.0
76    81   0.0
2587  0    0.0
77    81   0.0
2588  0    0.0
78    81   0.0
2589  0    0.0
79    81   0.0
2590  0    0.0
80    81   0.0
2591  0    0.0
81    81   0.0
2592  0    0.0
```

```
/VELOCITY IN THE OFFSHORE (Y) DIRECTION ON THE OFFSHORE BOUNDARY
/SHOULD BE ZERO
*BCNODE(UY)
73     81    0.0
2584   0     0.0
74     81    0.0
2585   0     0.0
75     81    0.0
2586   0     0.0
76     81    0.0
2587   0     0.0
77     81    0.0
2588   0     0.0
78     81    0.0
2589   0     0.0
79     81    0.0
2590   0     0.0
80     81    0.0
2591   0     0.0
81     81    0.0
2592   0     0.0
/VELOCITY IN THE VERTICAL (Z) DIRECTION ON THE OFFSHORE BOUNDARY
/SHOULD BE ZERO
*BCNODE(UZ)
73     81    0.0
2584   0     0.0
74     81    0.0
2585   0     0.0
75     81    0.0
2586   0     0.0
76     81    0.0
2587   0     0.0
77     81    0.0
2588   0     0.0
78     81    0.0
2589   0     0.0
79     81    0.0
2590   0     0.0
80     81    0.0
2591   0     0.0
81     81    0.0
2592   0     0.0
/VELOCITY IN THE LONGSHORE (X) DIRECTION ON THE BED BOUNDARY
/SHOULD BE ZERO
*BCNODE(UX)
1      81    0.0
2512   0     0.0
10     81    0.0
2521   0     0.0
19     81    0.0
2530   0     0.0
28     81    0.0
2539   0     0.0
37     81    0.0
2548   0     0.0
46     81    0.0
2557   0     0.0
55     81    0.0
2566   0     0.0
64     81    0.0
2575   0     0.0
```

```
73     81    0.0
2584   0     0.0
/VELOCITY IN THE OFFSHORE (Y) DIRECTION ON THE BED BOUNDARY
/SHOULD BE ZERO
*BCNODE(UY)
1      81    0.0
2512   0     0.0
10     81    0.0
2521   0     0.0
19     81    0.0
2530   0     0.0
28     81    0.0
2539   0     0.0
37     81    0.0
2548   0     0.0
46     81    0.0
2557   0     0.0
55     81    0.0
2566   0     0.0
64     81    0.0
2575   0     0.0
73     81    0.0
2584   0     0.0
/VELOCITY IN THE VERTICAL (Z) DIRECTION ON THE BED BOUNDARY
/SHOULD BE ZERO
*BCNODE(UZ)
1      81    0.0
2512   0     0.0
10     81    0.0
2521   0     0.0
19     81    0.0
2530   0     0.0
28     81    0.0
2539   0     0.0
37     81    0.0
2548   0     0.0
46     81    0.0
2557   0     0.0
55     81    0.0
2566   0     0.0
64     81    0.0
2575   0     0.0
73     81    0.0
2584   0     0.0
/FREE SURFACE NORMAL VELOCITY SHOULD BE ZERO
*BCNODE(UZ)
9      81    0.0
2520   0     0.0
18     81    0.0
2529   0     0.0
27     81    0.0
2538   0     0.0
36     81    0.0
2547   0     0.0
45     81    0.0
2556   0     0.0
54     81    0.0
2565   0     0.0
63     81    0.0
2574   0     0.0
```

```
72    81    0.0
2583  0     0.0
81    81    0.0
2592  0     0.0
/NORMAL & TANGENTIAL DIRECTIONS ON THE SHORELINE BOUNDARY EDGES
*BCNODE(COORDINATE)
1     81    1
2512  0     1
9     81    1
2520  0     1
1     1     1
9     0     1
2512  1     1
2520  0     1
*BCSYSTEM(SET=1,EDGE,1TANGENTIAL)
0,0,0,1,0,0,0,0,0
/NORMAL & TANGENTIAL DIRECTIONS ON THE OFFSHORE BOUNDARY EDGES
*BCNODE(COORDINATE)
73    81    2
2584  0     2
81    81    2
2592  0     2
73    1     2
81    0     2
2584  1     2
2592  0     2
*BCSYSTEM(SET=2,EDGE,1TANGENTIAL)
0,0,0,1,0,0,0,0,0
/NORMAL & TANGENTIAL DIRECTIONS ON THE BED BOUNDARY EDGES
*BCNODE(COORDINATE)
1     81    3
2512  0     3
73    81    3
2584  0     3
1     9     3
73    0     3
2512  9     3
2584  0     3
*BCSYSTEM(SET=3,EDGE,1TANGENTIAL)
0,0,0,1,0,0,0,0,0
*END
```

Appendix-C

Subroutine USRNOD for generation of nodal coordinates

```
      SUBROUTINE USRNOD (X,NFIRST,NLAST,NDFCD,SUB,IERR)
C     ==================================================
C     WITH SUBROUTINE SEDIM FOR 1984 ELEMENTS
C     ***************************************
C     SAND TRANSPORT TO BE CALCULATED USING ACKERS'S FORMULA
C     ======================================================
C
C     USER SUPPLIED SUBROUTINE FOR THE DEFINITION OF NODES CALLED WHEN
C     *NODES ( CART/CYLIN/SPHER, SUBROUTINE = SUB )
C
C     INPUT:
C     ======
C     SUB          VALUE SPECIFIED ON THE CONTROL CARD ...,SUBR=SUB
C     NDFCD = 2(3) COORDINATES DIMENSION, ACCORDING TO THE DEFINITION IN
C                  *PROBLEM ( 2-D/AXI- ..  OR .. 3-D )
C     IERR =  0    NORMAL COMPLETION
C         .GT.0    ERROR
C
C     OUTPUT:
C     =======
C     NFIRST (NLAST)           FIRST (LAST) POINT DEFINED
C     X(3,I) I=NFIRST,NLAST    CARTHESIAN COORDINATES OF THE POINTS
C
C     NOTE:
C     =====
C     THE LAST ORIGIN COMMAND PREVIOUS TO THE *NODE COMMAND IS TAKEN AS
C     THE CURRENT ORIGIN; THE COORDINATE SYSTEM IS TAKEN FROM THE *NODE
C     COMMAND.
C
C
      IMPLICIT DOUBLE PRECISION (A-H,O-Z)
      COMMON /TAPES/ IFMH,INP,INPS,IOUT,IOUTS,IOUTM,IFID,IERF,IPST,
     1               IECHFI,IECHF,IECHF1,IELM,IELMS,INP1,IUSER,
     2               LPDEV(15),IHLPF,IDEVF,IECHF2,IRADF
      COMMON /INTERN/ IBUF,NBUF,NCBUF,NKVLD,KEYSTR,KEYEND,INFLAG,
     1                MAJIND(160),MININD(750),KVERIF(85),IPVERF(85),
     2                IDVERF(85),INALTR,ILETP,IDATA,INPROG,INFLG1,MECHF,
     3                IHUNT,ISHOWN
      COMMON /INTERC/ BUFFER(80,15),FILNAM
      CHARACTER  BUFFER*1 , BUFF8R(15)*80 , FILNAM*20
      EQUIVALENCE (BUFFER,BUFF8R)
      DIMENSION UX(2592),UY(2592),U(33,10),V(33,10),UT(33,10),
     + SANDX(33,10),SANDY(33,10),BDX(33,10),BDY(33,10),H(33,10),
     + X(3,2592),AU(2592),AV(2592),XMOVE(33,10),YMOVE(33,10)
      NFIRST = 1
      NLAST  = 2592
      NDFCD  = 3
C
      OPEN(UNIT=100,
     + FILE='/home/pop/usr6/foreign/vithana/fidap/MXLOUT',
     + STATUS='OLD')
      OPEN(UNIT=200,
     + FILE='/home/pop/usr6/foreign/vithana/fidap/NEWBED',
     + STATUS='OLD')
C
```

```
C
C     INSERT HERE NORMAL EXECUTION COMMANDS
C
C  IN THE FIRST ITERATION, BED COORDINATES ARE GENERATED BY ANALYTICAL
C  FORMULA. IN ALL OTHER ITERATIONS THESE COORDINATES ARE READ FROM
C  THE OUTPUT FILE (MXLOUT) OF THE PREVIOUS ITERATION.
C
C
      ITE = 1
      IF(ITE.NE.1)GO TO 175
C
C
      DO 50 N = 1, 2592
      X(1,N) = 0.0
      X(2,N) = 0.0
      X(3,N) = 0.0
50    CONTINUE
C
C   GENERATION OF THE COORDINATES OF THE NODES AT THE BED LEVEL.
C
C   INITIAL BED ELEVATION FOR THE FIRST ITERATION
C
      DO 200 I = 1, 32
      DO 200 J = 1, 73, 9
      N = J + 81*(I-1)
      X(1,N) = 0.25*(I-1)
      X(2,N) = (J-1)/60.0
200   CONTINUE
C
      DO 201 N = 1, 244, 81
      X(3,N) = 0.424 - 0.25*0.001*(N-1)/81.0
201   CONTINUE
C
      DO 202 N = 10, 253, 81
      X(3,N) = 0.394 - 0.25*0.001*(N-10)/81.0
202   CONTINUE
C
      DO 203 N = 19, 343, 81
      X(3,N) = 0.364 - 0.25*0.001*(N-19)/81.0
203   CONTINUE
C
      DO 204 N = 28, 352, 81
      X(3,N) = 0.334 - 0.25*0.001*(N-28)/81.0
204   CONTINUE
C
      DO 205 N = 37, 442, 81
      X(3,N) = 0.304 - 0.25*0.001*(N-37)/81.0
205   CONTINUE
C
      DO 206 N = 46, 451, 81
      X(3,N) = 0.274 - 0.25*0.001*(N-46)/81.0
206   CONTINUE
C
      DO 207 N = 55, 541, 81
      X(3,N) = 0.244 - 0.25*0.001*(N-55)/81.0
207   CONTINUE
C
      DO 208 N = 64, 550, 81
      X(3,N) = 0.214 - 0.25*0.001*(N-64)/81.0
208   CONTINUE
C
```

```
C
      DO 209 N = 73, 640, 81
      X(3,N) = 0.184 - 0.25*0.001*(N-73)/81.0
209   CONTINUE
C
      DO 210 N = 325, 334, 9
      X(3,N) = X(3,244) - 0.25*0.001 - 0.125/3.75
210   CONTINUE
C
      DO 211 N = 406, 433, 9
      X(3,N) = X(3,325) - 0.25*0.001 - 0.25/3.75
211   CONTINUE
C
      DO 212 N = 487, 532, 9
      X(3,N) = X(3,406) - 0.25*0.001 - 0.25/3.75
212   CONTINUE
C
      DO 213 N = 568, 631, 9
      X(3,N) = X(3,487) - 0.25*0.001 - 0.25/3.75
213   CONTINUE
C
      DO 214 I = 649, 1297, 81
      DO 214 J = 9, 81, 9
      N = I + J - 9
      X(3,N) = 0.122 - 0.25*0.001*(I-649)/81.0
214   CONTINUE
C
      DO 215 N = 1378, 1441, 9
      X(3,N) = X(3,1297) - 0.25*0.001 + 0.25/3.75
215   CONTINUE
C
      DO 216 N = 1459, 1504, 9
      X(3,N) = X(3,1378) - 0.25*0.001 + 0.25/3.75
216   CONTINUE
C
      DO 217 N = 1540, 1567, 9
      X(3,N) = X(3,1459) - 0.25*0.001 + 0.25/3.75
217   CONTINUE
C
      DO 218 N = 1621, 1630, 9
      X(3,N) = X(3,1540) - 0.25*0.001 + 0.25/3.75
218   CONTINUE
C
      DO 219 N = 1702, 2512, 81
      X(3,N) = 0.424 - 21.0*0.25*0.001 - 0.25*0.001*(N-1702)/81.0
219   CONTINUE
C
      DO 220 N = 1711, 2521, 81
      X(3,N) = 0.394 - 21.0*0.25*0.001 - 0.25*0.001*(N-1711)/81.0
220   CONTINUE
C
      DO 221 N = 1639, 2530, 81
      X(3,N) = 0.364 - 20.0*0.25*0.001 - 0.25*0.001*(N-1639)/81.0
221   CONTINUE
C
      DO 222 N = 1648, 2539, 81
      X(3,N) = 0.334 - 20.0*0.25*0.001 - 0.25*0.001*(N-1648)/81.0
222   CONTINUE
C
```

```
C
      DO 223 N = 1576, 2548, 81
      X(3,N) = 0.304 - 19.0*0.25*0.001 - 0.25*0.001*(N-1576)/81.0
223   CONTINUE
C
      DO 224 N = 1585, 2557, 81
      X(3,N) = 0.274 - 19.0*0.25*0.001 - 0.25*0.001*(N-1585)/81.0
224   CONTINUE
C
      DO 225 N = 1513, 2566, 81
      X(3,N) = 0.244 - 18.0*0.25*0.001 - 0.25*0.001*(N-1513)/81.0
225   CONTINUE
C
      DO 226 N = 1522, 2575, 81
      X(3,N) = 0.214 - 18.0*0.25*0.001 - 0.25*0.001*(N-1522)/81.0
226   CONTINUE
C
      DO 227 N = 1450, 2584, 81
      X(3,N) = 0.184 - 17.0*0.25*0.001 - 0.25*0.001*(N-1450)/81.0
227   CONTINUE
C
      GO TO 228
C
175   CALL SEDIM(UX,UY,U,V,UT,SANDX,SANDY,BDX,BDY,H,X,AU,AV,
     + XMOVE,YMOVE,NLS,MOF,NLSI,MOFI,XL,YL,AREA,MTA)
C
      GO TO 229
C
C  GENERATION OF THE COORDINATES OF THE NODES IN THE FREE WATER SURFACE.
C
C
228   DO 230 I = 1, 32
      DO 230 J = 9, 81, 9
      N = J + 81 * (I-1)
      X(1,N) = 0.25 * (I-1)
      X(2,N) = (J-9)/60.0
      X(3,N) = 0.495 - 0.25 * (I-1)*0.001
230   CONTINUE
C
C   GENERATION OF THE COORDINATES OF THE NODES IN BETWEEN THE FREE
C   SURFACE AND THE BED.
C
229   DO 231 I = 1, 2584, 9
      DO 232 J = 1, 7
      N = I + J
      X(1,N) = X(1,I)
      X(2,N) = X(2,I)
232   CONTINUE
      X(3,I+1) = X(3,I) + (X(3,I+8) - X(3,I))/12
      X(3,I+2) = X(3,I) + (X(3,I+8) - X(3,I))*15/84
      X(3,I+3) = X(3,I) + (X(3,I+8) - X(3,I))*24/84
      X(3,I+4) = X(3,I) + (X(3,I+8) - X(3,I))*34/84
      X(3,I+5) = X(3,I) + (X(3,I+8) - X(3,I))*45/84
      X(3,I+6) = X(3,I) + (X(3,I+8) - X(3,I))*57/84
      X(3,I+7) = X(3,I) + (X(3,I+8) - X(3,I))*70/84
231   CONTINUE
C
C     WRITE THE NEW BED COORDINATES TO THE FILE 'NEWBED'
C
      DO 233 N = 1, 2592 , 9
      WRITE(UNIT=200, FMT=10)N, X(1,N), X(2,N), X(3,N), AU(N), AV(N)
10    FORMAT(2X, I5, 5F10.4)
233   CONTINUE
C
```

```
C
      CLOSE(UNIT=100)
      CLOSE(UNIT=200)
C
      RETURN
      END
C
      SUBROUTINE SEDIM(UX,UY,U,V,UT,SANDX,SANDY,BDX,BDY,H,X,AU,AV,
     + XMOVE,YMOVE,NLS,MOF,NLSI,MOFI,XL,YL,AREA,MTA)
C     ************************************************************
C     SUBROUTINE TO CALCULATE SAND TRANSPORT IN THE BED USING THE OUTPUT
C     NODAL VELOCITIES FROM THE FIDAP MODEL
C
      IMPLICIT DOUBLE PRECISION (A-H,O-Z)
      DIMENSION UX(2592), UY(2592), U(33,10), V(33,10), UT(33,10),
     +  SANDX(33,10), SANDY(33,10), BDX(33,10), BDY(33,10), H(33,10),
     +  X(3,2592), AU(2592), AV(2592), XMOVE(33,10), YMOVE(33,10)
C
C  UX,UY          = NODAL VELOCITIES IN X,Y DIRECTIONS
C  AU,AV          = DEPTH AVERAGED NODAL VELOCITIES IN X,Y DIRECTIONS
C  U(I,J),V(I,J)  = CELL VELOCITIES IN X,Y DIRECTIONS
C  UT(I,J)        = TOTAL CELL VELOCITY
C  H(I,J)         = MEAN CELL DEPTH
C  SANDX,SANDY    = CELL SAND TRANSPORT RATES IN X,Y DIRECTIONS
C  BDX,BDY        = CELL EDGE SAND TRANSPORT RATES IN X,Y DIRECTIONS
C  XMOVE,YMOVE    = NET TRANSPORT FOR EACH CELL IN X,Y DIRECTIONS
C
C  SETTING DIMENSIONS OF AREA
C  NLS  = NUMBER OF CELLS IN X-DIRECTION
C  MOF  = NUMBER OF CELLS IN Y-DIRECTION
C
      NLS = 31
      MOF = 8
      NLSI= NLS + 2
      MOFI= MOF + 2
C
C  SETTING DIMENSIONS OF GRIDS IN X-Y PLANE-ALL DIMENSIONS TO BE IN METRIC
C  XL,YL = LENGTH OF EACH CELL IN X,Y DIRECTIONS
C
      XL = 0.25
      YL = 0.15
      AREA = XL*YL
C
C  READ NODAL VELOCITY COMPONENTS FROM THE FIDAP OUTPUT FILE MXLOUT
C
      DO 300 N = 1, 2592
      READ(UNIT=100,FMT=11)N,X(1,N),X(2,N),X(3,N),UX(N),UY(N)
11    FORMAT(2X,I6,4X,3(F15.11),2X,2(F18.14))
300   CONTINUE
C
C  CONVERT THE NODAL VELOCITIES TO DEPTH AVERAGED VELOCITIES-(M/SEC)
C
      DO 301 I=1,2584,9
      DO 301 J=1,9
      N = I + J-1
      A = (UX(I)   + UX(I+1))/2 * (X(3,I+1) - X(3,I))   +
     1    (UX(I+1) + UX(I+2))/2 * (X(3,I+2) - X(3,I+1)) +
     2    (UX(I+2) + UX(I+3))/2 * (X(3,I+3) - X(3,I+2)) +
     3    (UX(I+3) + UX(I+4))/2 * (X(3,I+4) - X(3,I+3)) +
     4    (UX(I+4) + UX(I+5))/2 * (X(3,I+5) - X(3,I+4)) +
     5    (UX(I+5) + UX(I+6))/2 * (X(3,I+6) - X(3,I+5)) +
     6    (UX(I+6) + UX(I+7))/2 * (X(3,I+7) - X(3,I+6)) +
     7    (UX(I+7) + UX(I+8))/2 * (X(3,I+8) - X(3,I+7))
C
```

```
C
      B = X(3, I+8) - X(3,I)
      AU(I) =A/B
C
      C = (UY(I)   + UY(I+1))/2 * (X(3,I+1) - X(3,I))   +
     1    (UY(I+1) + UY(I+2))/2 * (X(3,I+2) - X(3,I+1)) +
     2    (UY(I+2) + UY(I+3))/2 * (X(3,I+3) - X(3,I+2)) +
     3    (UY(I+3) + UY(I+4))/2 * (X(3,I+4) - X(3,I+3)) +
     4    (UY(I+4) + UY(I+5))/2 * (X(3,I+5) - X(3,I+4)) +
     5    (UY(I+5) + UY(I+6))/2 * (X(3,I+6) - X(3,I+5)) +
     6    (UY(I+6) + UY(I+7))/2 * (X(3,I+7) - X(3,I+6)) +
     7    (UY(I+7) + UY(I+8))/2 * (X(3,I+8) - X(3,I+7))
C
      D = X(3, I+8) - X(3,I)
      AV(I) = C/D
C
301   CONTINUE
C
C  CONVERT DEPTH AVERAGED NODAL VELOCITIES TO CELL VELOCITIES
C
      DO 302 I = 2, NLS+1
      DO 302 J = 2, MOF+1
      N = 1 + (I-2)*81
      N1 = N + (J-2)*9
      N2 = N1 + 9
      N3 = N1 + 81
      N4 = N1 + 90
      U(I,J) = (AU(N1) + AU(N2) + AU(N3) + AU(N4))/4.0
      V(I,J) = (AV(N1) + AV(N2) + AV(N3) + AV(N4))/4.0
302   CONTINUE
C
C  DETERMINATION OF TOTAL CELL VELOCITIES (METRES/SEC)
C
      DO 303 I = 2, NLS+1
      DO 303 J = 2, MOF+1
      B = U(I,J)**2 + V(I,J)**2
      UT(I,J) = ABS(SQRT(B))
303   CONTINUE
C
C  CONVERTING NODAL HEIGHTS TO CELL DEPTHS-(METRES)
C
      DO 304 I = 2, NLS+1
      DO 304 J = 2, MOF+1
      N = 1 + (I-2)*81
      N1 = N + (J-2)*9
      N2 = N1 + 9
      N3 = N1 + 81
      N4 = N1 + 90
      H(I,J) = (X(3,N1) + X(3,N2) + X(3,N3) + X(3,N4))/4.0
      H(I,J) = 0.494 - H(I,J)
304   CONTINUE
C
C  SAND TRANSPORT ROUTINE
C
C  SET TIME INTERVAL IN SECONDS
C
      MTA = 600
C
C  TRANSPORT RATES FOR EACH CELL
C
```

```
C
C  COMMENT OUT THE METHOD WHICH IS NOT APPLICABLE
C
C  METHOD 1: USING ACKERS AND WHITE METHOD
C  ========
C
      DO 305 J = 2, MOF+1
      DO 305 I = 2, NLS+1
      A = (H(I,J)**0.0936) * ((LOG10(41667*H(I,J)))**0.4382)
      B = (7.7019*UT(I,J)/A) - 1.0
      IF(B.LT.0.0)GO TO 306
      C = B**2.9343
      SAND = 0.000012567*UT(I,J)*C*(H(I,J)**0.0936)
      GO TO 307
306   SAND = 0.0
C
C  METHOD 2: USING SHIELD'S BED LOAD FORMULA
C  ========
C
C      DO 305 J = 2, MOF+1
C      DO 305 I = 2, NLS+1
C      S = 0.0009*(UT(I,J)**2)/(H(I,J)**1.33333333)
C      SAND = 9.573*UT(I,J)*H(I,J)*S*((995.38*H(I,J)*S) - 0.0462)
C      IF(SAND.GT.0.0)GO TO 307
C      SAND = 0.0
C
307   THETA = ATAN(V(I,J)/U(I,J))
      SANDX(I,J) = SAND * COS(THETA*3.1415926/180.0)
      SANDY(I,J) = SAND * SIN(THETA*3.1415926/180.0)
305   CONTINUE
C
C  TRANSPORT RATES FOR BOUNDARY CELLS
C
      DO 308 J = 2, MOF+1
      SANDX(1,J) = SANDX(2,J)
      SANDX(NLSI,J) = SANDX(NLS+1,J)
308   CONTINUE
C
      DO 309 I = 2, NLS+1
      SANDY(I,1) = 0.0
      SANDY(I,MOFI) = 0.0
309   CONTINUE
C
C  CELL EDGE VALUES
C
      DO 310 I = 1, NLS+1
      DO 310 J = 2, MOF+1
      BDX(I,J) = (SANDX(I,J) + SANDX(I+1,J))/2.0
310   CONTINUE
C
      DO 311 J = 1, MOF+1
      DO 311 I = 2, NLS+1
      BDY(I,J) = (SANDY(I,J) + SANDY(I,J+1))/2.0
311   CONTINUE
C
C  NET SAND TRANSPORT INTO EACH CELL
C
      DO 312 J = 2, MOF+1
      DO 312 I = 2, NLS+1
      XMOVE(I,J) = BDX(I-1,J) - BDX(I,J)
      YMOVE(I,J) = BDY(I, J-1) - BDY(I,J)
312   CONTINUE
C
```

```
C
C  AMOUNT OF EROSION OR DEPOSITION
C
      DO 313 J = 2, MOF+1
      DO 313 I = 2, NLS+1
      RISE = (YL*XMOVE(I,J) + XL*YMOVE(I,J)) * MTA / AREA
      H(I,J) = H(I,J) - RISE
313   CONTINUE
C
      DO 314 J = 2, MOF+1
      H(1,J) = H(2,J)
      H(NLSI,J) = H(NLS+1,J)
314   CONTINUE
C
      DO 315 I = 1, NLSI
      H(I,1) = H(I,2)
      H(I,MOFI)  = H(I,MOF+1)
315   CONTINUE
C
C  CONVERSION OF CELL DEPTH VALUES TO NODAL HEIGHTS
C
      DO 316 I = 2, NLSI
      DO 316 J = 2, MOFI
      N = 1 + (I-2)*81 + (J-2)*9
      X(3,N) = (H(I-1,J-1) + H(I-1,J) + H(I,J-1) + H(I,J))/4.0
      X(3,N) = 0.494 - X(3,N)
316   CONTINUE
C
      DO 317 N = 1, 2512, 81
      X(3,N) = 2*X(3,N) - X(3,N+9)
317   CONTINUE
C
      DO 318 N = 73, 2584, 81
      X(3,N) = 2*X(3,N) - X(3,N-9)
318   CONTINUE
C
      RETURN
      END
```

Appendix-D

Subroutine USRELM for generation of nodal connectivities

```
      SUBROUTINE USRELM (NECARD,NDP,NGROUP,SUB,NELGRP,IERR)
C     ============================================================
C     FOR NO. OF ELEMENTS = 1984(31X8X8), NO. OF NODES = 2592(32X9X9)
C     ============================================================================
C
C     USER SUPPLIED SUBROUTINE FOR THE DEFINITION OF ELEMENTS
C
C     INPUT:
C     =====
C     SUB,NDP,NGROUP ARE THE VALUES SPECIFIED ON THE CONTROL CARD
C     ... , SUBR=SUB , NODE=NDP , GROUP=NGROUP , ...
C
C     OUTPUT:
C     =======
C     NELGRP : NUMBER OF ELEMENTS IN THIS GROUP
C     NECARD(NDP,NELGRP) ELEMENTS DEFINITION FOR THIS GROUP
C     IERR =  0 NORMAL COMPLETION
C          .GT.0 ERROR
C
      IMPLICIT DOUBLE PRECISION (A-H,O-Z)
      COMMON /TAPES/ IFMH,INP,INPS,IOUT,IOUTS,IOUTM,IFID,IERF,IPST,
     1               IECHFI,IECHF,IECHF1,IELM,IELMS,INP1,IUSER,
     2               LPDEV(15),IHLPF,IDEVF,IECHF2,IRADF
      COMMON /INTERN/ IBUF,NBUF,NCBUF,NKVLD,KEYSTR,KEYEND,INFLAG,
     1                MAJIND(160),MININD(750),KVERIF(85),IPVERF(85),
     2                IDVERF(85),INALTR,ILETP,IDATA,INPROG,INFLG1,MECHF,
     3                IHUNT,ISHOWN
      COMMON /INTERC/ BUFFER(80,15),FILNAM
      CHARACTER  BUFFER*1 , BUFF8R(15)*80 , FILNAM*20
      EQUIVALENCE (BUFFER,BUFF8R)
C
      DIMENSION NECARD (NDP,*)
C
      IF(NGROUP.EQ.2) GO TO 222
      IF(NGROUP.EQ.3) GO TO 333
      IF(NGROUP.EQ.4) GO TO 444
C
      NELGRP = 1984
C
C     INSERT HERE NORMAL EXECUTION COMMANDS
C
C   GENERATION OF THE GLOBAL NODE NUMBERS OF THE ELEMENT NODES.
C   ELEMENT GROUP=1, 3-D BRICK ELEMENTS, NODES=8
C
      NE = 0
      DO 100 I = 1, 2431, 81
      DO 100 J = 1, 8
      DO 100 K = 1, 8
      N = (I-1) + 9*(J-1) + K
      NE = NE + 1
      NECARD(1,NE) = N
      NECARD(2,NE) = N + 81
      NECARD(3,NE) = N + 9
      NECARD(4,NE) = N + 90
      NECARD(5,NE) = N + 1
      NECARD(6,NE) = N + 82
      NECARD(7,NE) = N + 10
      NECARD(8,NE) = N + 91
100   CONTINUE
C
      RETURN
C
```

```
222   NELGRP = 248
C
C     GENERATION OF THE GLOBAL NODE NUMBERS OF THE ELEMENT NODES ON WALL
C     SURFACES
C
C     NE = ELEMENT NUMBER
C
C     1-SHOREEND WALL
C     ===============
C     ELEMENT GROUP=2, 2-D QUADRILATERAL ELEMENTS, NODES=4
C
      NE = 0
      DO 200 I = 1, 2431, 81
      DO 200 J = 1, 8
      N = (I-1) + J
      NE = NE + 1
      NECARD(1,NE) = N
      NECARD(2,NE) = N + 81
      NECARD(3,NE) = N + 82
      NECARD(4,NE) = N + 1
200   CONTINUE
C
      RETURN
C
333   NELGRP = 248
C
C     2-OFFSHOREEND WALL
C     ==================
C     ELEMENT GROUP=3, 2-D QUADRILATERAL ELEMENTS, NODES=4
C
      NE = 0
      DO 300 I = 73, 2503, 81
      DO 300 J = 1, 8
      N  = (I-1) + J
      NE = NE + 1
      NECARD(1,NE) = N + 81
      NECARD(2,NE) = N
      NECARD(3,NE) = N + 1
      NECARD(4,NE) = N + 82
300   CONTINUE
C
      RETURN
C
444   NELGRP = 248
C
C     3-BED WALL BOUNDARY
C     ===================
C     ELEMENT GROUP=4, 2-D QUADRILATERAL ELEMENTS, NODES=4
C
      NE = 0
      DO 400 I = 1, 2431, 81
      DO 400 J = 9, 72, 9
      N  = I + (J-9)
      NE = NE + 1
      NECARD(1,NE) = N + 81
      NECARD(2,NE) = N
      NECARD(3,NE) = N + 9
      NECARD(4,NE) = N + 90
400   CONTINUE
C
      RETURN
      END
```

Appendix-E

Subroutine USRMXL for generation of mixing lengths

```
      SUBROUTINE USRMXL (NELT,NE,NG,VMU,TEMP,SPEC1,SPEC2,UV,DUV,VEL,SHP,
     1                   DSDX,DSDY,DSDZ,NDP,XL,YL,ZL,PROP,MDVSC,TIME,
     2                   NIP,MNDP,DEN)
C     ******************************************************************
C     FOR 1984 (31X8X8) ELEMENTS AND 2592 (32X9X9) NODES
C     ==================================================
C
C     USER DEFINED MIXING LENGTH
C
C     NELT  = GLOBAL ELEMENT NUMBER
C     NE    = LOCAL ELEMENT NUMBER
C     NG    = GROUP NUMBER
C     VMU   = VISCOSITIES
C     TEMP  = TEMPERATURE
C     SPEC1 = SPECIES 1
C     SPEC2 = SPECIES 1
C     XL    = X COORDINATES
C     YL    = Y COORDINATES
C     ZL    = Z COORDINATES
C     UV    = VELOCITY COMPONENTS
C     DUV   = VELOCITY GRADIENT COMPONENTS
C     SHP   = ELEMENT SHAPE FUNCTIONS
C     DSDX  = SHAPE FUNCTION DERIVATIVES IN THE X DIRECTION
C     DSDY  = SHAPE FUNCTION DERIVATIVES IN THE Y DIRECTION
C     DSDZ  = SHAPE FUNCTION DERIVATIVES IN THE Z DIRECTION
C     VEL   = VALUES OF NODAL DEGREES OF FREEDOM AT NODAL
C             POINTS OF ELEMENT NELT
C     PROP  = USER DEFINED PARAMETERS
C     MDVSC = NUMBER OF COMPONENTS OF VISCOSITY ARRAY
C     TIME  = TIME
C     MNDP  = FIRST DIMENSION OF SHAPE FUNCTION MATRICES
C     NIP   = NUMBER OF INTEGRATION POINTS
C
      IMPLICIT DOUBLE PRECISION (A-H,O-Z)
      DIMENSION VMU(9,NIP),SHP(MNDP,NIP),DSDX(MNDP,NIP)
      DIMENSION DSDY(MNDP,NIP),DSDZ(MNDP,NIP),VEL(*),PROP(*)
      DIMENSION TEMP(NIP),SPEC1(NIP),SPEC2(NIP),XL(NIP)
      DIMENSION YL(NIP),ZL(NIP),UV(3,NIP),DUV(9,NIP),R(1984)
      ZRO = 0.D0
C
C  DETERMINATION OF R , THE MEAN DEPTH OF FLOW
C
      IF(NE.LT.513) GO TO 301
      IF(NE.GT.512.AND.NE.LT.1025) GO TO 302
      IF(NE.GT.1024) GO TO 303
C
301   CONTINUE
      DO 201 I = 1, 129, 64
      DO 201 J = 1, 8
      N = I + (J-1)
      R(N) = 0.085
201   CONTINUE
C
      DO 202 I = 9, 201, 64
      DO 202 J = 1, 8
      N = I + (J-1)
      R(N) = 0.115
202   CONTINUE
C
```

```
C
      DO 203 I = 17, 209, 64
      DO 203 J = 1, 8
      N = I + (J-1)
      R(N) = 0.145
203   CONTINUE
C
      DO 204 I = 25, 281, 64
      DO 204 J = 1, 8
      N = I + (J-1)
      R(N) = 0.175
204   CONTINUE
C
      DO 205 I = 33, 289, 64
      DO 205 J = 1, 8
      N = I + (J-1)
      R(N) = 0.205
205   CONTINUE
C
      DO 206 I = 41, 361, 64
      DO 206 J = 1, 8
      N = I + (J-1)
      R(N) = 0.235
206   CONTINUE
C
      DO 207 I = 49, 369, 64
      DO 207 J = 1, 8
      N = I + (J-1)
      R(N) = 0.265
207   CONTINUE
C
      DO 208 I = 57, 441, 64
      DO 208 J = 1, 8
      N = I + (J-1)
      R(N) = 0.295
208   CONTINUE
C
      DO 209 N = 193, 200
      R(N) = 0.094
209   CONTINUE
C
      DO 210 N = 257, 272
      R(N) = 0.137
210   CONTINUE
C
      DO 211 N = 273, 280
      R(N) = 0.158
211   CONTINUE
C
      DO 212 N = 321, 352
      R(N) = 0.203
212   CONTINUE
C
      DO 213 N = 353, 360
      R(N) = 0.221
213   CONTINUE
C
      DO 214 N = 385, 432
      R(N) = 0.270
214   CONTINUE
C
```

```
C
      DO 215 N = 433, 440
      R(N) = 0.250
215   CONTINUE
C
      DO 216 N = 449, 512
      R(N) = 0.337
216   CONTINUE
C
      GO TO 304
C
302   CONTINUE
C
      DO 217 N = 513, 1024
      R(N) = 0.370
217   CONTINUE
C
      GO TO 304
C
303   CONTINUE
C
      DO 218 N = 1025, 1088
      R(N) = 0.337
218   CONTINUE
C
      DO 219 N = 1089, 1136
      R(N) = 0.270
219   CONTINUE
C
      DO 220 N = 1137, 1144
      R(N) = 0.250
220   CONTINUE
C
      DO 221 N = 1153, 1184
      R(N) = 0.203
221   CONTINUE
C
      DO 222 N = 1185, 1192
      R(N) = 0.221
222   CONTINUE
C
      DO 223 N = 1217, 1232
      R(N) = 0.137
223   CONTINUE
C
      DO 224 N = 1233, 1240
      R(N) = 0.158
224   CONTINUE
C
      DO 225 N = 1281, 1288
      R(N) = 0.094
225   CONTINUE
C
      DO 226 I = 1345, 1921, 64
      DO 226 J = 1, 8
      N = I + J - 1
      R(N) = 0.085
226   CONTINUE
C
```

```
C
      DO 227 I = 1289, 1929, 64
      DO 227 J = 1, 8
      N = I + J - 1
      R(N) = 0.115
227   CONTINUE
C
      DO 228 I = 1297, 1937, 64
      DO 228 J = 1, 8
      N = I + J - 1
      R(N) = 0.145
228   CONTINUE
C
      DO 229 I = 1241, 1945, 64
      DO 229 J = 1, 8
      N = I + J - 1
      R(N) = 0.175
229   CONTINUE
C
      DO 230 I = 1249, 1953, 64
      DO 230 J = 1, 8
      N = I + J - 1
      R(N) = 0.205
230   CONTINUE
C
      DO 231 I = 1193, 1961, 64
      DO 231 J = 1, 8
      N = I + J - 1
      R(N) = 0.235
231   CONTINUE
C
      DO 232 I = 1201, 1969, 64
      DO 232 J = 1, 8
      N = I + J - 1
      R(N) = 0.265
232   CONTINUE
C
      DO 233 I = 1145, 1977, 64
      DO 233 J = 1, 8
      N = I + J - 1
      R(N) = 0.295
233   CONTINUE
C
304   CONTINUE
C
C  CALCULATE CENTROD X AND Y FOR ELEMENT
C
      XT = 0.0
      YT = 0.0
      ZT = 0.0
      DO 234 J = 1, NIP
      XT = XT + XL(J)
      YT = YT + YL(J)
      ZT = ZT + ZL(J)
234   CONTINUE
C
      FNIP = FLOAT(NIP)
      XAVG = XT/FNIP
      YAVG = YT/FNIP
      ZAVG = ZT/FNIP
C
```

```
C
C  MINIMUM WALL DISTANCE
C
      W = 1.2
      YD = W - YAVG
      ZD = R(NE) - (0.490 - ZAVG)
      Y = MIN(YAVG,YD,ZD)
C
      YR = Y/R(NE)
      PRPIPE = 0.14 - 0.08*(1.0 - YR)**2  - 0.06*(1.0 - YR)**4
      FMIXL = R(NE)*PRPIPE
      IF(FMIXL.LT.0.0) FMIXL = 0.0
C
C  MIXING LENGTH FOR ELEMENT
C
c      XML = FMIXL(XAVG,YAVG,ZAVG)
      XML = FMIXL
      XML2 = DEN*XML*XML
C
C  CALCULATE AVERAGE DUDX, DUDY AND DUDZ FOR ELEMENT
C
      DO 100 J = 1, NIP
      DUXDX = DUV(1,J)
      DUXDY = DUV(2,J)
      DUXDZ = DUV(3,J)
      DUYDX = DUV(4,J)
      DUYDY = DUV(5,J)
      DUYDZ = DUV(6,J)
      DUZDX = DUV(7,J)
      DUZDY = DUV(8,J)
      DUZDZ = DUV(9,J)
C
      DUDX = SQRT (DUXDX*DUXDX + DUYDX*DUYDX + DUZDX*DUZDX)
      DUDY = SQRT (DUXDY*DUXDY + DUYDY*DUYDY + DUZDY*DUZDY)
      DUDZ = SQRT (DUXDZ*DUXDZ + DUYDZ*DUYDZ + DUZDZ*DUZDZ)
      DUDN = SQRT (DUDX*DUDX + DUDY*DUDY + DUDZ*DUDZ)
      VSC = XML2*DUDN
      DO 50 I = 1, 9
      VMU(I,J) = VSC
50    CONTINUE
100   CONTINUE
      RETURN
C
      END
```

Bibliography

[1] Ackers, Peter and White, W.R. *Sediment Transport: New Approach and Analysis.* Journal of the Hydraulics Division, Vol.99, No.HY11, November 1973, pp.2041-2060.

[2] Baines, W.Douglas. *Tidal Currents in Constricted Inlets.* Proc. of the 6th International Conference on Coastal Engineering, Dec.1957, Vol.6,pp.545-561.

[3] Bechteler, W. and Schrimpf, W. *Improved Numerical Model for Sedimentation.* Journal of the Hydraulic Engineering, Vol.110, No.3, March 1984, pp.234-246.

[4] Blench, T. *Hydraulics of Canals and Rivers of Mobile Boundary.* Butterworth's Civil Engineering Reference Book, 2nd ed., Butterworth, London, England, 1961.

[5] Brian, A. O'Connor. *Mathematical Model for Sediment Distribution.* Proc. of the 14th IAHR Conference, Paper D-23, Paris, France, 1971.

[6] Brian, A. O'Connor. *Suspended Load Calculations in a Tidal Estuary.* Proc. of the 12th International Conference on Coastal Engineering, Sept.1970, pp.1931-1950.

[7] Brown, E.I. *Inlets on Sandy Coasts.* Proc. of the ASCE, Vol. 54, 1928, pp.505-553.

[8] Coleman,N.L. *Flume Studies of the Sediment Transfer Coefficient.* Water Resources Research, Vol.6, No.3, 1970, USA.

[9] Coles, D. *The Law of the Wake in the Turbulent Boundary Layer.* Journal of Fluid Mechanics, Vol.1,1965.

[10] Curtis Mason. *Regime Equations and Tidal Inlets.* Journal of the Waterways, Harbours and Coastal Engineering Division, WW3, Aug.1973, Vol.99, pp.393-397.

[11] Delft Hydraulic Laboratory. *Semi-Empirical Model for the Flow in Dredged Trenches.* Report R 1267 III, Delft, The Netherlands, 1980.

[12] Dennis, W.A., Lanan, G.A. and Dalrymple, R.A. *Case Studies of Delaware's Tidal Inlets: Roosevelt and Indian Riner Inlets.* Proc. of the 16th International Conference on Coastal Engineering, Aug.1978, pp.1283-1301.

[13] Djunkovski, N.N. and Smirnov, G.S. XIX International Navigation Congress, London, 1957, Section II, Communication-3.

[14] Dobbins, W.E. *Effect of Turbulence on Sedimentation.* Transactions of ASCE, 1944, Vol.109, pp.629-656.

[15] Einstein, H.A. *Computation of Tides and Tidal Currents.* United States Practice, Proc. of the ASCE, Vol.81, Separate No.715, June 1955.

[16] Escoffier, F.F. *The Stability of Tidal Inlets.* Shore and Beach, Vol.8, No.4, pp.114-115.

[17] Forman, James W. and Vallianos, Limberios. *Procedure for Determining Dredging Requirements in Coastal Inlet Channels.* 19th International Conference on Coastal Engineering, Sept.1984, Vol.II, pp.1668-1684.

[18] French, R.H. *Open-Channel Hydraulics.* McGraw-Hill Book Company, 1985, pp.351.

[19] Galvin, Cyril. *Shoaling with Bypassing for Channels at Tidal Inlets.* 18th International Conference on Coastal Engineering, Nov.1982, Vol.II, pp.1496-1513.

[20] Graf, W.H. *Hydraulics of Sediment Transport.* Mc Graw-Hill Book Company, 1971.

[21] Hiller, M.E. and Jenkin, R.D. *Digital Coastal Outflow Simulation.* University of Adelaide, Oct.1976.

[22] Hunt, J.N. *The Turbulent Transport of Suspended Sediment in Open Channels.* Proc. of the Royal Society of London, Series A, Vol.224, No.1158, pp.322-335.

[23] Hurst, H.E. *The Suspension of Sand in Water.* Proc. of the Royal Society of London, Series A, Vol.24, 1929, pp.196-201.

[24] Jacobus van de Kreeke. *Water-Level Fluctuations and Flow in Tidal Inlets.* Journal of the Waterways and Harbours Division, ASCE, Vol.93, No.WW4, Nov.1967, pp.97-106.

[25] Jarrett, J.T. *Tidal Prism-Inlet Area Relationships.* GITI Report 3, U.S. Army Coastal Engineering Research Center, Fort Belvoir, Feb.1976.

[26] Johnson, J.W. *Tidal Inlets on the California, Oregon and Washington Coasts.* HEL-24-12, Hydraulic Engineering Laboratory, University of California, Feb.1972.

[27] Kalinske, A.A. *Suspended Material Transportation Under Non-Equilibrium Conditions.* Transactions of the American Geophysical Union, Vol.21, 1940, pp.613-617.

[28] Kalinske, A.A. *Movement of Sediment as Bedload in Rivers.* Transactions of the American Geophysical Union, Vol.28, No.4, pp.616-620.

[29] Kerssens, P.J.M., Prins, A. and Rijn, L.C. van. *Model for Suspended Sediment Transport.* Journal of the Hydraulics Div., ASCE, HY5, May 1979,pp.461-476.

[30] Keulegan, G.H. *Tidal Flow in Entrances. Water Level Fluctuations of Basins in Communication with Seas.* 3rd Progress Report, National Bureau of Standards, Report No.1146, 1951.

[31] Lacey, G. *Stable Channels in Alluvium.* Minutes of the Proc. of the Institution of Civil Engineers, Vol.229, 1929.

[32] Launder, B.E., Morse, A., Rodi, W, and Spalding, D.B. *Prediction of Free Shear Flows - A Comparison of the Performance of Six Turbulence Models.* Proceedings of NASA, July 1972, pp.361-414.

[33] Launder, B.E. and Spalding, D.B. *The Numerical Calculation of Turbulent Flows.* Computer Methods in Applied Mechanics and Engineering, Vol.3, 1974, pp.269.

[34] Leschziner, M.A. and Rodi, W. *Calculation of Strongly Curved Open Channel Flow.* Journal of the Hydraulics Division, ASCE, Vol.105, HY10, October 1979, pp. 1297-1313.

[35] Muthusamy, K. *Tidal Prism of Equilibrium Inlets.* Journal of the Waterway, Port, Coastal and Ocean Division, Nov.1977, Vol.103, WW4, pp.423-432.

[36] O'Brien, M.P. *Estuary Tidal Prisms Related to Entrance Area.* Civil Engineering, ASCE, Vol.1, No.8, 1931, pp.738-739.

[37] O'Brien, M.P. *Review of the Theory of Turbulent Flow and Its Relation to Sediment Transportation.* Transactions of the American Geophysical Union, April 1933, pp.487-491.

[38] O'Brien, M.P. *Equilibrium Flow Areas of Inlets on Sandy Coasts.* Journal of the Waterways and Harbours Division, ASCE, Vol.95, No.WW1, Feb.1969, pp.43-52.

[39] O'Brien, M.P. and Dean, R.G. *Hydraulics and Sedimentary Stability of Coastal Inlets.* Proc. of the 13th International Conference on Coastal Engineering, July 1972, Vol.II, pp.761-780.

[40] Rijn, L.C. van *Mathematical Modelling of Suspended Sediment in Non-Uniform Flows.* Journal of Hydraulic Engineering, ASCE, Vol.112, No.6, June 1986, pp.433-455.

[41] Rodi, W. *Turbulence Models and their Application in Hydraulics.* IAHR Section on Fundamentals, Delft, The Netherlands, 1980.

[42] Rouse, Hunter. *Experiments on the Mechanics of Sediment Suspension.* Proc. of the 5th International Congress for Applied Mechanics, Vol.55, John Wiley & Sons,Inc., New York, 1938.

[43] Schlichting, H. *Boundary Layer Theory.* Mc.Graw Hill, New York, 1969.

[44] Schmidt, Wilhelm. *"Der Massenaustausch in Freir Luft und Verwandte Erscheinungen".* Propleme der Kosmischen Physik, Band 7, Hamburg, Germany, 1925.

[45] Shemdin, O.H. and Forney, R.M. *Tidal Motion in Bays.* Proc. of the 12th International Conference on Coastal Engineering, Sept. 1970, Vol.III, pp.2225-2242.

[46] Schields, A. *"Anwendung der Aehnlichkeitsmechanik und der Turbulenzforschung auf die Geschiebebewegung"*, Mitteilungen der Preussischen Versuchsanstalt fur Wasserbau und Schiffbau, Berlin, Germany, Vol.26, 1936.

[47] Simons, D.B. and Albertson, M.L. *Uniform Water Conveyance Channels in Alluvial Material.* Transactions of ASCE, Vol.128, Part I, Paper No.3399, 1963, pp.65-107.

[48] Smith, T.J. and O'Connor, B.A. *A Two-Dimensional Model for Suspended Sediment Transport.* 17th IAHR Congress, Baden-Baden, West Germany, 1977, pp.79-86.

[49] Trawle, M.J. *Effects of Depth on Dredging Frequency.* Report 2, Methods of Estuariene Shoaling Analysis, U.S. Army Waterways Experiment Station, Technical Report H-78-5.

[50] Vincente, C.M. and Uva, L.P. *Sedimentation in Dredged Channels and Basins.* Proc. of the 19th International Conference on Coastal Engineering, Sept.1984, Vol.II, pp.1863-1878.

[51] Vreugdenhill, C.B. *Numerical Solution of a Convective-Diffusion Equation using Finite Elements.* Delft Hydraulics Laboratory, Internal Note X59, Delft, The Netherlands.

[52] William, N.Seelig and Robert, M.Sorensen. *Numerical Model Investigation of Selected Tidal Inlet-Bay System Characteristics.* Proc. of the 16th International Conference on Coastal Engineering, Aug.1978, Vol.II, pp.1302-1319.